WADC TECHNICAL REPORT 54-616
PART V
ASTIA DOCUMENT NO. 209378

HYDROGEN CONTAMINATION IN TITANIUM AND TITANIUM ALLOYS
PART V. HYDROGEN EMBRITTLEMENT

D. N. WILLIAMS
F. R. SCHWARTZBERG
R. I. JAFFEE

BATTELLE MEMORIAL INSTITUTE

FEBRUARY 1959

MATERIALS LABORATORY
CONTRACT NO. AF 33(616)-5007
AIRCRAFT LABORATORY

WRIGHT AIR DEVELOPMENT CENTER
AIR RESEARCH AND DEVELOPMENT COMMAND
UNITED STATES AIR FORCE
WRIGHT-PATTERSON AIR FORCE BASE, OHIO

McGregor & Werner Midwest Corp., Dayton, O.
25-545-500-3-27-59

FOREWORD

This report was prepared by Battelle Memorial Institute under USAF Contract No. AF 33(616)-5007. This contract was initiated under Project No. 7351, "Metallic Materials", Task No. 73510, "Titanium and Titanium Alloys". The project was administered under the direction of the Materials Laboratory, Directorate of Laboratories, Wright Air Development Center, with Lt. T. Cooper, Capt. E. J. Myers, and Mr. H. J. Middendorp acting as project engineers.

This project was conducted during the period March, 1957, to March, 1958.

ABSTRACT

Extensive investigations intended to provide information relating to the mechanism of hydrogen embrittlement in titanium-base alloys were carried out. Studies included detailed measurements of the effects of temperature, strain rate, and hydrogen content on hydrogen embrittlement; examination of all-alpha and all-beta alloys for susceptibility to hydrogen embrittlement; calculations of probable hydrogen solubility in alpha and beta titanium; and several other informative investigations. An embrittlement mechanism is outlined. Alloys previously prepared and examined to determine the effects of alloy content and microstructure on hydrogen embrittlement (WADC TR 54-616, Part IV) were further studied by means of notched stress-rupture tests. This work has resulted in some alteration in previously expressed conclusions regarding alloying and microstructural effects.

PUBLICATION REVIEW

This report has been reviewed and approved.

FOR THE COMMANDER:

R R Kennedy

R. R. KENNEDY
Chief, Metals Branch
Materials Laboratory

TABLE OF CONTENTS

	Page
SUMMARY	1
INTRODUCTION	2
MECHANISM OF LOW-STRAIN-RATE HYDROGEN EMBRITTLEMENT	2
Recovery of Ductility at Subzero Temperature	2
Stress-Dependent Diffusion	20
Critical Nucleation Stress	21
Loss of Ductility Near Room Temperature	26
Hydrogen Embrittlement in an All-Beta Alloy	33
Low-Strain-Rate Embrittlement in an All-Alpha Alloy	35
Effect of Cyclic Loading on Low-Strain-Rate Embrittlement	40
Pretreatment to Minimize Hydrogen Embrittlement	43
Segregation of Hydrogen at the Fracture	46
Hydride Formation in Torsion and Compression	47
Hydride Re-Solution During Heat Treatment	47
Discussion of Results	48
THE EFFECT OF ALLOY COMPOSITION AND HEAT TREATMENT ON LOW-STRAIN-RATE EMBRITTLEMENT	51
Experimental Procedure	52
Preparation of Material	52
Notched Stress-Rupture Testing	54
Metallographic and Hardness Examination	64
Results	65
Effect of Alloy Content	65
Effect of Heat Treatment	75
Strain-Induced Hydride	76
Discussion of Results	77
REFERENCES	80
APPENDIX	83

LIST OF TABLES

Table 1.	Effect of Temperature, Testing Speed, and Hydrogen Content on the Tensile Properties of Ti-2Fe-2Cr-2Mo	16
Table 2.	Tensile Properties of Hydrogen-Containing Ti-2Fe-2Cr-2Mo Tested at 0.005 Inch Per Minute	30
Table 3.	Hydrogen Embrittlement of an All-Beta Alloy, Ti-20Mo	34
Table 4.	Results of Tensile Tests of Unalloyed Titanium Conducted Immediately After Heat Treatment	37
Table 5.	Notched Stress-Rupture Properties of Ti-5Al at Four Hydrogen Levels	41
Table 6.	Results of Interrupted Stress-Rupture Tests on Unnotched Ti-8Mn Alloy Containing 370 PPM Hydrogen	41
Table 7.	Interrupted Stress-Rupture-Test Results on Ti-2Fe-2Cr-2Mo Alloy	42
Table 8.	Effect of Pretreatment on the Susceptibility to Low-Strain-Rate Embrittlement	44
Table 9.	Summary of X-Ray Tests to Check for Hydrogen Segregation at the Fracture	46
Table 10.	Selected Test Data Showing Equivalence of Three Notched Stress-Rupture Specimens	55
Table 11.	Notched Tensile Properties of Alloys Tested at 0.005 Inch/Minute Platen Speed	62

LIST OF TABLES
(Continued)

Page

Table 12. Low-Strain-Rate Embrittlement in Binary Titanium-Base Alloys 66

Table 13. Low-Strain-Rate Embrittlement in Titanium-Base Alloys Containing Multiple Beta Stabilizers 67

Table 14. Low-Strain-Rate Embrittlement in Aluminum- and Tin-Containing Titanium-Base Alloys 70

Table 15. Low-Strain-Rate Embrittlement in Titanium-Base Alloys for Varying Interstitial Content 71

Table 16. Effect of Heat Treatment on the Hydrogen Tolerance of Five Titanium-Base Alloys 73

Table 17. The Effect of Grain Size on the Hydrogen Tolerance of Four Titanium Alloys 74

Table A-1. Complete Results of the Room-Temperature Notched Stress-Rupture Test Program 83

LIST OF ILLUSTRATIONS

Figure 1. Photograph of Equipment Used to Attain Temperatures Below -110 F 6

Figure 2. Close-Up of Isopentane Bath and Cooling Coil 7

Figure 3. Effect of Testing Speed and Temperature on the Tensile Ductility of Ti-2Fe-2Cr-2Mo Containing 20 PPM Hydrogen 8

Figure 4. Effect of Testing Speed and Temperature on the Tensile Ductility of Ti-2Fe-2Cr-2Mo Containing 375 PPM Hydrogen 9

Figure 5. Activation-Energy Plot for the 375-PPM-Hydrogen Level 10

Figure 6. Activation-Energy Plot for the 250-PPM-Hydrogen Level, Lot A 11

Figure 7. Activation-Energy Plot for the 250-PPM-Hydrogen Level, Lot B 12

Figure 8. Activation-Energy Plot for the 500-PPM-Hydrogen Level 13

Figure 9. Activation-Energy Plot for the 750-PPM-Hydrogen Level 14

Figure 10. Plot of Per Cent Retained Fracture Stress Versus Log Time for Material Containing 375 PPM Hydrogen 22

Figure 11. Activation-Energy Plot for the 375-PPM-Hydrogen Level (Retained Fracture Stress) 23

Figure 12. Determination of Activation Energy by Using the Concept of a Critical Nucleation Stress 25

Figure 13. Effect of Temperature on the Solubility of Hydrogen in Titanium 28

Figure 14. Effect of Temperature on the Tensile Ductility of Hydrogen-Containing Ti-2Fe-2Cr-2Mo 31

Figure 15. Effect of Heat Treatment on Hydride Structure Near the Tensile Fracture of Unalloyed Titanium Containing 400 ppm Hydrogen and Tested at 0.005 Inch/Inch/Minute Immediately After Heat Treatment 38

Figure 16. Hydride in an All-Alpha Ti-5Al Alloy 39

Figure 17. Localized Precipitation of Hydride in a Ti-6Mn Alloy Containing 600 ppm Hydrogen 51

Figure 18. Notched Test Specimens Used in this Investigation 53

LIST OF ILLUSTRATIONS
(Continued)

Page

Figure 19. The Effect of Hydrogen on the Notched Stress-Rupture Properties of Ti-2Mn-2Cr 56

Figure 20. The Effect of Hydrogen on the Notched Stress-Rupture Properties of Ti-4Fe (F-15) 57

Figure 21. The Effect of Hydrogen on the Notched Stress-Rupture Properties of Ti-4Mo (K-1) 58

Figure 22. The Effect of Hydrogen on the Notched Stress-Rupture Properties of Ti-4Al-4Mn in the As-Stabilized, Fine Equiaxed Alpha Condition (K-38-1) 59

Figure 23. The Effect of Hydrogen on the Notched Stress-Rupture Properties of Ti-20Mo (K-3) 60

Figure 24. The Effect of Hydrogen on the Notched Stress-Rupture Properties of Ti-4Al-4Mn in the As-Solution Heat-Treated, Fine Equiaxed Alpha Condition (K-38-2) 61

Figure 25. Grain Boundary Hydride in Ti-8Mn (K-13-6) Containing 200 PPM Hydrogen 77

Figure 26. Massive Hydride in Ti-2Mn-2Fe (K-24) Containing 200 PPM Hydrogen. 78

Figure 27. Acicular Hydride in the Alpha Phase in Ti-6Al-2Fe (K-41) Containing 600 PPM Hydrogen 78

Figure 28. Secondary Strain-Induced Hydride in a Fractured-Notched-Stress-Rupture Sample of Ti-4V-0.95O_2 Alloy (K-52) Containing 100 PPM Hydrogen 79

HYDROGEN CONTAMINATION IN TITANIUM AND TITANIUM ALLOYS

PART V. HYDROGEN EMBRITTLEMENT

SUMMARY

The present investigation is a continuation of work described in WADC TR 54-616, Part IV. Two separate studies were conducted, one aimed at the development of a more complete understanding of the mechanism of low-strain-rate hydrogen embrittlement and the other aimed at determining the effect of alloy composition and structure on the hydrogen tolerance as determined by notched stress-rupture tests.

Tensile tests on Ti-2Fe-2Cr-2Mo alloy over a range of hydrogen contents, temperatures, and strain rates showed the low-strain-rate embrittlement to be a rate-controlled process, having an activation energy of 3100 calories per mole. It was also shown that the limited temperature range in which embrittlement was observed could be explained satisfactorily on the basis of decreasing hydrogen solubility in beta and alpha titanium with decreased temperature, and a beta solubility curve was calculated on the basis of the test data.

Low-strain-rate embrittlement was shown to occur in all-beta and in all-alpha alloys at relatively high hydrogen contents. Thus, susceptibility to embrittlement is not a characteristic of alpha-beta alloys only but is a general trait of titanium-base alloys.

Evaluation of the notched stress-rupture tests led to the revision of the minimum hydrogen contents capable of inducing low-strain-rate embrittlement previously reported in WADC TR 54-616, Part IV. Although some alloys were apparently unaffected by the presence of a notch, the majority of the alloys showed evidence of embrittlement at hydrogen contents from 100 to 200 ppm lower than previously observed. The general alloy trends previously observed were again apparent in most cases. Molybdenum was found to be the most beneficial beta-stabilizing addition from the standpoint of retarding embrittlement, while aluminum was the most beneficial alpha-stabilizing addition. Interstitial additions were detrimental, and multiple beta-stabilizing additions appeared to be no better than equivalent amounts of the various single components. Structural effects were also generally confirmed. A pronounced dependence of hydrogen tolerance on final heat treatment was again observed, and increased alpha grain size was slightly detrimental. A complete tabulation of all notched stress-rupture data is included in the report.

Manuscript released by authors 24 November 1958 for publication as a WADC Technical Report.

INTRODUCTION

This investigation is a continuation of research initiated under Contract No. AF 33(616)-2813. During the present research, which was conducted during the period from March 1, 1957, to February 28, 1958, two separate studies were undertaken: (1) the determination of the origin of low-strain-rate embrittlement in titanium alloys and (2) the measurement of the hydrogen tolerance of a number of alloys on the basis of notched stress-rupture tests at room temperature. The results of these studies are described in this report.

MECHANISM OF LOW-STRAIN-RATE HYDROGEN EMBRITTLEMENT

Low-strain-rate hydrogen embrittlement may be described as a loss of ductility due to hydrogen at relatively low strain rates. It is most pronounced at or slightly below room temperature and is observed to be much less prominent, or even absent, when straining is conducted at either very low (about -200 F) or slightly elevated (about 200 F) temperatures. Thus, embrittlement is characterized both by a sudden loss of ductility near room temperature and a recovery of ductility at low temperatures. Much of the effort during the past year has been devoted to a study of these two phenomena. Work also has been conducted, however, to amplify several previously reported characteristics of hydrogen embrittlement and to determine whether low-strain-rate embrittlement may occur in all types of titanium alloys or is restricted only to alpha-beta alloys. The above studies have led to a number of advances in the theory of hydrogen embrittlement.

Recovery of Ductility at Subzero Temperature

As an initial attempt to develop a mechanistic picture to explain the recovery behavior of hydrogen-containing alpha-beta alloys at various temperatures and strain rates, the following assumptions were made regarding the effects of hydrogen and strain:

(1) Hydrogen partitions primarily to the beta phase.

(2) At the low temperatures where embrittlement is observed, the beta phase is supersaturated with hydrogen.

(3) Hydride cannot precipitate easily within the beta phase.

(4) Under the influence of an applied stress, there is a directed net flux of hydrogen* toward the alpha-beta interface.

(5) Accumulation of hydrogen at the interface causes a critical concentration of hydrogen atoms or precipitation of a stable titanium hydride phase, either of which would limit plastic deformation. **

(6) The hydrogen atoms are present in the beta phase as an atmosphere that can follow moving dislocations during straining.

(7) When the dislocation velocity is rapid, the hydrogen atmosphere cannot diffuse as rapidly as the dislocations, so directional diffusion no longer occurs and ductile behavior is observed.

(8) Similarly, when straining occurs at very low temperatures, the low diffusivity of the hydrogen atoms will not allow the atmosphere to follow the moving dislocations and ductile behavior is observed.

It was then proposed that at the critical temperature, defined as the temperature where complete recovery of ductility is just observed (for a given strain rate), the velocity at which the dislocations travel is equal to the rate at which the hydrogen atmosphere diffuses in the beta phase. The shift of the reciprocal of the critical temperature of recovery with strain rate was then used to determine the activation energy for the embrittlement process. If the above assumptions are correct, this activation energy should equal that for diffusion of hydrogen in the beta phase. Mathematically, this model can be expressed as follows:

(1) $\frac{dx_D}{dt} = \frac{dx_H}{dt}$ at the critical temperature, T, where $\frac{dx_D}{dt}$ is the dislocation velocity and $\frac{dx_H}{dt}$ is the linear velocity of diffusing hydrogen.

(2) $\frac{dx_D}{dt} = A\,\dot{\epsilon}$. The dislocation velocity is directly related to strain rate, $\dot{\epsilon}$. Since A is an arbitrary constant, $\dot{\epsilon}$ can be expressed either as strain rate (inches/inch/minute) or testing speed (inches/minute). The latter method is used in this study.

*Diffusion of hydrogen may occur as protons rather than atoms.

**Since either of these conditions might act similarly to cause brittle behavior, accumulation of hydrogen and hydride precipitation are often used synonomously in this report. Where a distinction between the two is intended it will be so noted.

(3) $\frac{dx_H}{dt} \cdot \frac{dC}{dx} = \frac{dC}{dt} = D \frac{d^2D}{dx^2}$, where

$\frac{dC}{dx}$ is the concentration gradient during diffusion

$\frac{dC}{dt}$ is the rate of accumulation of hydrogen

$\frac{dC}{dt} = D \frac{d^2D}{dx^2}$ is Fick's second law for diffusion.

(4) Combining Equations (2) and (3) by means of Equation (1) and using the relationship $D = D_o e^{-Q/RT}$, where Q is the activation energy for the process:

$$\dot{\epsilon} = \frac{D_o \frac{d^2C}{dx^2}}{A \, dC/dx} e^{-Q/RT}.$$

If the factors D_o, $\frac{d^2D}{dx^2}$, A, and $\frac{dC}{dx}$ are assumed independent of temperature and strain rate at the critical point,

$$\dot{\epsilon} = Be^{-Q/RT}, \text{ where B is constant.}$$

(5) By expressing this equation in logarithmic form

$$\ln \dot{\epsilon} = \left(-\frac{Q}{R}\right) \frac{1}{T} + \ln B,$$

a graphical representation of the critical points in terms of $\ln \dot{\epsilon}$ and $\frac{1}{T}$ should result in straight line having a slope equal to $-\frac{Q}{R}$.

The proposed model used to explain the recovery of ductility pictures two important concepts: (1) recovery of ductility with decreasing temperature is a rate-controlled process and (2) the rate-controlling step is the diffusion of hydrogen in the beta phase. To confirm this mechanistic picture, tensile tests were performed at various temperatures, testing speeds, and hydrogen concentrations.

Commercial 5/8-inch-diameter rod of the Ti-2Fe-2Cr-2Mo alloy was obtained from the Titanium Metals Corporation of America. Hydrogenation of the as-received rod to the 250, 375, 500, and 750 ppm levels was performed by the thermal addition of hydrogen in a Sieverts' apparatus. During hydrogenation the rods were heated to 1470 F, held 24 hours, and

furnace cooled to room temperature. Rods for testing in the low hydrogen (20 ppm) condition were vacuum annealed following the same thermal cycle used for hydrogen addition.

Following hydrogenation or vacuum annealing, the 5/8-inch-diameter rods were hot swaged to 1/4-inch diameter at temperatures progressively reduced from 1400 to 1300 F during the first 50 per cent reduction. Temperature was maintained at 1300 F for the final 50 per cent reduction. Swaged rods were annealed at 1300 F for 1 hour, slowly cooled to 1100 F, held 2 hours at 1100 F, and air cooled.

Standard 0.125-inch-gage-diameter tensile specimens were machined from the heat-treated rods. Tensile testing was performed on a Baldwin-Southwark testing machine; a strain pacer was used to maintain constant testing speed. Temperatures in the range 80 F to -110 F were attained by using a cooling mixture of dry ice and methanol. Below -110 F, the desired temperature was attained by cooling isopentane, a low-freezing-point alcohol, with liquid nitrogen circulated through a cooling coil. Nitrogen or helium gas pressure was used to force the liquid nitrogen through the coil. Temperature was controlled by adjusting gas pressure to vary the liquid-nitrogen flow rate. Figures 1 and 2 show photographs of the equipment used at the lower temperatures.

Tensile test results showed that the ductility of specimens containing 20 ppm hydrogen decreased gradually from 56 to 30 per cent reduction in area* in the temperature range 80 F to -320 F. This is shown graphically in Figure 3. Ductility was apparently independent of testing speed within the limits of the test reliability. Tensile strength showed very slight strain sensitivity over the hundredfold change in testing speed used.

The results of tensile tests of material containing 375 ppm hydrogen over a broad temperature and strain-rate range are shown in Figure 4. At the highest testing speed, 1.0 inch/minute, no embrittlement was observed; ductility gradually decreased with temperature from 80 F to -160 F. At the lower speeds, hydrogen embrittlement was observed from room temperature to approximately -200 F, depending upon rate of straining. Below -200 F, a ductile-to-brittle transition was detected. The critical temperature for each strain rate (the temperature at which ductility is recovered) can be selected quite easily from data presented in the form shown in Figure 4. For example, at a test speed of 0.025 inch/minute, the critical temperature is about -200 F. However, a more exact selection of critical temperature may be made by replotting the data in the manner illustrated in Figure 5. Here, the reduction in area is shown for each test

*Ductility in this work refers to reduction in area measurements only. No elongation measurements were obtained because of the generally adverse effect of punched gage marks on specimens that fail in a brittle manner.

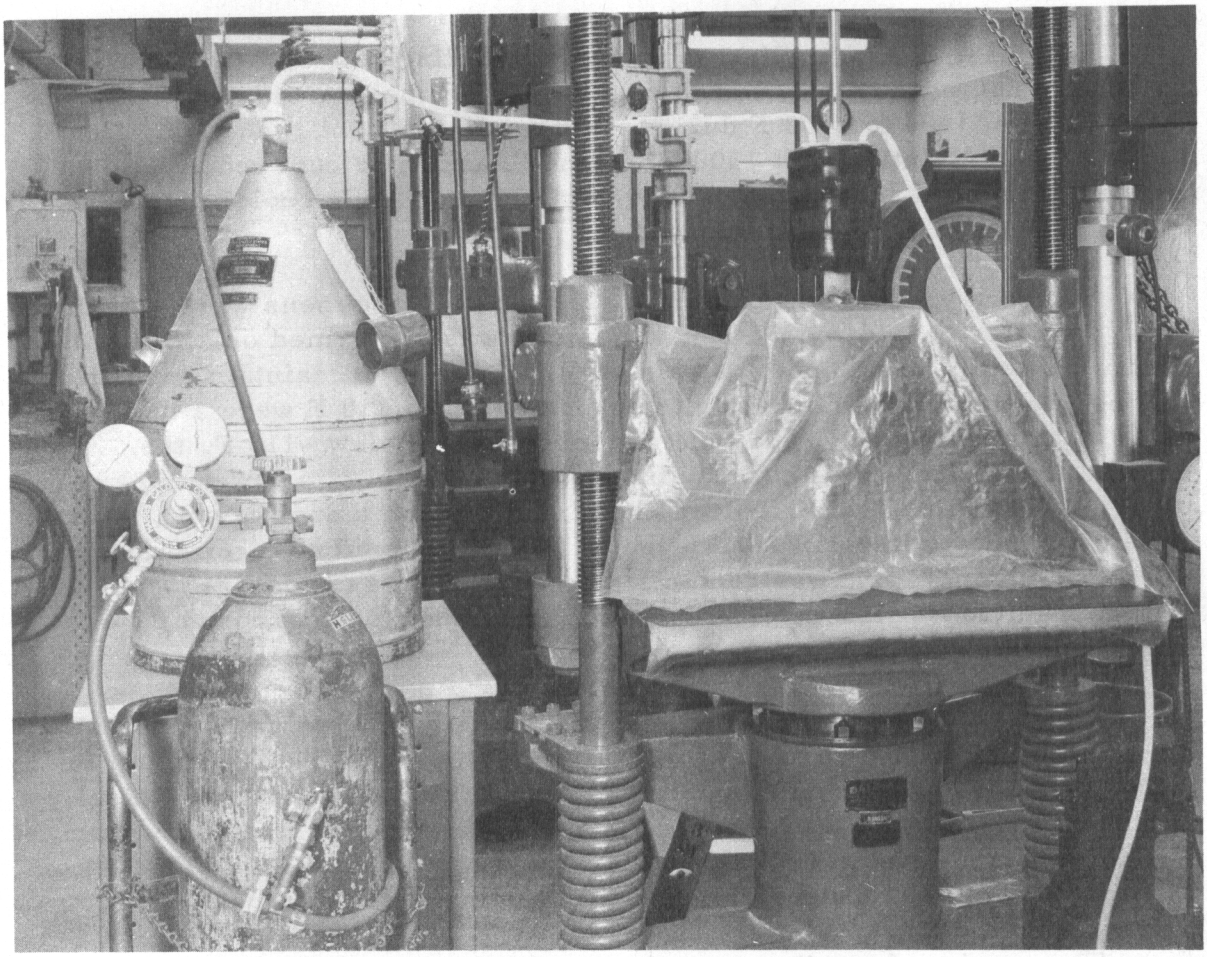

N45773

A. Helium or nitrogen gas cylinder
B. Bleed valve used to control flow rate
C. Liquid nitrogen
D. Isopentane bath with cooling coil

FIGURE 1. PHOTOGRAPH OF EQUIPMENT USED TO ATTAIN TEMPERATURES BELOW -110 F

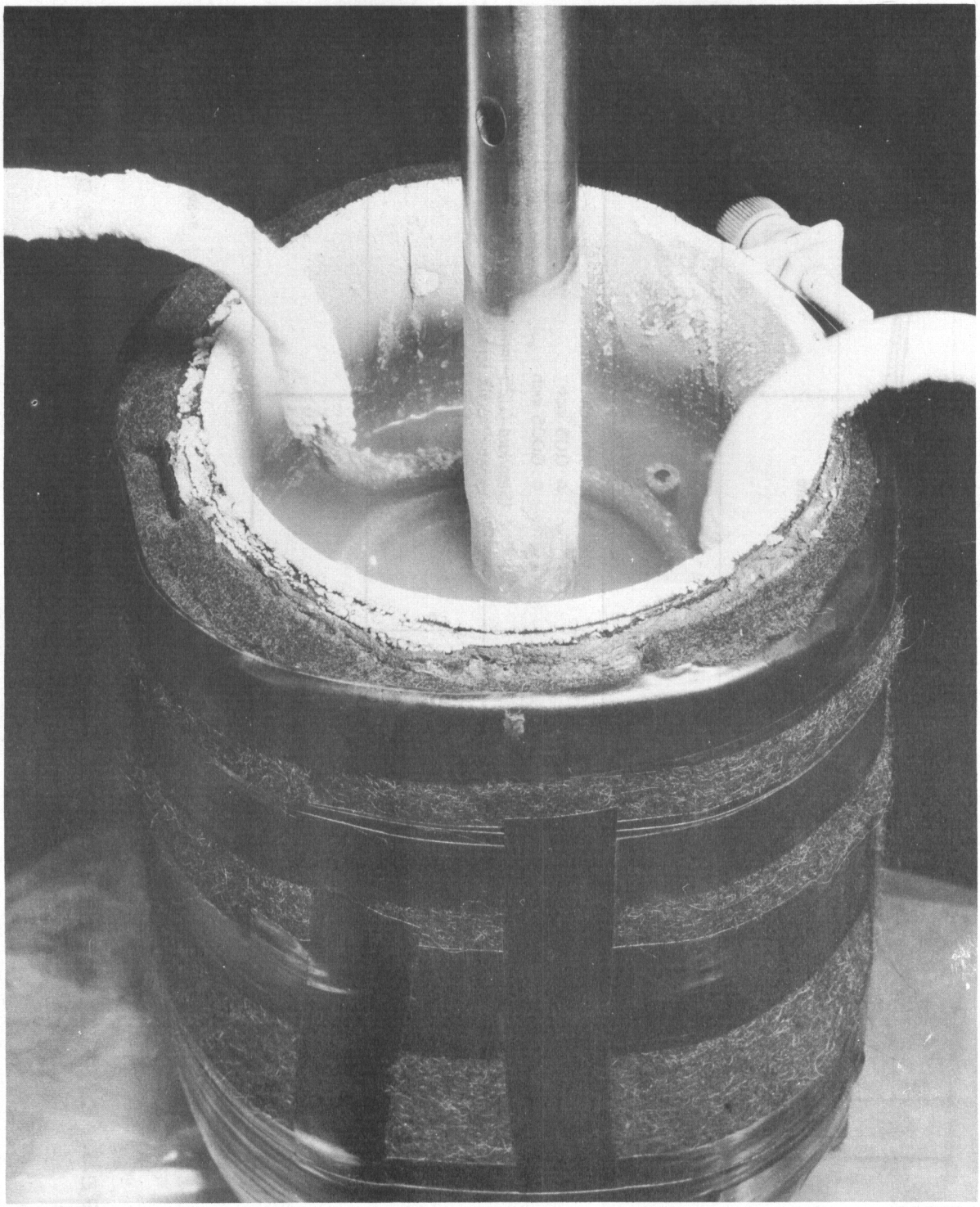

N45774

FIGURE 2. CLOSE-UP OF ISOPENTANE BATH AND COOLING COIL

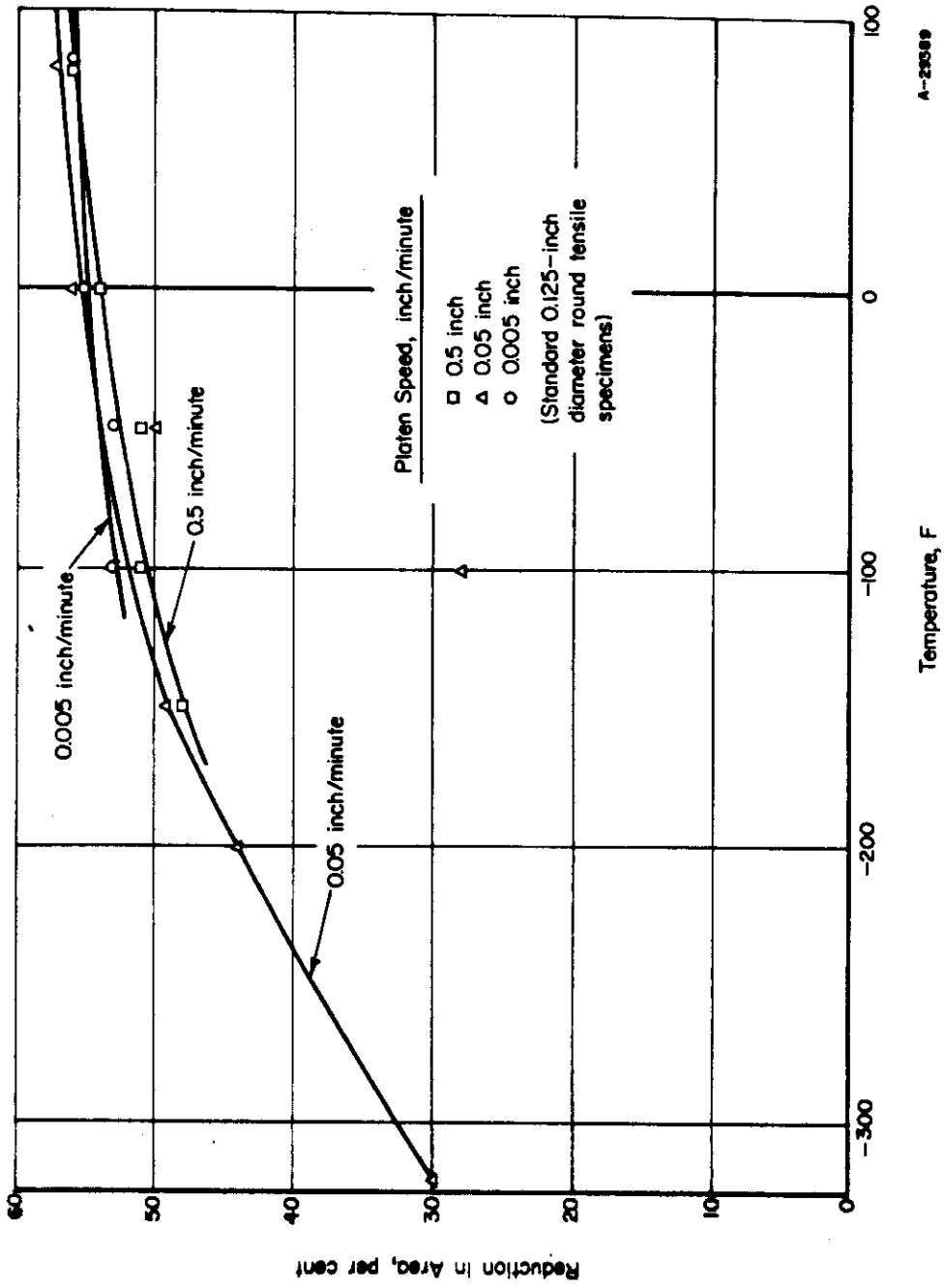

FIGURE 3. EFFECT OF TESTING SPEED AND TEMPERATURE ON THE TENSILE DUCTILITY OF Ti-2Fe-2Cr-2Mo CONTAINING 20 PPM HYDROGEN

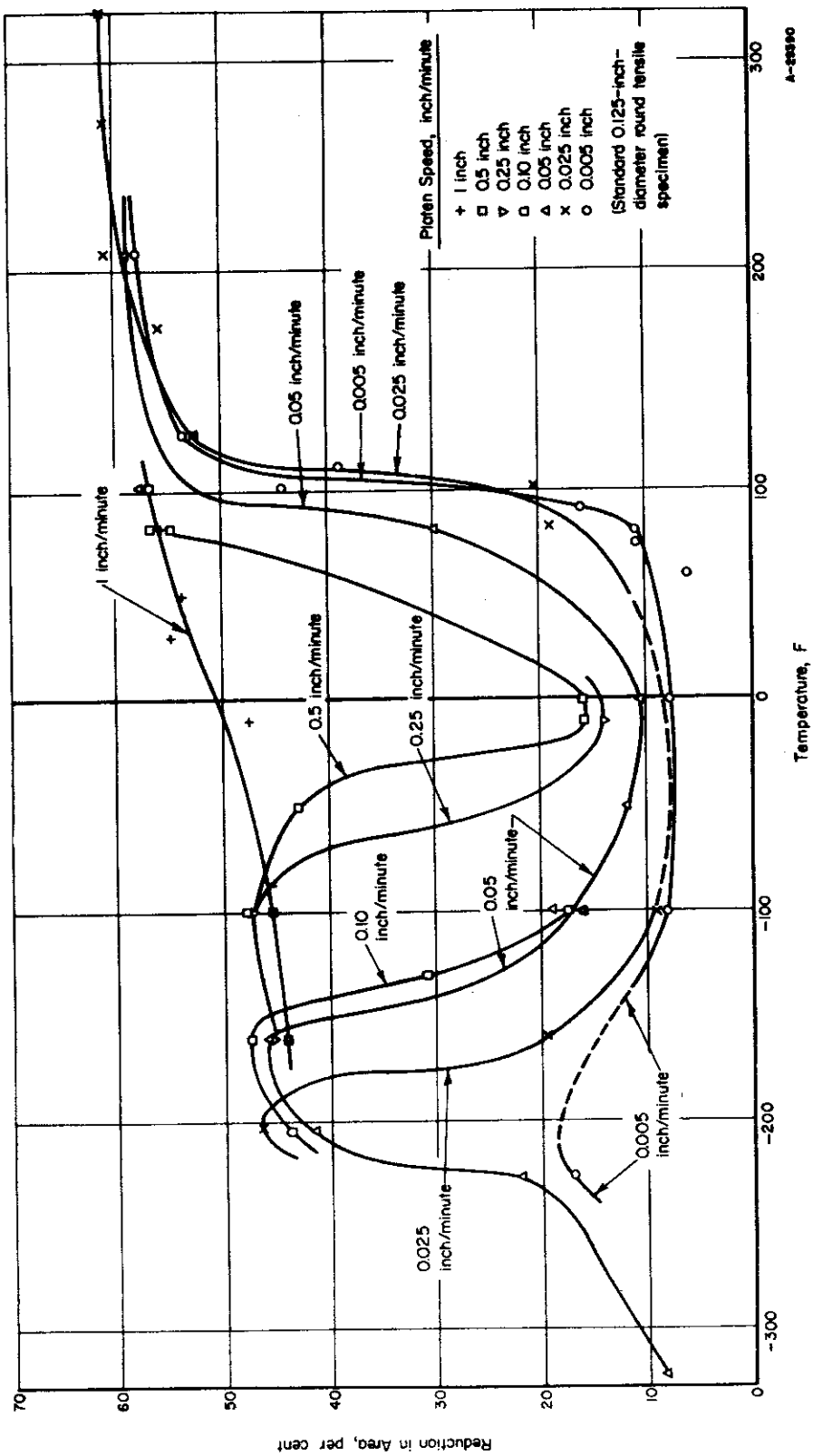

FIGURE 4. EFFECT OF TESTING SPEED AND TEMPERATURE ON THE TENSILE DUCTILITY OF Ti-2Fe-2Cr-2Mo CONTAINING 375 PPM HYDROGEN

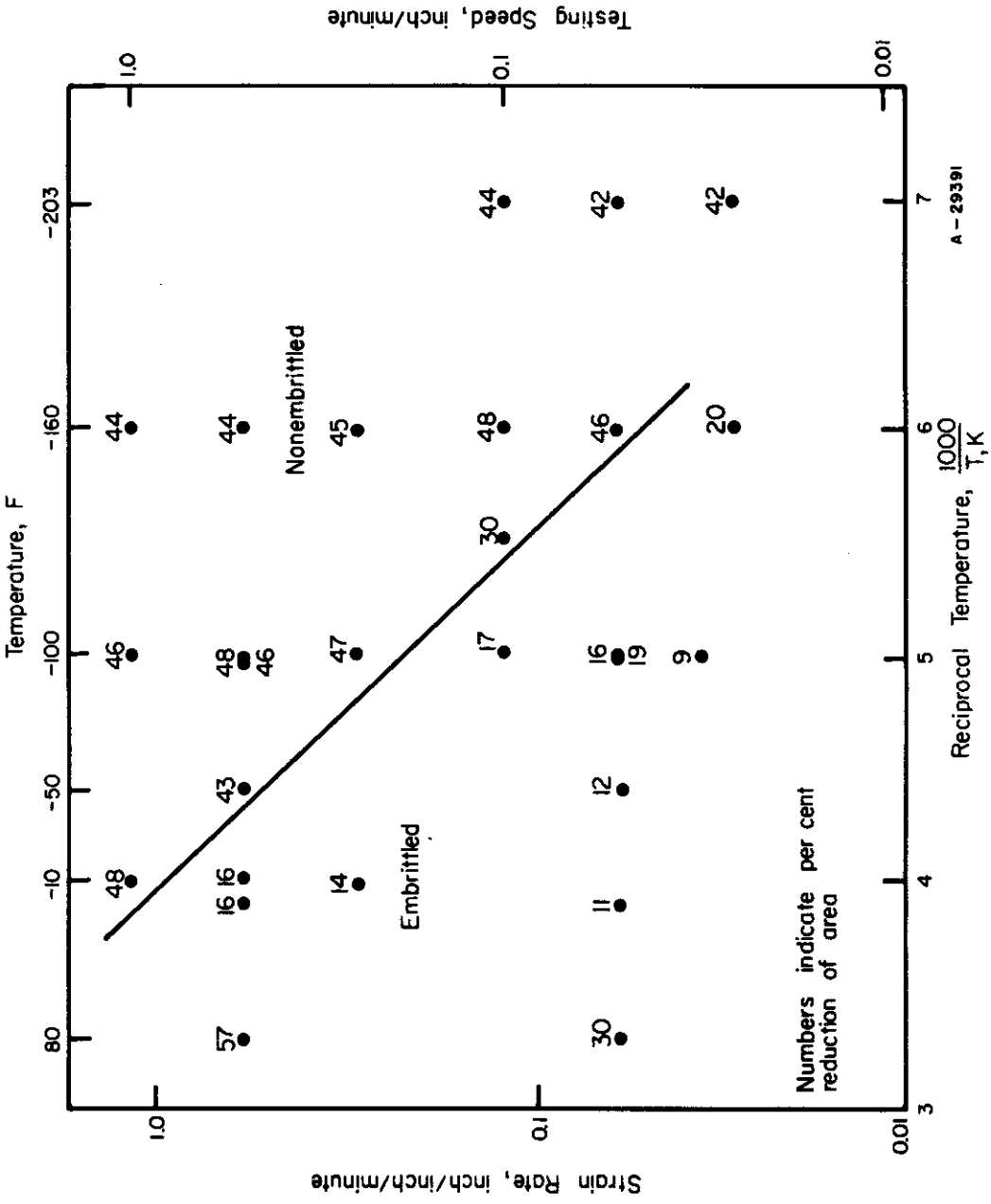

FIGURE 5. ACTIVATION-ENERGY PLOT FOR THE 375-PPM-HYDROGEN LEVEL

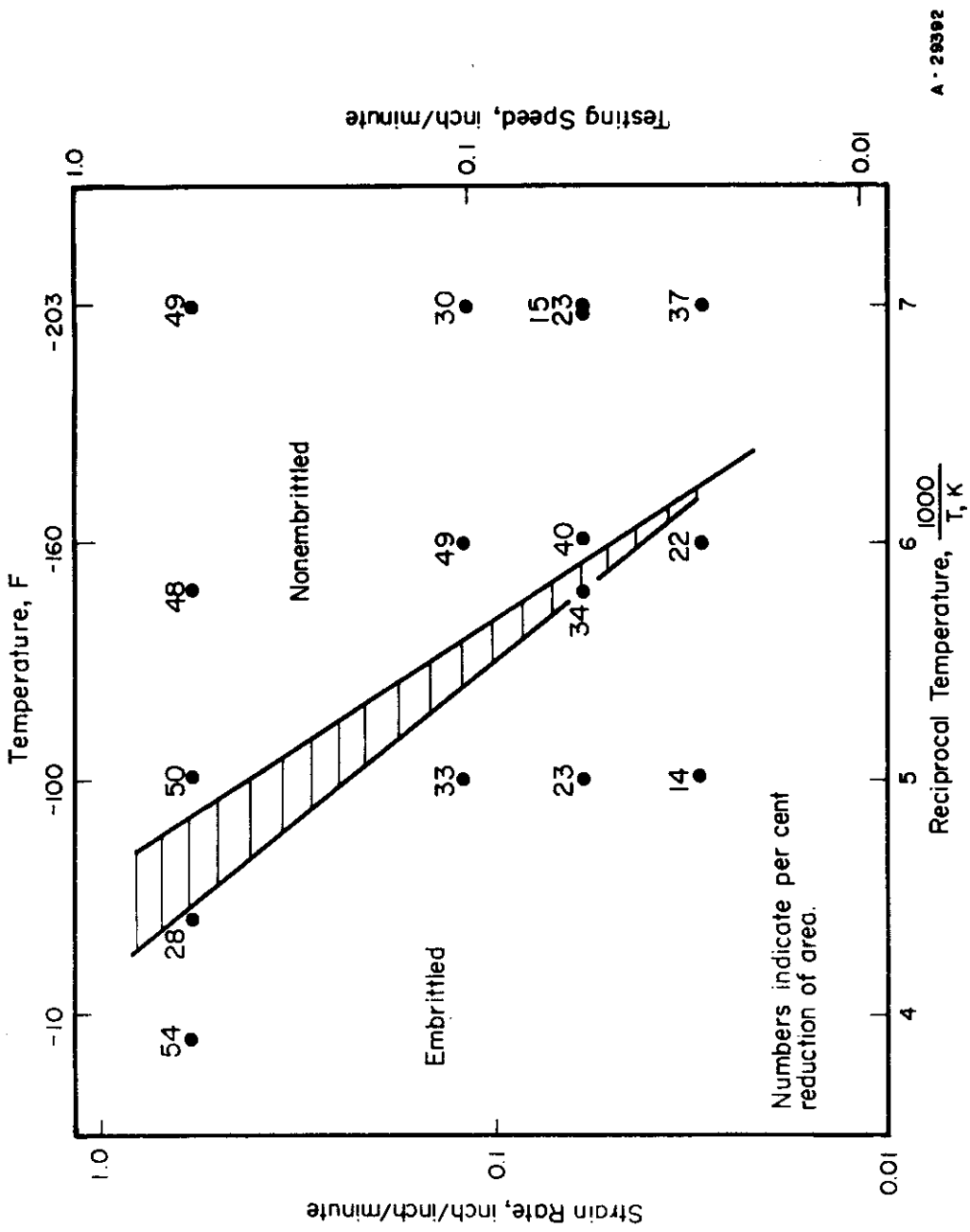

FIGURE 6. ACTIVATION-ENERGY PLOT FOR THE 250-PPM-HYDROGEN LEVEL, LOT A

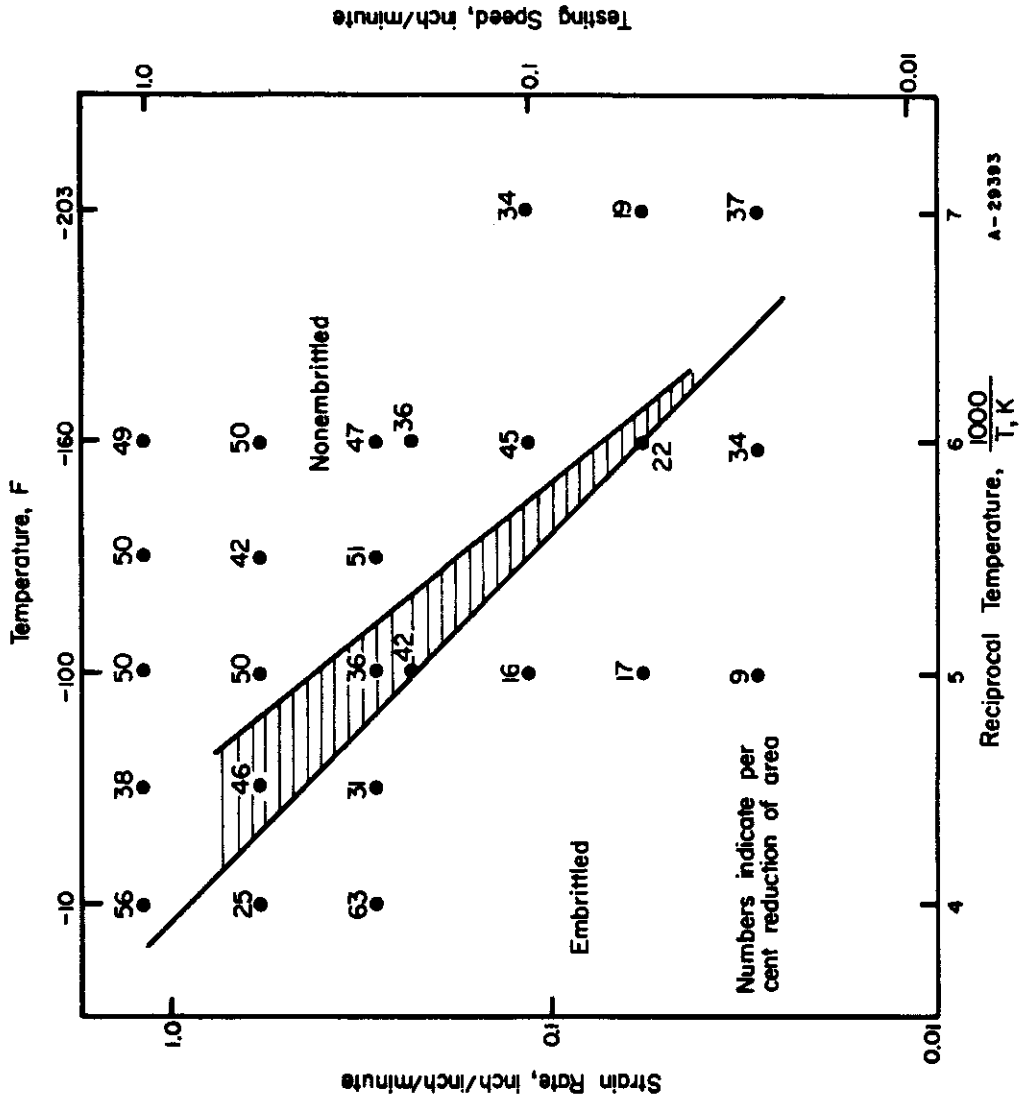

FIGURE 7. ACTIVATION-ENERGY PLOT FOR THE 250-PPM-HYDROGEN LEVEL, LOT B

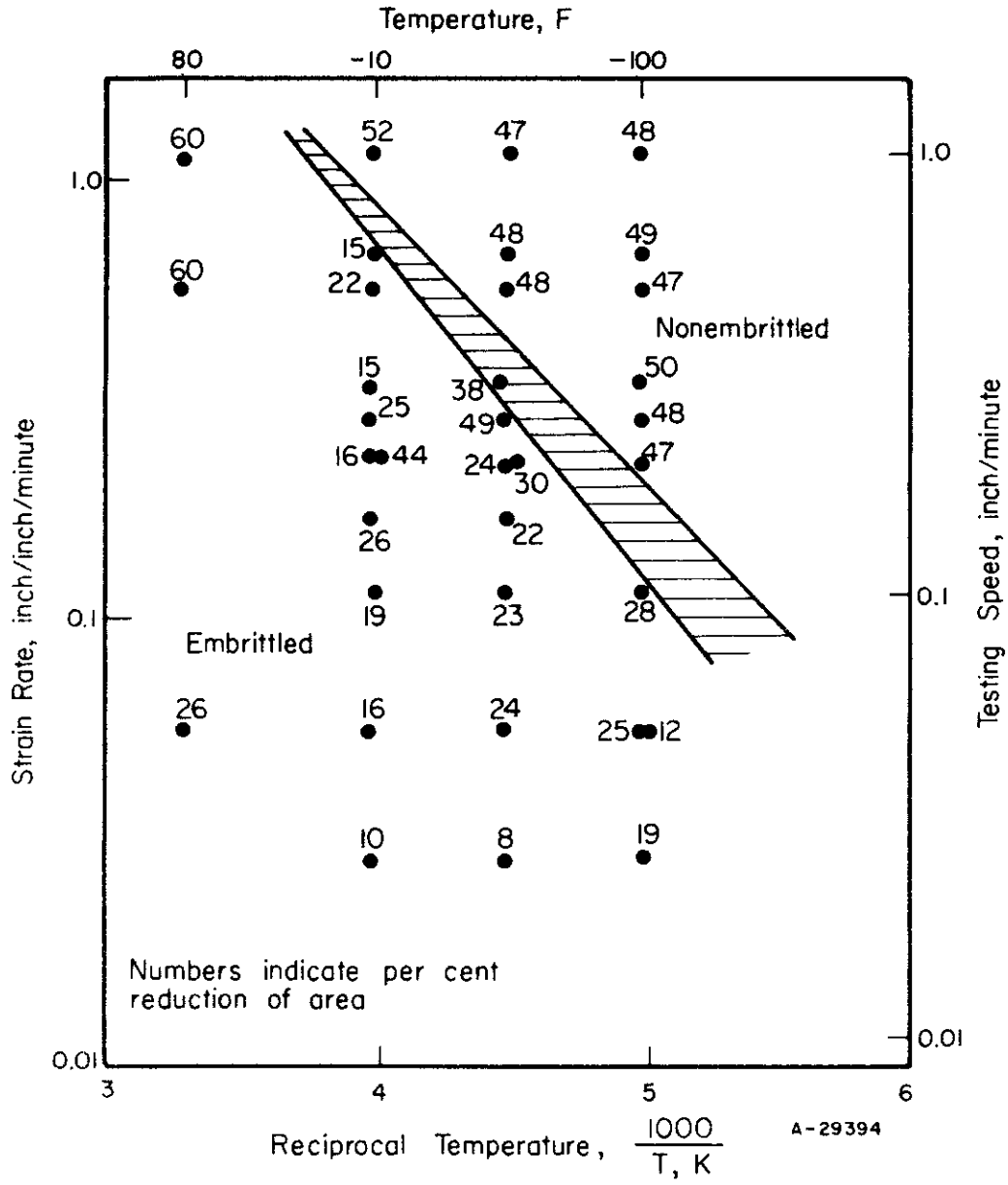

FIGURE 8. ACTIVATION-ENERGY PLOT FOR THE 500-PPM-HYDROGEN LEVEL

on a graph of reciprocal temperature versus logarithm of strain rate. It is seen that a straight line may be conveniently drawn separating embrittled from nonembrittled material. The slope of this line is equal to -Q/R [see Equation (5), page 4]. From Figure 5, an activation energy of 3000 cal/mole is obtained.

Tests at the 250-ppm hydrogen level were performed on specimens prepared from rods hydrogenated at different times (designated Lots A and B). Reduction-in-area measurements for both lots showed maximum embrittlement occurring above -50 F. Recovery of ductility occurred over the temperature range -50 F to -150 F. At approximately -200 F, a sharp decrease in reduction of area was observed, probably due to a low temperature ductile-to-brittle transition. Plots of the data (logarithm of strain rate versus reciprocal of absolute temperature) give activation energies of 3400 to 4200 and 2700 to 3500 calories/mole for the recovery-temperature shift of the specimens from Lot A and B, respectively, as shown in Figures 6 and 7. No reason for the different behavior of the two lots of material was indicated by the results obtained.

Tests at the 500-ppm level suggest a minimum between room temperature and 0 F. Recovery for the 0.5-inch/minute speed occurs between -10 and -60 F, while only slight recovery is apparent for the 0.05-inch/minute speed at temperatures as low as -100 F. The activation-energy plot for this level gives a value of 2200 to 3500 calories/mole, as shown in Figure 8.

Only six specimens were available for testing at the 750 ppm level. Test conditions for these specimens were carefully selected on the basis of the data obtained at the other hydrogen levels. The activation-energy plot, Figure 9, for these tests gives a value of between 2300 and 2800 calories/mole.

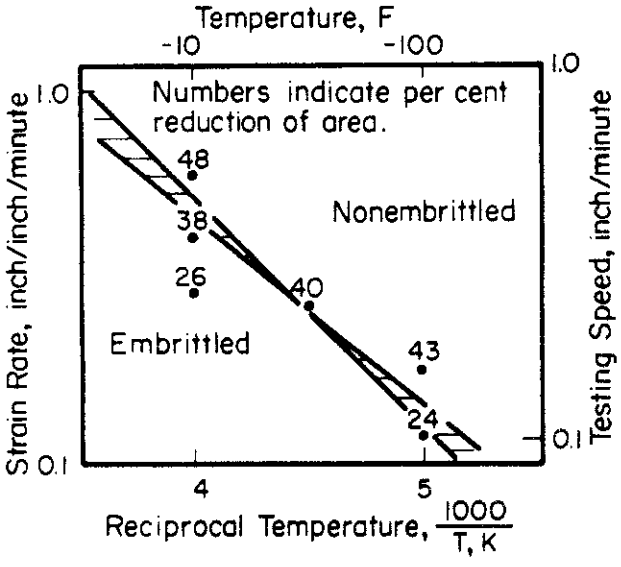

FIGURE 9. ACTIVATION-ENERGY PLOT FOR THE 750-PPM-HYDROGEN LEVEL

Activation energy values for the various hydrogen levels were as follows:

Hydrogen Content, ppm	Activation Energy, calories/mole
20	No embrittlement
250 (Lot A)	3400-4200
250 (Lot B)	2700-3500
375	3000
500	2200-3500
750	2300-2800

Complete test results are presented in Table 1.

It should be noted that although the activation-energy values were determined by plotting reduction of area, similar values of the activation energy can be obtained by using other embrittlement-sensitive parameters such as elongation at fracture or true fracture stress.

In addition to the graphical solutions presented, the data at the 375 ppm level were analyzed statistically by the Battelle Mathematical Physics Division.* As a result of this analysis the following linear equation was derived:

$$y = -683.0\ x + 3.431$$

where

x = reciprocal temperature (absolute)

y = logarithm of tensile-testing speed.

The constant -683.0 is equal to the slope of the line and represents $-\frac{Q}{2.303\ R}$. The activation energy determined by statistical means was therefore 3100 calories/mole, which agrees closely with the graphical solution of 3000 calories/mole.

These test data, which resulted in the determination of an average activation energy of 3100 calories/mole for five hydrogen test conditions, clearly confirm the first concept of the mechanistic picture, that the recovery of ductility is a rate-controlled process. Since embrittlement occurs only in the presence of hydrogen, it is probable that the rate-controlled process is one involving hydrogen. The second concept pictured

*Statistical analysis performed by A. E. Mace and G. Beatty.

TABLE I. EFFECT OF TEMPERATURE, TESTING SPEED, AND HYDROGEN CONTENT ON THE TENSILE PROPERTIES OF Ti-2Fe-2Cr-2Mo

Temperature, F	Testing Speed, inch/minute	Ultimate Tensile Strength, psi	True Stress at Fracture, psi	Reduction in Area, per cent	Test Time, seconds
		20 PPM Hydrogen			
80	0.5	146,000	254,000	56	23
80	0.05	146,000	263,000	57	243
80	0.005	142,000	238,000	56	3115
0	0.5	161,000	281,000	54	26
0	0.05	157,000	271,000	56	249
0	0.005	154,000	258,000	55	2555
-50	0.5	168,000	286,000	51	24
-50	0.05	166,000	266,000	50	238
-50	0.005	164,000	268,000	53	2100
-100	0.5	174,000	299,000	51	26
-100	0.05	175,000	234,000	28	250
-100	0.005	170,000	281,000	52	3062
-150	0.5	188,000	292,000	48	20
-150	0.05	192,000	305,000	49	244
-200	0.05	200,000	298,000	44	208
-320	0.05	250,000	338,000	30	118
		250 PPM Hydrogen (Lot A)			
0	0.5	167,000	287,000	54	28
-50	0.5	179,000	238,000	28	21
-100	0.5	192,000	302,000	50	26
-100	0.1	189,000	281,000	33	110
-100	0.05	186,000	230,000	23	75
-100	0.025	187,000	219,000	14	314
-150	0.5	205,000	306,000	48	21
-150	0.05	204,000	276,000	34	211
-160	0.1	212,000	316,000	49	90
-160	0.05	204,000	299,000	46	189
-160	0.025	203,000	253,000	22	333
-175	0.05	212,000	282,000	34	192
-200	0.5	222,000	324,000	49	21
-200	0.05	221,000	276,000	23	162
-203	0.1	221,000	284,000	30	50
-203	0.05	218,000	252,000	15	162
-203	0.025	220,000	299,000	37	229
-225	0.5	228,000	289,000	36	16
		250 PPM Hydrogen (Lot B)			
-10	1.0	162,000	316,000	56	19
-10	0.5	165,000	215,000	25	28
-10	0.25	165,000	302,000	63	48
-25	0.005	158,000	--	8	1125
-60	1.0	175,000	261,000	38	15
-60	0.5	172,000	285,000	46	32
-60	0.25	171,000	235,000	31	60
-100	1.0	180,000	287,000	50	15
-100	0.5	183,000	265,000	50	25
-100	0.25	181,000	251,000	36	43
-100	0.2	180,000	282,000	42	63
-100	0.1	180,000	211,000	17	115

TABLE 1. (Continued)

Temperature, F	Testing Speed, inch/ minute	Ultimate Tensile Strength, psi	True Stress at Fracture, psi	Reduction in Area, per cent	Test Time, seconds
		250 PPM Hydrogen (Lot B) (Continued)			
-100	0.05	181,000	216,000	17	169
-100	0.025	178,000	189,000	9	312
-130	1.0	179,000	321,000	50	11
-130	0.5	181,000	313,000	42	21
-130	0.25	185,000	313,000	51	43
-160	1.0	201,000	187,000	49	9
-160	0.5	200,000	296,000	50	20
-160	0.25	202,000	300,000	47	38
-160	0.2	200,000	273,000	36	36
-160	0.1	193,000	296,000	45	173
-160	0.05	192,000	216,000	25	220
-160	0.025	201,000	282,000	34	470
-203	0.1	202,000	279,000	34	80
-203	0.05	209,000	252,000	19	188
-203	0.025	213,000	285,000	37	185
		375 PPM Hydrogen			
80	1.0	146,000	--	56	15
80	0.5	147,000	244,000	57	23
80	0.5	147,000	--	55	--
80	0.05	147,000	199,000	30	240
80	0.025	148,000	--	19	326
80	0.005	144,000	--	11	--
50	1.0	156,000	--	54	11
32	1.0	154,000	--	55	10
0	0.5	166,000	196,000	16	17
0	0.05	162,000	181,000	11	115
0	0.005	154,000	166,000	8	820
-10	1.0	168,000	282,000	48	15
-10	0.5	169,000	201,000	16	21
-10	0.25	166,000	193,000	14	37
-50	0.5	176,000	273,000	43	23
-50	0.05	173,000	194,000	12	105
-100	1.0	188,000	305,000	46	10
-100	0.5	189,000	294,000	48	19
-100	0.5	187,000	297,000	46	24
-100	0.25	187,000	295,000	47	43
-100	0.1	185,000	219,000	17	113
-100	0.05	184,000	218,000	19	120
-100	0.05	184,000	198,000	16	205
-100	0.025	184,000	203,000	9	270
-100	0.005	--	--	8	855
-130	0.1	196,000	259,000	30	108
-160	1.0	204,000	294,000	44	9
-160	0.5	212,000	302,000	44	16
-160	0.25	208,000	297,000	45	32
-160	0.1	203,000	308,000	47	107
-160	0.05	204,000	302,000	46	203
-160	0.025	201,000	247,000	20	420
-203	0.1	223,000	315,000	44	96
-203	0.05	219,000	--	42	108
-203	0.025	219,000	332,000	47	426
-225	0.5	222,000	313,000	22	183
-225	0.005	218,000	259,000	17	1512
-320	0.05	269,000	293,000	8	80

TABLE 1. (Continued)

Temperature, F	Testing Speed, inch/ minute	Ultimate Tensile Strength, psi	True Stress at Fracture, psi	Reduction in Area, per cent	Test Time, seconds
		500 PPM Hydrogen			
80	1.0	143,000	271,000	60	12
80	0.5	145,000	266,000	60	25
80	0.05	144,000	187,000	26	231
80	0.005	142,000	159,000	12	1067
25	0.05	148,000	169,000	11	177
-10	1.0	161,000	295,000	52	12
-10	0.6	163,000	190,000	15	21
-10	0.5	163,000	197,000	22	25
-10	0.3	160,000	189,000	15	42
-10	0.25	164,000	213,000	26	41
-10	0.2	165,000	195,000	16	--
-10	0.2	159,000	253,000	44	60
-10	0.15	164,000	216,000	28	62
-10	0.1	165,000	189,000	14	89
-10	0.05	157,000	186,000	16	127
-10	0.025	155,000	172,000	10	313
-10	0.005	155,000	164,000	7	484
-60	1.0	168,000	289,000	47	12
-60	0.6	169,000	282,000	48	17
-60	0.5	173,000	279,000	48	27
-60	0.3	174,000	251,000	38	35
-60	0.25	169,000	281,000	49	40
-60	0.2	172,000	221,000	24	--
-60	0.2	171,000	212,000	20	43
-60	0.15	172,000	216,000	22	52
-60	0.1	171,000	214,000	23	91
-60	0.05	167,000	213,000	24	149
-60	0.025	166,000	180,000	8	332
-100	1.0	167,000	311,000	48	9
-100	0.6	186,000	278,000	49	19
-100	0.5	180,000	296,000	47	23
-100	0.3	183,000	288,000	50	39
-100	0.25	182,000	301,000	48	27
-100	0.2	182,000	292,000	48	43
-100	0.15	181,000	275,000	17	63
-100	0.1	182,000	240,000	28	109
-100	0.05	176,000	196,000	12	139
-100	0.05	179,000	231,000	25	178
-100	0.025	178,000	218,000	19	297
		750 PPM Hydrogen			
-10	0.5	166,000	275,000	48	25
-10	0.35	171,000	250,000	38	32
-10	0.25	168,000	215,000	26	52
-60	0.225	179,000	270,000	40	53
-100	0.15	188,000	285,000	43	72
-100	0.1	193,000	241,000	24	78

in the initially proposed mechanism stated that the rate-controlling step was the diffusion of hydrogen in the beta phase. The values of the experimentally determined data strongly indicate that this was a correct assumption. The value of approximately 3000 calories/mole is of the same order of magnitude as the activation energy for diffusion of hydrogen in the beta phase of unalloyed titanium at high temperatures, 6600 calories/mole.[1]*

In considering explanations to account for the lower value of the activation energy obtained by the experimental procedure described in this section, several possibilities become apparent. The first of these, and possibly the most significant, is the fact that the value of the activation energy reported by Wasilewshi and Kehl[1] was obtained at elevated temperature (>1620 F) and for unalloyed beta. It is very probable that the activation energy for diffusion of hydrogen does not remain constant over such a large range of temperature. Furthermore, alloying can be expected to alter the diffusivity. Although the value of 6000 calories per mole reported for Ti-8Mn[2] suggests that the activation energy is not altered by alloying or over large magnitudes of temperature change, it should be noted that this value is subject to some doubt and may well be lower than the reported energy due to shortcomings of the experimental technique.

Plastic deformation could lower the activation energy for diffusion of hydrogen in beta titanium. Numerous references can be found in the literature to show that plastic strain decreases the activation energy for various substitutional diffusion processes. No specific information regarding the effect of plastic strain on interstitial diffusion has been discovered in a literature search, but it is not unreasonable to expect that a lowering of the activation energy would occur.

Another possible explanation to account for a low value may be associated with grain-boundary diffusion. Hydrogen already present at the alpha-beta interface could diffuse to the area of high stress in the direction of applied stress and contribute hydrogen or precipitate as hydride and therefore decrease the amount of hydrogen necessary from the bulk-phase diffusion. The value of the activation energy for grain-boundary diffusion is generally lower by a factor of 1/2 to 1/3 than the energy for bulk diffusion and could lower the total observed activation energy.

Other explanations include the accuracy of the experimental technique and possible oversimplifications in the original model. It is very difficult to evaluate the former. By comparison, an investigation of the hydrogen embrittlement of SAE 1020 steel[3] shows an experimentally determined activation energy of 5000 to 6000 calories/mole, which is about twice the value for diffusion of hydrogen in α-iron, 2900 to 3050 calories/mole.[4,5] This may suggest that the method is subject to considerable experimental error.

*Reference list is at end of report.

Of the several explanations proposed to account for the apparent low energy value, the first and second appear quite probable, while the third, which would act in the correct direction, is probably of minor significance. The last two explanations could shift the energy in either direction. Collectively, the above possibilities could easily explain the difference between the 3000 calories/mole obtained by the tensile-test technique and the 6000 calories/mole obtained by degassing and internal-friction tests.

During the examination of the test data it was discovered that an activation energy could be obtained by at least two other methods of handling the test data, other than the criticality between dislocation velocity and hydrogen velocity initially proposed. These methods are described briefly below.

Stress-Dependent Diffusion

Failure occurs during tensile testing when the applied stress equals the fracture stress of the material. If the fracture stress of the alloy is assumed to decrease linearly with increased hydrogen accumulation or hydride precipitation, it would be possible to express the concentration of hydride in terms of the fracture stress. That is,

$$\sigma_f = \sigma_o - A[H] ,$$

where

σ_f is the measured true fracture stress

$[H]$ is the concentration of hydride precipitate (or of hydrogen segregated at the interface)

A is an arbitrary constant

σ_o is the true fracture stress of unembrittled material.

At the same time, the reaction time can be expressed in terms of the time to failure, such that $[H] = f(t)$, where t is the time to failure in the tensile test. This reasoning necessarily assumes the reaction will not proceed in the absence of stress but it does not require an assumption of dislocation-directed diffusion and can be handled by convention chemical kinetic methods. Moreover, all of the data can be applied to a solution instead of just those data at the critical point. It should also be noted that strain rate is of importance only by its inverse relationship with time.

A plot of measured fracture stress (which correlates with hydrogen concentration) versus time to failure for data of three temperatures is

shown for the material containing 375 ppm hydrogen in Figure 10. The per cent retained fracture stress is defined as

$$\frac{\text{fracture stress of sample in question, } \sigma_f}{\text{fracture stress of unembrittled samples, } \sigma_o} \times 100.$$

The fracture stress of unembrittled samples was obtained from tests at a high strain rate. When no hydride is present, the per cent retained fracture stress is equal to 100. As increasing amounts of hydride are formed (time in test increases), it decreases gradually to a minimum of about 60, as shown in Figure 10. Since time can be assumed inversely proportional to the rate constant, k, when concentration (fracture-stress ratio) is held constant,

$$\frac{1}{t} \sim k = Ae^{-Q/RT} \Big] \frac{\sigma_f}{\sigma_o} = \text{constant}$$

A plot of log $\left(\frac{1}{\text{time}}\right)$ versus reciprocal absolute temperature should permit an activation energy to be determined. As shown in Figure 11, a value of 3200 calories/mole is obtained using these assumptions.

Critical Nucleation Stress

The previously described method is similar to the originally proposed mechanism in that it was assumed the diffusion will occur only when the material is under stress, even though no attempt was made to relate diffusion directly to dislocation velocity. The present method assumes that diffusion occurs freely, but that hydrogen precipitation cannot start until nucleation is forced to occur. The onset of nucleation is then assumed dependent upon the development in the sample of a critical stress sufficient to trigger nucleation. That is, the function of strain is not to accelerate growth of hydride but rather to develop a stress state sufficient to induce nucleation. Once nucleation occurs, hydride grows according to normal reaction kinetics, and embrittlement follows as soon as a finite amount of hydride is formed. As in the previous case, the apparent dependence of embrittlement on strain rate is assumed to represent instead a dependence on time (reciprocal strain rate). In the present mathematical treatment, the fracture stress is assumed relatively independent of amount of hydride formed, and ductility is assumed dependent only upon the stress which the sample must reach before nucleation occurs and upon the time required to grow an embrittling amount of hydride from the nuclei. On the basis of these assumptions, a strain equation may be written for the tensile data obtained in this study:

$$\dot{\epsilon}_n + t\dot{\epsilon} = \dot{\epsilon}_f \quad , \qquad (6)$$

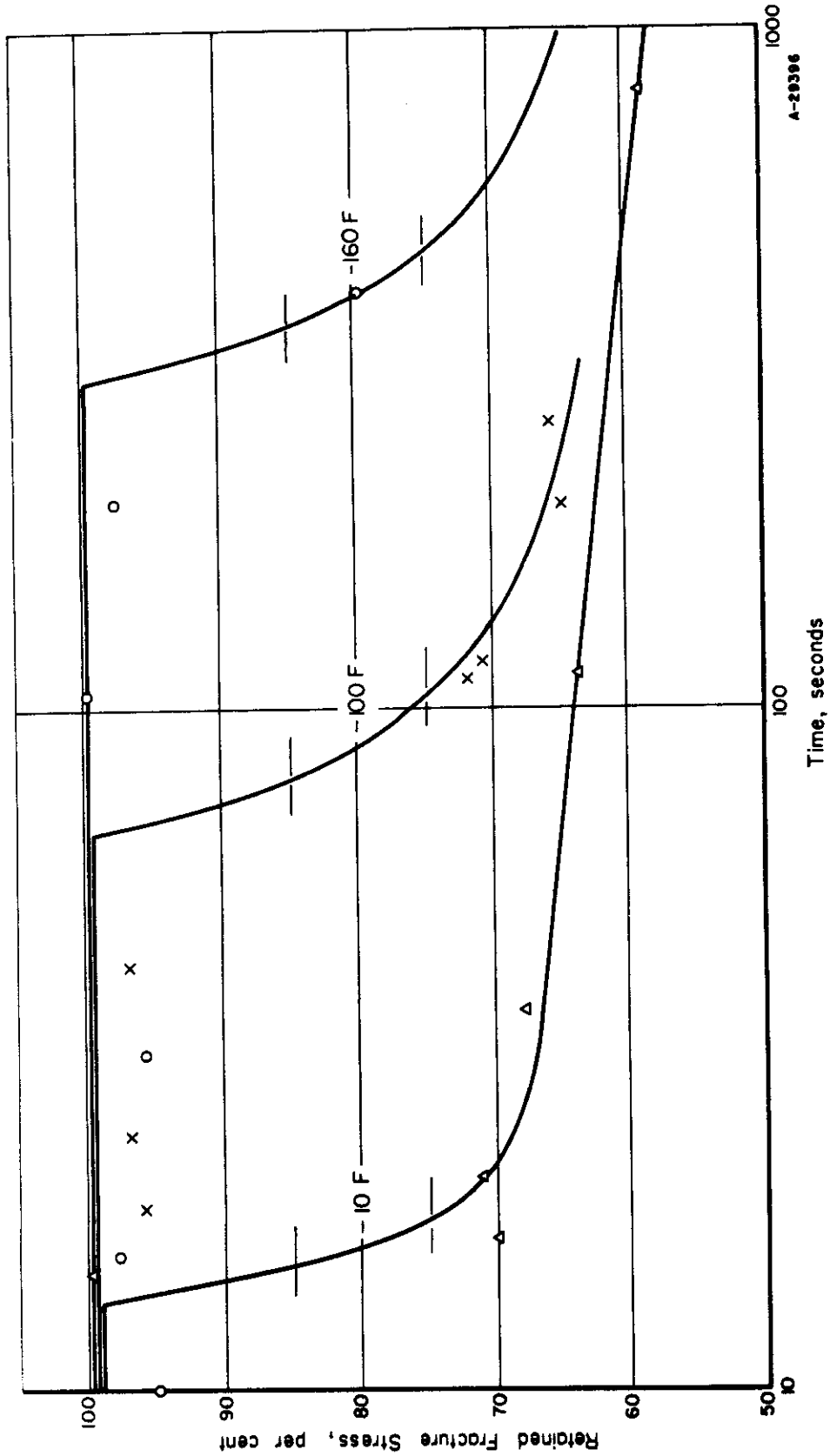

FIGURE 10. PLOT OF PER CENT RETAINED FRACTURE STRESS VERSUS LOG TIME FOR MATERIAL CONTAINING 375 PPM HYDROGEN

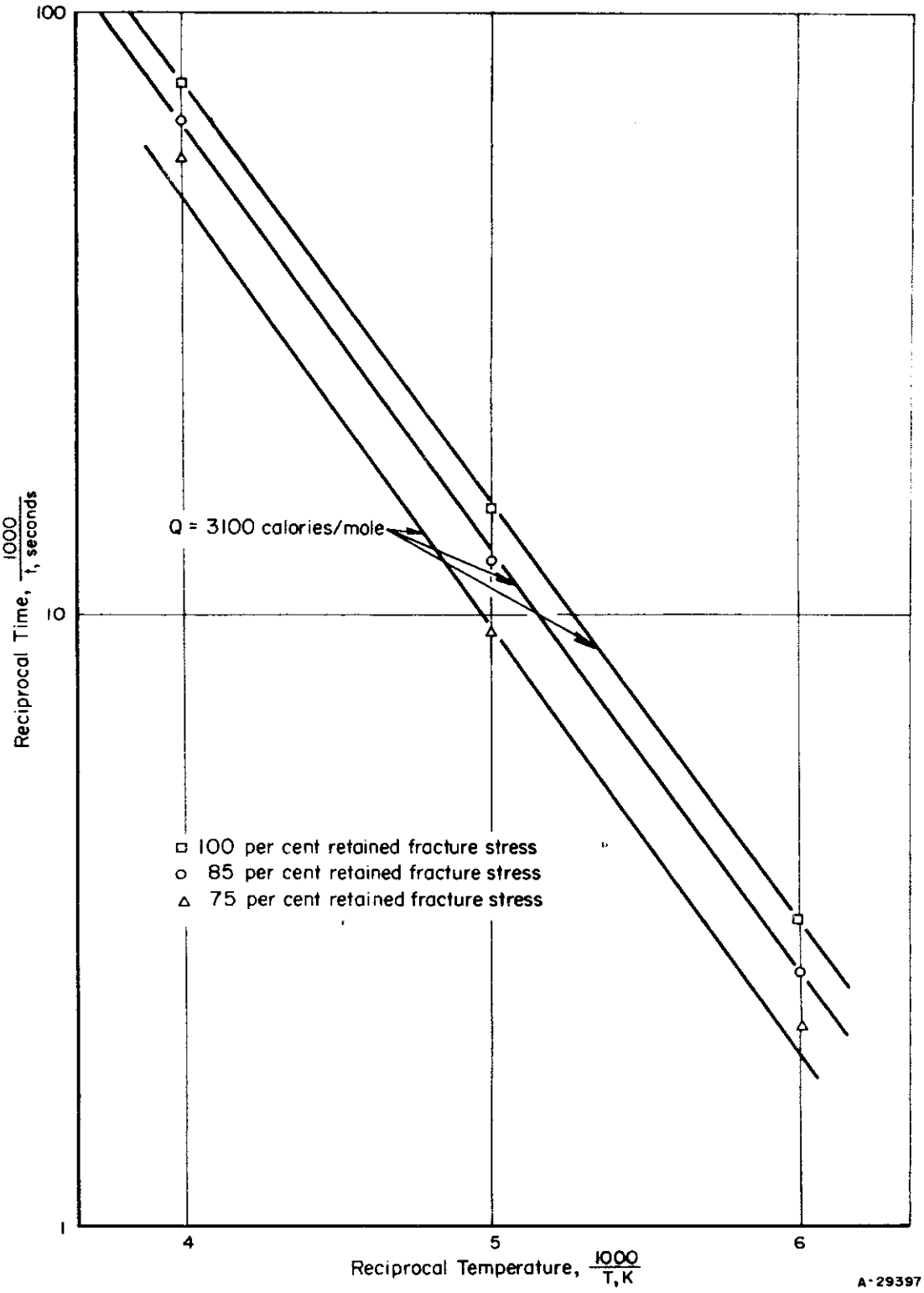

FIGURE 11. ACTIVATION-ENERGY PLOT FOR THE 375-PPM-HYDROGEN LEVEL (RETAINED FRACTURE STRESS)

where

ϵ_n is the total strain which must be applied before nucleation occurs. (Nucleation is assumed to require the attainment in the sample of a fixed value of stress. To reach this critical stress, appreciable plastic strain, with accompanying work hardening, may be required. This value of stress, within a limited temperature and strain-rate range, can be represented equally well by a strain value.)

t is the time necessary to precipitate an embrittling amount of hydride (a function of temperature and hydrogen concentration) upon the stress-induced nuclei.

$\dot{\epsilon}$ is the strain rate. Multiplying the strain rate by the reaction time will give the strain imposed on the sample while hydride growth is occurring.

ϵ_f is the strain at fracture.

This equation was applied to the test data at the 375-ppm-hydrogen level. In the absence of necking, σ_f should equal the total time in test multiplied by strain rate. All data in which the measured total strain $\left(\ln \frac{Ao}{A}\right)$ did not agree within 25 per cent of the calculated total strain (total time in test multiplied by strain rate) were eliminated from consideration.* The remaining data were examined using measured values of $\dot{\epsilon}$ and ϵ_f. At only three temperatures (0 F, -10 F, and -100 F) could independent solutions be obtained. At -160 F and -225 F only one suitable test point was available, so values for ϵ_n were assumed, based on calculated values of ϵ_n at 0 F, -10 F, and -100 F to estimate a reaction time. A plot of the reciprocal of the calculated reaction time, t, versus 1/T** permitted an activation energy to be determined as shown in Figure 12. The slope of the line in this figure is equivalent to an activation energy of 3500 calories/mole.

The calculated value of ϵ_n varied from 9.6 to 11.4 per cent, which would indicate the nucleating stress of the material considered was quite close to the ultimate strength of the alloy when tested at conventional strain rates.

*The reason for selecting the data in this manner was as follows: In the equation $\epsilon_f = \epsilon_n + t\dot{\epsilon}$, the only measurable quantities were ϵ_f and $\dot{\epsilon}$. Neither was known with a high degree of accuracy. A third easily measured factor was known, the total time consumed in the test, t_o. ϵ_f should equal $t_o \times \dot{\epsilon}$ if all factors were measured accurately, and a deviation from this equality indicated an error in measurement. Generally, samples showing necking were eliminated from consideration by applying this criterion. This is not unexpected since loading rates, not strain rates, were controlled during testing.

**Since the embrittling amount of hydride was assumed independent of stress, the previously expressed proportionally between rate constant, k, and reciprocal time could be used. Use of this relationship carries with it the implication that a constant amount of hydride is necessary to cause embrittlement regardless of temperature or stress at which embrittlement is observed.

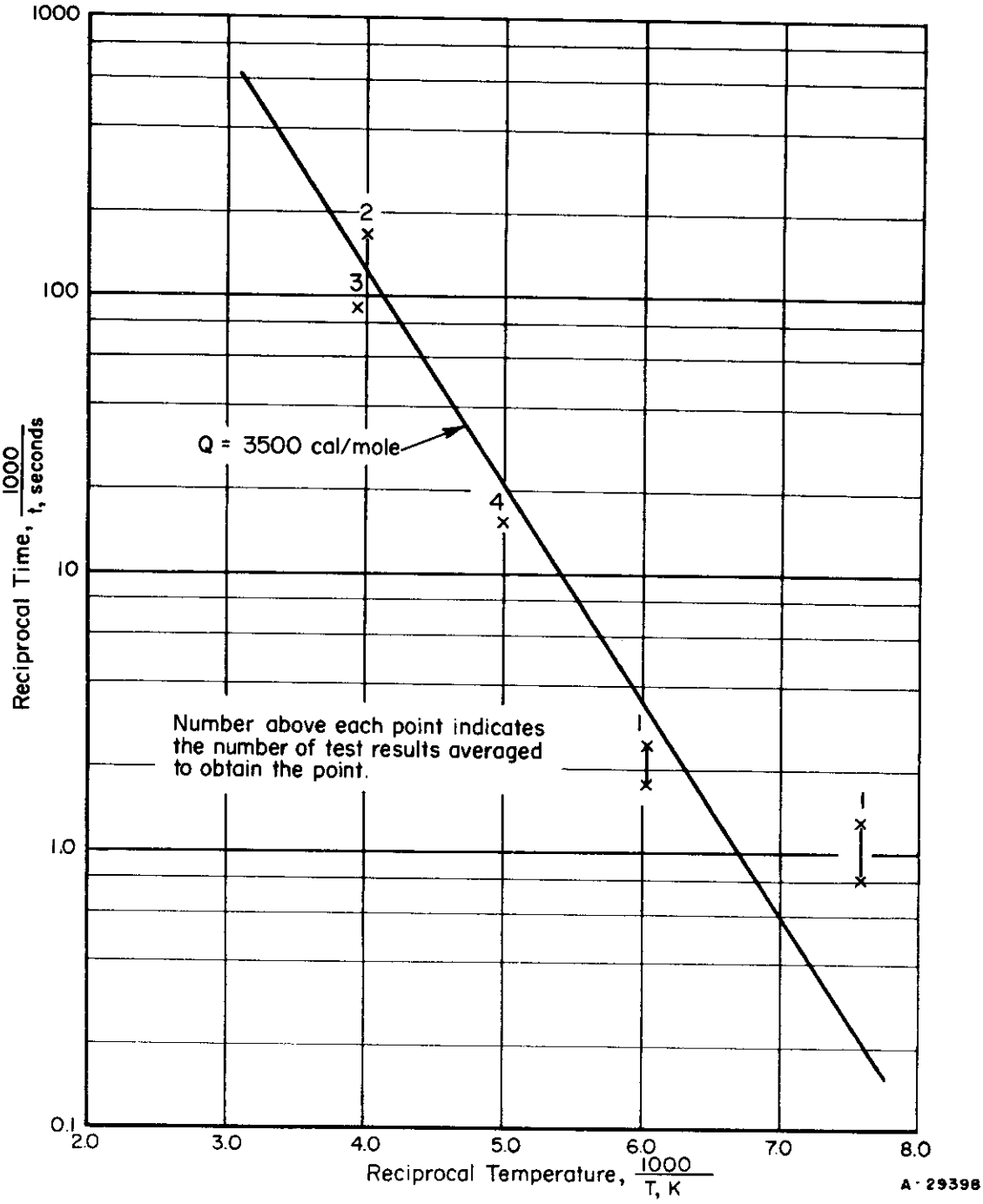

FIGURE 12. DETERMINATION OF ACTIVATION ENERGY BY USING THE CONCEPT OF A CRITICAL NUCLEATION STRESS

Loss of Ductility Near Room Temperature

Low-strain-rate embrittlement in hydrogen-containing alpha-beta alloys is not observed at temperatures slightly in excess of room temperature but becomes quite pronounced as the temperature is lowered to or slightly below room temperature. The reason for the sudden loss of ductility near room temperature has not been satisfactorily explained. Ductility minima of the type observed in the hydrogen-containing titanium alloys are occasionally related to dislocation-locking mechanisms. However, in this type of process, the maximum temperature at which embrittlement is observed generally increases as strain rate increases, while a tendency for the opposite effect to occur is observed in hydrogen-induced low-strain-rate embrittlement, as shown in Figure 4.

Another possible explanation for an abrupt loss of ductility near room temperature would be a change in the solubility of hydrogen with temperature such that hydrogen solubility decreases rapidly at temperatures approaching room temperature. Inherent in this theory is the assumption that low-strain-rate embrittlement is due to the precipitation of hydride or the formation of hydrogen clusters under strain from a super-saturated solid solution of hydrogen in titanium. That is, the alloy is assumed to exist in a nonequilibrium state before embrittlement such that a tendency toward hydride precipitation exists. This process would be expected to result in a shift in the maximum temperature of embrittlement to lower temperatures as strain rate increased, since the faster the strain rate the less time is allowed for hydrogen segregation and precipitation. Thus, more hydrogen would be required to cause embrittlement, which would be made available only by lowering the temperature (and the equilibrium solubility).

As shown in Figure 4, a very abrupt loss of ductility occurred in Ti-2Fe-2Cr-2Mo tested at a platen speed of 0.005 inch/minute. This permitted the selection of the maximum temperature of embrittlement at this strain rate with a high degree of precision and provided a means of checking the feasibility of a theory based on solubility changes by setting up an equation to express the hydrogen distribution in the alloy at the maximum temperature of embrittlement:

$$f_a H_a + f_b H_b + H_e = H_t \ , \qquad (7)$$

where

H_a is the equilibrium hydrogen solubility in alpha at the maximum temperature of embrittlement

H_b is the equilibrium hydrogen solubility in beta at the maximum temperature of embrittlement

H_e is the hydrogen in excess of soluble amount just sufficient to cause embrittlement

H_t is the total hydrogen content of the alloy

f_a and f_b are the fractional parts of alpha and beta in the alloy.

Both H_a and H_b were assumed strongly temperature dependent, and the hydrogen solubility was expressed as a function of temperature by means of the following equation:

$$H = A\ 10^{B/T} \tag{8}$$

where H is the hydrogen content in atomic per cent, A and B are constants, and T is the temperature in degrees Rankine. Within the range of hydrogen contents of interest, less than 10 atomic per cent, only a slight error is involved in expressing the hydrogen contents in weight rather than atomic per cent, so, for convenience, hydrogen contents were expressed in parts per million. The above equation was used only to express the solubility of hydrogen in beta titanium. It was assumed that the solubility of hydrogen in the alpha phase of Ti-2Fe-2Cr-2Mo would not differ significantly from that in unalloyed titanium, and the variation of hydrogen solubility in alpha was determined directly from published experimental results[6,7,8] for unalloyed alpha titanium. A solubility curve of hydrogen in alpha titanium based on these data is given in Figure 13.

The manner in which H_e varies with temperature cannot be predicted, although it seems likely that less hydride, and therefore less excess hydrogen, would be required to cause embrittlement as temperature decreased. However, in the present examinations, H_e was assumed independent of temperature.

Equation (7) was expanded by replacing H_b with the value of H given in Equation (8):

$$f_a H_a + f_b \times A\ 10^{B/T} + H_e = H_t\ . \tag{9}$$

For each hydrogen content (H_t) the maximum temperature of embrittlement (T), the hydrogen solubility of alpha (H_a), and the fractions by weight of alpha and beta (f_a and f_b) can be measured. Thus, measurements at three different hydrogen levels would permit calculation of the three unknown factors, A, B, and H_e, that is, the beta/hydride + beta solvus line and the minimum hydrogen content in excess of the soluble amount necessary to result in embrittlement. Testing speed was held constant at 0.005 inch/minute throughout these studies.

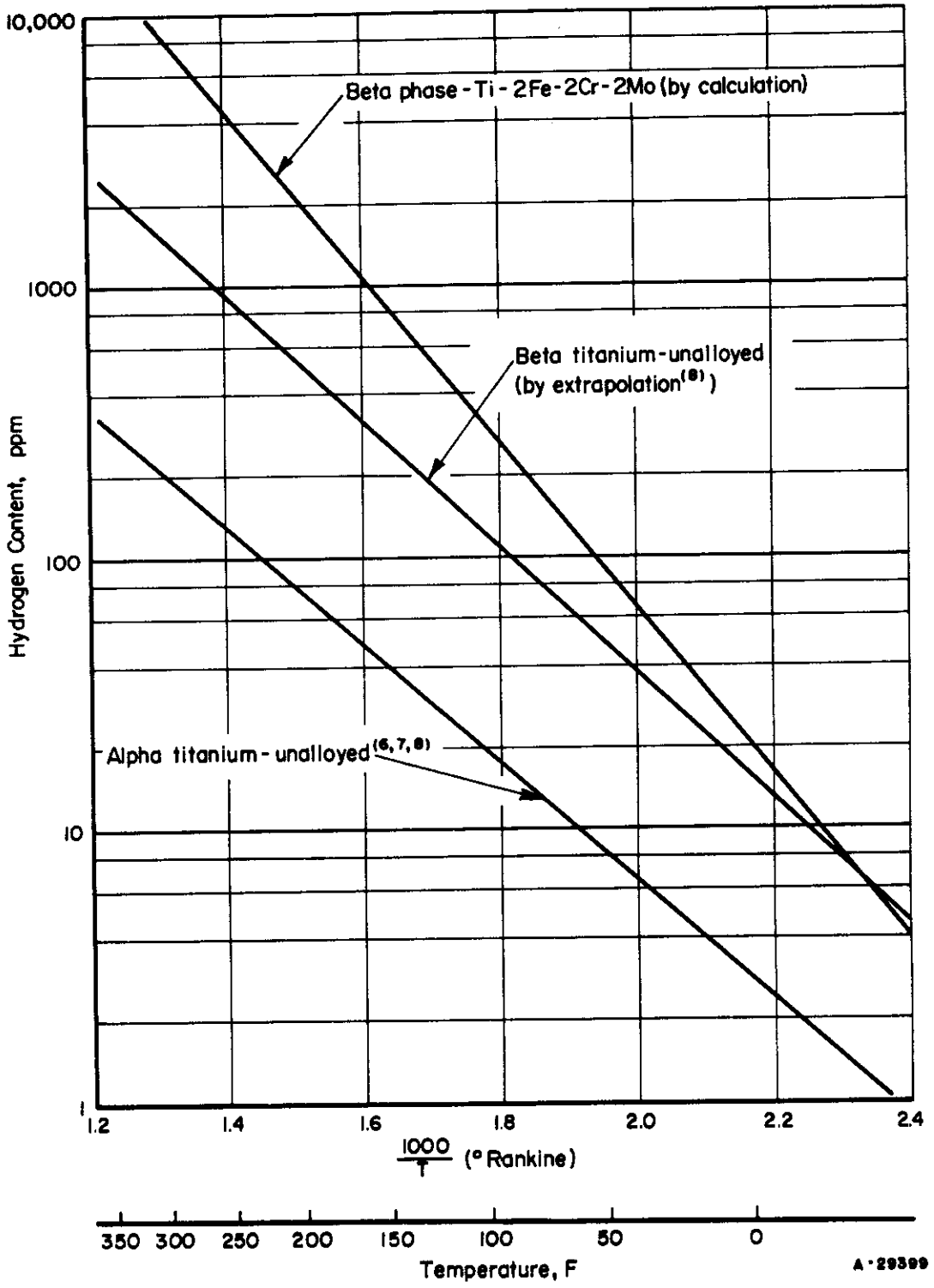

FIGURE 13. EFFECT OF TEMPERATURE ON THE SOLUBILITY OF HYDROGEN IN TITANIUM

Ti-2Fe-2Cr-2Mo material was prepared containing 20, 250, 375, and 750 ppm hydrogen. Hydrogenation and stabilization treatments were performed as described in the previous section on low-temperature recovery of ductility. The hydrogenated alloys all showed a fine equiaxed alpha-beta structure. The tensile properties of these samples were determined over a range of temperatures and are given in Table 2. Figure 14 is a graphical presentation of the reduction in area data. From this figure, the maximum temperature of embrittlement is seen to be:

Hydrogen Content, ppm	Max Temp of Embrittlement F	Rankine
20	None	None
250	68	528
375	116	576
750	172	632

The volume fraction of alpha and beta in the alloys was determined by the lineal-intercept method, with the following results:

Hydrogen Content, ppm	Volume Per Cent Alpha	Volume Per Cent Beta
250	71.4	28.6
375	64.1	35.9
750	60.0	40.0

Since the density of Ti-2Fe-2Cr-2Mo is 0.169 lb/in.^{3} as compared with 0.163 for unalloyed titanium, it is apparent that the beta phase in the alloy is more dense than the alpha phase. Using an approximate density for beta of 0.180 lb/in.^{3} (based on an alpha-beta ratio of 65:35), the above values were converted to weight fractions of alpha and beta, as follows:

Hydrogen Content, ppm	f_a	f_b
250	0.69	0.31
375	0.62	0.38
750	0.58	0.42

From these data, by substitution of the appropriate experimental values into Equation (9), three equations were obtained:

$$7 \text{ ppm} + 0.31A\ 10^{B/528} + H_e = 250 \text{ ppm}$$

$$15 \text{ ppm} + 0.38A\ 10^{B/576} + H_e = 375 \text{ ppm}$$

$$30 \text{ ppm} + 0.42A\ 10^{B/632} + H_e = 750 \text{ ppm}.$$

A solution of the above equations resulted in the following values for H_e and H_b:

TABLE 2. TENSILE PROPERTIES OF HYDROGEN-CONTAINING Ti-2Fe-2Cr-2Mo TESTED AT 0.005 INCH PER MINUTE

	Test Temperature, F	Ultimate Tensile Strength, psi	Reduction in Area, per cent
		20 PPM Hydrogen	
	212	127,500	59
	70	147,100	56
	0	145,900	57
	-58	169,200	56
		250 PPM Hydrogen	
Lot A	212	126,500	53
Lot B	85	142,000	58
Lot A	70	147,300	59
Lot B	60	146,000	14
Lot B	40	149,500	14
Lot A	32	148,700	12
Lot B	32	153,000	28
Lot B	20	152,500	10
Lot A	0	153,500	8
Lot B	-25	157,500	8
Lot A	-50	165,100	8
Lot A	-100	180,500	8
		375 PPM Hydrogen	
	212	127,000	58
	125	139,500	54
	110	142,000	39
	100	141,000	44
	85	146,500	16
	75	144,000	11
	60	146,000	6
	0	153,500	7
	-100	--	8
		750 PPM Hydrogen	
	250	123,000	61
	200	130,000	56
	190	131,200	59
	180	131,000	55
	170	134,000	54
	160	135,000	25
	150	136,000	16
	140	136,000	10
	130	139,500	12
	100	142,500	9
	75	146,000	13

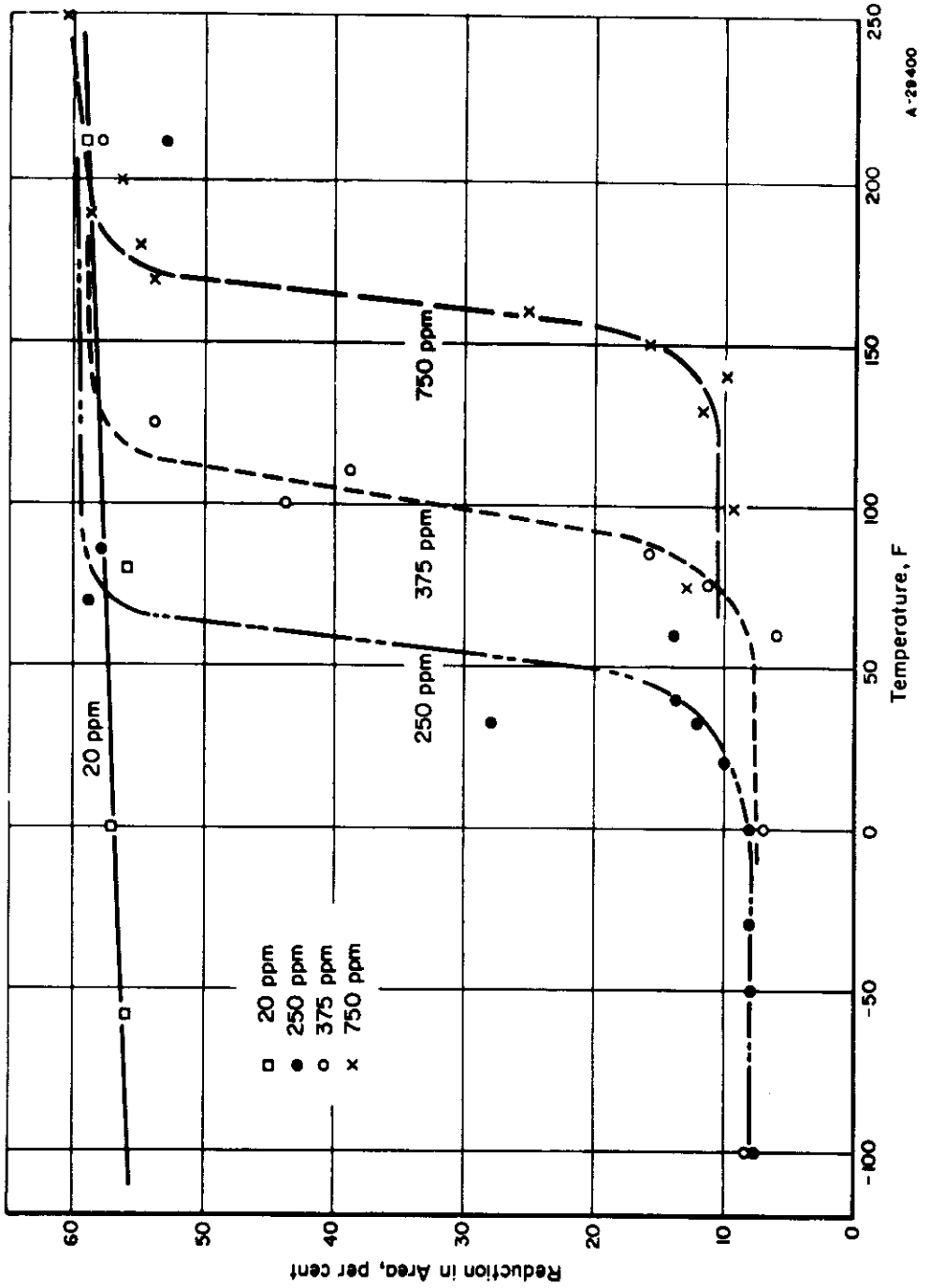

FIGURE 14. EFFECT OF TEMPERATURE ON THE TENSILE DUCTILITY OF HYDROGEN-CONTAINING Ti-2Fe-2Cr-2Mo

Test speed: 0.005 inch/minute.

$$H_e = 200 \text{ ppm}$$

$$H_b = 8 \times 10^7 \times 10^{-3040/T} = 10^{(7.903 - 3040/T)}.$$

An indication of the validity of the assumption that changes in hydrogen solubility are the basic cause of low-strain-rate embrittlement can be gained by considering the value of the above two calculated factors.

The variation of hydrogen solubility in beta with temperature has been plotted in Figure 13. It is seen that the hydrogen solubility increases from 140 ppm at room temperature to 2000 ppm at 200 F. In an extrapolation from hydrogen-pressure studies of unalloyed titanium at elevated temperatures, it was predicted that the room-temperature hydrogen solubility in beta titanium might be as low as 66 ppm[8]. A solubility curve for hydrogen in beta based on this extrapolation is also included in Figure 13. Considering the expected variation in solubility with alloying, the agreement is very good and lends considerable support to the assumption that changes in hydrogen solubility near room temperature are the basic cause of embrittlement.

The second important variable calculated from these data was H_e, the amount of hydrogen in excess of the soluble amount necessary to cause embrittlement. A value of 200 ppm does not seem unreasonable for the minimum hydrogen content in excess of the soluble amount required to result in embrittlement in unnotched tensile tests, based on the known hydrogen tolerance of Ti-2Fe-2Cr-2Mo. This factor may be considered as a rough indication of severity of test condition. Although H_e was assumed independent of temperature, it is probable that it decreases with temperature. Strain rate and notches should also affect its value, such that it becomes smaller as strain rate is decreased (since more of the excess hydrogen would be effective in embrittling the alloy) or as notches are introduced (since less hydrogen would be necessary to cause embrittlement, the stress being concentrated in a more restricted area). Increased alpha grain size might also be expected to decrease the magnitude of H_e.

Assuming the most severe testing conditions, such that H_e approaches zero, the limiting hydrogen content necessary to result in embrittlement would equal the hydrogen solubility. It is of interest that the solubility in an alloy such as that tested decreases very rapidly with temperature, as shown below:

Temperature, F	H_2 Solubility (From Figure 13), ppm
68	62
32	25
0	10
-40	2

Evidence of embrittlement in Ti-2Fe-2Cr-2Mo alloy at -40 F in notched tensile testing has been reported at hydrogen contents of less than 60 ppm.[9]

Hydrogen Embrittlement in an All-Beta Alloy

To determine whether all-beta alloys might be susceptible to hydrogen embrittlement, material available from a Ti-20Mo alloy (K-3) was examined. This alloy had previously been prepared for hydrogen-tolerance measurements and was known to be free from both low-strain-rate and impact embrittlement at 800 ppm. Sufficient hydrogen was added to 1/4-inch swaged bars of this alloy to produce hydrogen contents of 3000, 3600, and 4200 ppm. Following hydrogenation, the bars were homogenized at 1470 F for 24 hours and air cooled.

The properties of the alloy are shown in Table 3. Test procedures were analogous to those used in the studies to determine the effect of alloy content on hydrogen embrittlement described in this and a previous report[2]. Impact testing showed the alloy to be quite brittle, even at 20 ppm. The iodide-base Ti-20Mo alloy containing 2000 ppm hydrogen had better impact properties than did the vacuum-annealed sponge-base Ti-20Mo alloy. The poor impact resistance of this alloy is therefore believed to be related to interstitial content. The unnotched fast tensile test (0.5 inch/minute) indicates that impact embrittlement in unnotched material is occurring between 3600 and 4200 ppm hydrogen.

Low-strain-rate embrittlement is apparent in comparison of slow and fast unnotched-tensile-test data at 4200, 3600, and to a lesser extent, 3000 ppm. Notched stress-rupture tests also indicate embrittlement at 4200, 3600, and 3000 ppm. The notched-tensile-test data suggest, however, that the 3000 ppm material is extremely notch sensitive. Thus, the notched-stress-rupture data for this alloy are probably not reliable, and the slight reduction in ductility in the low-speed unnotched tensile test may also be related to the apparent notch sensitivity of the materials. The hydrogen tolerance for low-strain-rate embrittlement is believed to lie between 3000 and 3600 ppm.

All-beta titanium alloys are apparently susceptible to both impact and low-strain-rate embrittlement when very large amounts of hydrogen are present. Based on the known effects of molybdenum in alpha-beta alloys, molybdenum-free beta alloys should be susceptible to embrittlement at much lower hydrogen contents than those observed in Ti-20Mo. In all cases, however, the hydrogen tolerances of all beta alloys should be quite high.

Microstructural examination showed the Ti-20Mo alloy to consist of equiaxed fine-grained beta containing a few stringers of small alpha

TABLE 3. HYDROGEN EMBRITTLEMENT OF AN ALL-BETA ALLOY, Ti-20Mo

Hydrogen Content, ppm:	20[a]	800[a]	2000[b]	3000	3600	4200		
Unnotched Tensile Properties, 0.005 Inch/Minute								
Ultimate Strength, psi	136,400	136,800	110,000	133,000	134,000	136,500		
0.2% Offset Yield Strength, psi	129,300	135,800	110,000	132,000	133,000	136,500		
Elongation, % in 4 Diameters	16	10	22	8[c]	7	0		
Reduction in Area, %	37	36	67	28	11	0		
Unnotched Tensile Properties, 0.5 Inch/Minute								
Ultimate Strength, psi	142,100	143,400	119,000	146,500	148,000	150,700		
Elongation, % in 4 Diameters	20	10	16	6	--	--		
Reduction in Area, %	43	38	69	39	32	5		
Notched Tensile Properties, 0.005 Inch/Minute								
Ultimate Strength, psi	209,600	207,000	171,000	134,000	176,500	107,500		
Reduction in Area, %	6.0	4.3	37	2.0	1.0	0.7		
Micro Impact Properties								
Energy Absorbed at 75 F, inch-pounds	8	6	31	--	--	5		
Energy Absorbed at -80 F, inch-pounds	6	6	19	--	--	2		
Notched Stress-Rupture Properties								
Stress, psi	149,400	149,400	--	146,300	147,000	149,400	108,600	101,800
Stress, % of Unnotched Tensile Strength	110	110	--	110	110	110	80	75
Rupture Time, hours	206.9[d]	216.7[d]	--	0.1	9.8	Unloading	4.2	137.7[d]
Reduction in Area, %	0.9[d]	1.5[d]	--	5.0	1.1	0.0	0.7	0.5[d]

(a) From Reference (2).
(b) Iodide-base alloy. From Reference (10).
(c) Broke outside gage mark.
(d) Sample removed from test before failure.

spheroids. As the hydrogen content increased, the amount of alpha decreased. No hydride was observed in any of these samples, even in the fracture region of embrittled samples. The fineness of the beta grain size and rounding of the fracture area during metallographic preparation prevented an accurate determination of the path of fracture.

The hydrogen content necessary to embrittle this alloy was very high. Calculations of the hydrogen solubility in the beta phase of Ti-2Fe-2Cr-2Mo suggested that the solubility at room temperature was only about 140 ppm. Molybdenum is known to increase the hydrogen tolerance of alpha-beta alloys appreciably. Assuming that the Ti-4Mo alloy (K-1) is representative of molybdenum alloys, the hydrogen solubility in molybdenum-stabilized beta might be as high as 5000 ppm. (The data[2] suggest that embrittlement would be observed in this alloy in slow tensile testing at 1000 ppm. If so, the beta solubility might be as high as the result obtained by solving the following equation; 0.8 x 10 ppm + 0.2 x beta solubility = 1000 ppm, assuming that alpha solubility is not changed significantly.) This does not include provision for the hydrogen in excess of the soluble amount necessary to result in embrittlement. It has been suggested[8] that hydride cannot nucleate easily in beta titanium due to structural misfit between the hydride and beta lattices. Grain boundaries or alpha-beta interfacial regions would presumably provide suitable nucleation sites. Difficulty in nucleating hydride would tend to increase the hydrogen content in excess of the soluble amount necessary to cause embrittlement. Again using the Ti-4Mo to illustrate this effect, and assuming beta solubility is equal in all alloys (140 ppm), the excess hydrogen necessary to cause embrittlement in Ti-4Mo would be 964 ppm as compared with 200 ppm in Ti-2Fe-2Cr-2Mo. (By solution of the equation: 0.8 x 10 ppm + 0.2 x 140 ppm + excess hydrogen = 1000 ppm.) Since the hydrogen tolerance of the Ti-20Mo was much higher than the 1104 ppm which would be predicted assuming the beta solubility was 140 ppm and was actually quite close to the 5000 ppm predicted assuming the beta solubility was 5000 ppm, it is probable that molybdenum is effective in increasing the tolerance of alpha-beta titanium alloys principally through its ability to increase the solubility of hydrogen in beta titanium.

Low-Strain-Rate Embrittlement in an All-Alpha Alloy

Low-strain-rate embrittlement is generally assumed to occur in alloys containing appreciable amounts of beta. However, recent work has indicated that alpha-compound alloys, such as Ti-4Al-7Cu, are susceptible to embrittlement.[2] Since these alloys contain no beta phase, embrittlement cannot be a characteristic of beta-containing alloys only. The present investigation was undertaken to determine whether all-alpha alloys might be susceptible to low-strain-rate embrittlement.

Unalloyed titanium was selected for initial investigation. It has been reported that hydrogen can be retained in the alpha phase for short times by quenching[7], and progressive loss of impact properties with time was known to occur in quenched unalloyed titanium on aging.[6] Tests were therefore conducted immediately after a solution heat treatment to determine whether strain-induced hydride precipitation might lead to embrittlement. Results of tensile tests on unalloyed titanium at two hydrogen levels are shown in Table 4. It is apparent that no low-strain-rate embrittlement occurred. Strain-induced precipitation may be indicated, however, by the large difference in ultimate strength observed at 400 ppm in quenched material tested at different test speeds. At low test speeds, the tensile strength is about equal to that of the air-cooled samples. At fast tensile-testing speeds, in which the hydrogen would presumably remain in solution, significant strengthening was observed.

The structure near the tensile fracture of two of the high-hydrogen samples is shown in Figure 15. A noticeable difference in hydride precipitate was observed; the air-cooled alloy showed needlelike hydride while the quenched alloy showed uniform dispersion of fine hydride particles. Since the unstrained portion of the test sample of the quenched samples tested at fast test speeds also showed the same type of precipitate, it is not known how much, if any, of the fine precipitate came out during straining.

No strain-induced hydride precipitation in unalloyed titanium was observed, and no strain-induced embrittlement was noted. Additional studies were carried out on a Ti-5Al alloy to determine whether this more highly alloyed alpha alloy would be susceptible to embrittlement. Notched stress-rupture properties of this alloy at four hydrogen levels are shown in Table 5. Slight embrittlement apparently occurred at 300 and 450 ppm. However, since both of these alloys contained some thermally precipitated hydride, it is possible that the test is indicating notch sensitivity rather than low-strain-rate embrittlement.

Strain-induced hydride was observed in Ti-5Al containing 150 ppm and was tentatively identified in the alloys containing 300 and 450 ppm. The presence of thermally precipitated hydride in these latter alloys prevented a conclusive detection of strain-induced hydride, however. Photomicrographs of hydride in Ti-5Al are shown in Figure 16.

Although conclusive evidence of embrittlement was not observed, the study of all-alpha alloys showed evidence of strain-induced hydride precipitation. It seems likely that low-strain-rate embrittlement will not be a problem in alpha alloys, since the amount of hydrogen required to result in strain-induced hydride is large and the degree of brittleness induced is relatively slight compared with that found in alpha-beta alloys.

TABLE 4. RESULTS OF TENSILE TESTS OF UNALLOYED TITANIUM CONDUCTED IMMEDIATELY AFTER HEAT TREATMENT

Heat Treatment	Strain Rate, inch/inch/minute	Ultimate Tensile Strength, psi	Elongation, % in 4 diameters	Reduction in Area, %
		20 PPM Hydrogen		
1 hr at 1475 F, air cooled	0.005	70,600	36	57
1 hr at 800 F, quenched	0.005	70,600	35	55
1/4 hr at 1650 F, quenched[a]	0.005	69,600	40	69
		400 PPM Hydrogen		
1 hr at 1675 F, air cooled	0.005	73,200	30	54
1 hr at 800 F, quenched	0.005	75,000	30	58
1 hr at 800 F, quenched	0.5	83,600	27	53
1/4 hr at 1650 F, quenched[a]	0.005	75,300	--	54
1/4 hr at 1650 F, quenched[a]	0.5	84,300	24	39

(a) Encapsulated during heat treatment to prevent contamination.

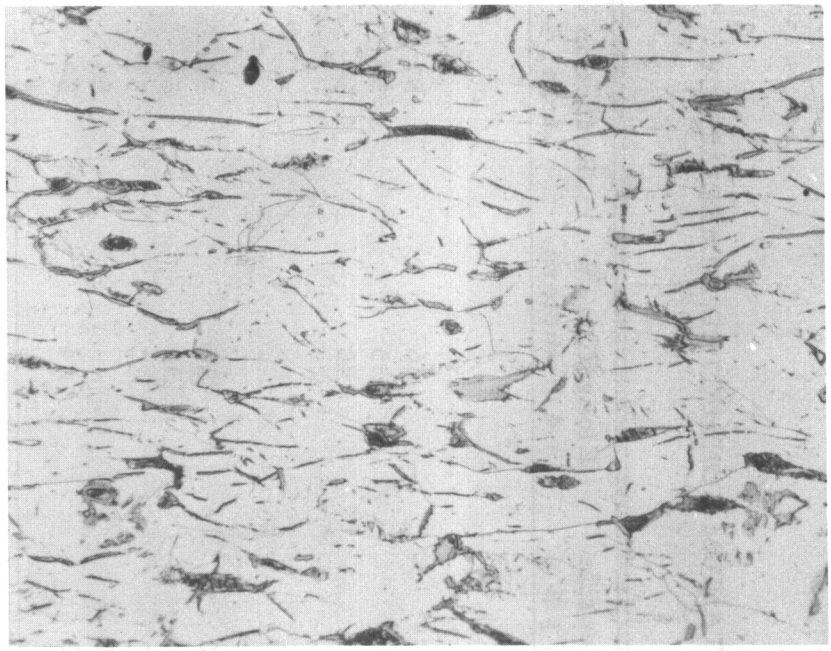

500X N44805

a. 1 Hr at 1675 F, Air Cooled

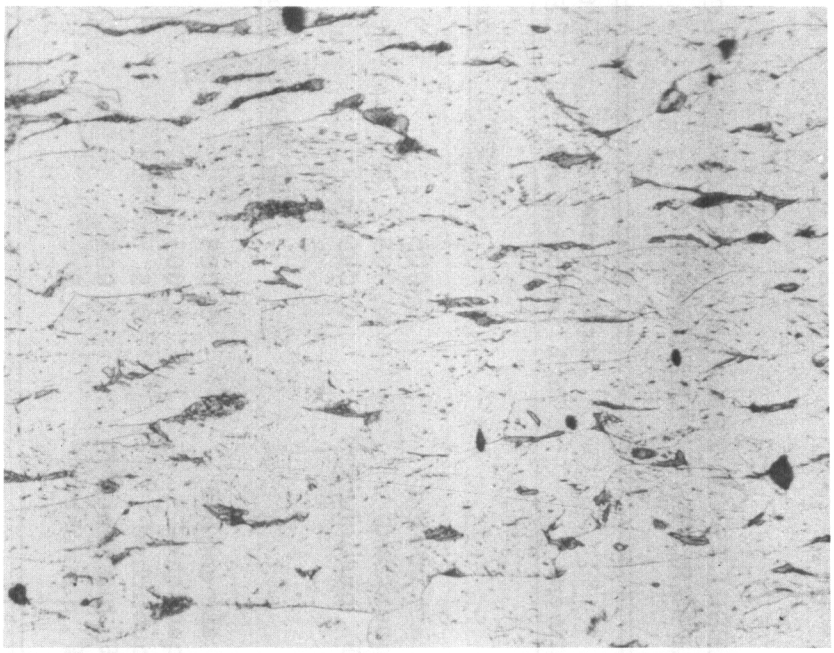

500X N44803

b. 1 Hr at 800 F, Quenched

FIGURE 15. EFFECT OF HEAT TREATMENT ON HYDRIDE STRUCTURE NEAR THE TENSILE FRACTURE OF UNALLOYED TITANIUM CONTAINING 400 PPM HYDROGEN AND TESTED AT 0.005 INCH/INCH/MINUTE IMMEDIATELY AFTER HEAT TREATMENT

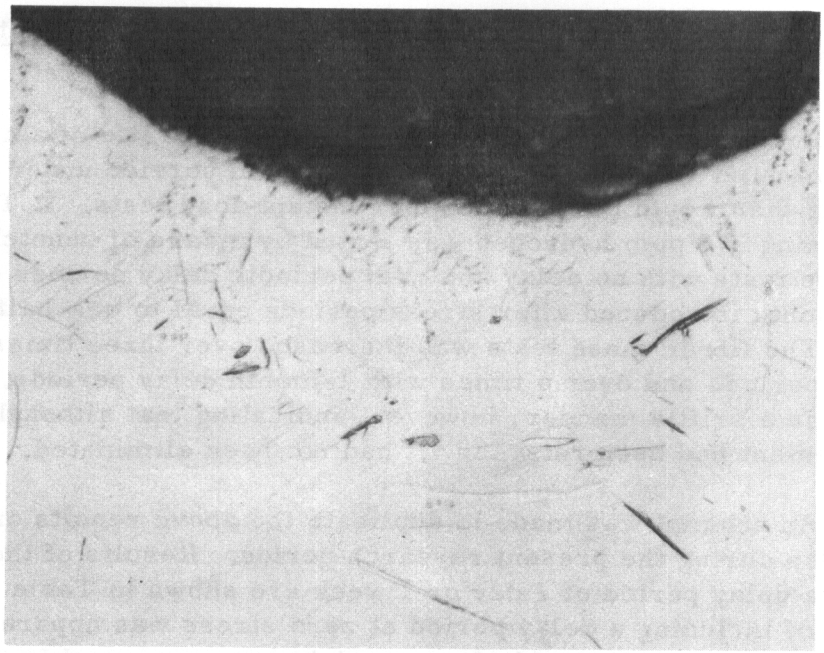

500X Stress direction N47179

a. Strain-induced hydride; 150 ppm hydrogen

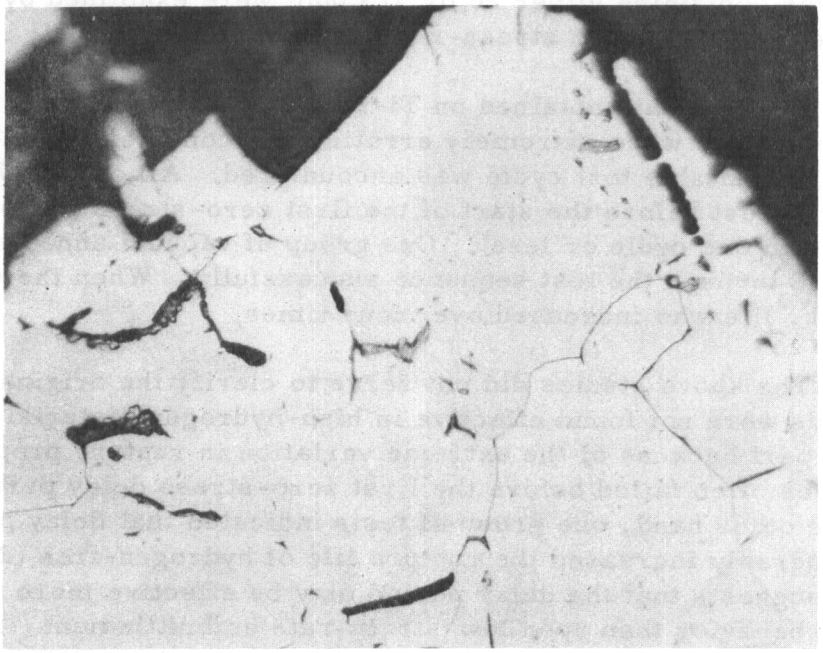

500X N47180

b. Fracture region; 300 ppm hydrogen

FIGURE 16. HYDRIDE IN AN ALL-ALPHA Ti-5Al ALLOY

Effect of Cyclic Loading on Low-Strain-Rate Embrittlement

Previous work[2] indicated that the rupture life of a hydrogen-contaminated alloy might be much greater in service under interrupted loading than would be indicated by constant-load tests. A Ti-8Mn alloy containing 370 ppm hydrogen was tested by means of unnotched stress-rupture tests with no delay and with periodic delay periods of 1 day and of 1 month introduced after stress periods equal to one-half the expected life. The life in these tests was increased over three times with 1-day delay periods and over 6 times with 1-month delay periods. All samples failed in a brittle manner, however, indicating that although hydrogen embrittlement had been retarded, it had not been eliminated.

An attempt was made to duplicate the above results on the same alloy samples during the present research period. Results of these tests when using a delay period of 1 day or 1 week are shown in Table 6. No beneficial effect of including a delay period at zero stress was apparent. It was felt that microsegregation of hydrogen might have occurred in the year between running the two groups of samples which could explain the lack of agreement. Therefore, new test specimens were prepared from Ti-2Fe-2Cr-2Mo alloy available from studies of the low temperature recovery of ductility. Samples containing either 20 or 375 ppm were examined by using both notched and unnotched stress-rupture loading.

The test data obtained on Ti-2Fe-2Cr-2Mo are given in Table 7. These results were extremely erratic, and considerable difficulty in obtaining a suitable test cycle was encountered. All of the 375-ppm material failed in test before the start of the first zero-stress period (indicated by failure in one cycle or less). One group of vacuum annealed material was carried through the test sequence successfully. When the delay period was 1 week, life was increased over four times.

The above studies did not serve to clarify the original results. Delay periods were not found effective in high-hydrogen material, probably in large part because of the extreme variation in rupture properties such that samples often failed before the first zero-stress delay period was reached. On the other hand, one group of tests indicated that delay periods of 1 week considerably increased the rupture life of hydrogen-free (20 ppm) material. This suggests that the delay period may be effective more for its effect on creep behavior than upon low-strain-rate embrittlement. It would appear that, pending a more conclusive investigation, the resistance of hydrogen-contaminated material to embrittlement in cyclic loading should not be considered significantly different from that in continuous loading.

TABLE 5. NOTCHED STRESS-RUPTURE PROPERTIES OF Ti-5Al AT FOUR HYDROGEN LEVELS

Stress concentration factor = 3.

Hydrogen Content, ppm	Applied Stress		Time to Failure, hours	Reduction in Area, %
	PSI	% of Unnotched Tensile Strength		
20	104,500	110	221.2(a)	1.0(a)
150	115,500	110	213.5(a)	2.7(a)
300	115,500	110	111.1	3.6
450	117,700	110	177.2	3.5

(a) Sample removed from test before failure.

TABLE 6. RESULTS OF INTERRUPTED STRESS-RUPTURE TESTS ON UNNOTCHED Ti-8Mn ALLOY CONTAINING 370 PPM HYDROGEN

Stress = 123,500 psi (90 per cent of ultimate tensile strength).

Intended Stress Cycle, hours		Time to Rupture, hours	Number of Cycles	Reduction in Area, %
At Stress	Delay Period			
--	--	15.9	2.0	10
--	--	12.9	1.6	5
8	40	11.3	1.4	5
8	160	13.3	1.7	10
8	160	1.7	0.2	6

TABLE 7. INTERRUPTED STRESS-RUPTURE-TEST RESULTS ON Ti-2Fe-2Cr-2Mo ALLOY

Type of Specimen	Applied Stress: Per Cent of Unnotched Ultimate Tensile Strength	Applied Stress: PSI	Intended Stress Cycle: At Stress	Intended Stress Cycle: Delay Period	Total Time to Rupture, hours	Number of Cycles	Reduction in Area, per cent
			Nominal Hydrogen Content 20 PPM				
Unnotched	97	142, 800	--	--	50.4	--	43
	98	144, 200	--	--	3.6	--	41
Notched, K_t = 3	137	197, 000	--	--	40.5[a]	--	4.1[a]
	140	201, 000	--	--	7.0	--	9.6
	140	201, 000	--	--	117.3[a]	--	4.6[a]
	145	208, 000	--	--	0.3	1.8	5.4
	145	208, 000	--	--	0.3	1.8	8.6
	145	208, 000	10 min	1 week	1.53	9.2	9.2
	145	208, 000	10 min	1 week	1.17	7.4	7.4
			Nominal Hydrogen Content 375 PPM				
Unnotched	93	130, 200	--	--	90.0[a]	--	0[a]
	97.5[b]	136, 200[b]	--	--	11.6	1.4	2
	97.5	136, 200	--	--	2.4	0.3	10
	97.5	136, 200	--	--	25.3	3.2	8
	97.5	136, 200	8 hours	1 week	1.7	0.2	4
	97.5	136, 200	8 hours	1 week	1.9	0.2	8
Notched, K_t = 3	110	157, 000	--	--	0.6	--	2.6
	95	136, 200	--	--	6.9	2.3	4.2
	95	136, 200	--	--	6.7	2.2	1.6
	95	136, 200	3 hours	1 week	1.9	0.6	--
	95	136, 200	3 hours	1 week	2.9	1.0	1.6

(a) Sample did not rupture.

(b) Retest of sample previously stressed 90 hours at 130, 200 psi.

Pretreatment to Minimize Hydrogen Embrittlement

If low-strain-rate embrittlement is due to the precipitation or segregation under strain of nonequilibrium hydrogen retained in solid solution on cooling, a pretreatment designed to relocate this excess hydrogen might prove beneficial. If a random thermal precipitation of hydride could be induced, the high degree of segregation apparently causing embrittlement would be prevented. It is possible, of course, that pretreatment could cause segregation of hydrogen without precipitation and thereby lead to a condition of increased susceptibility to hydrogen embrittlement. The present study was initiated to study the effect of pretreatment.

Ti-2Fe-2Cr-2Mo containing 375 ppm hydrogen (nominal) was selected for study. After thermal treatment, the samples were tested to failure at 75 F at a strain rate of 0.025 inch/inch/minute. These test conditions were selected on the basis of data shown in Figure 4 to produce a fracture of intermediate ductility such that either increased or decreased embrittlement tendencies would be obvious.

The results of the first series of tests, in which annealing treatments between 100 and 1000 F were examined, are given in Table 8, Test Group 1. Embrittlement was apparently reduced considerably by annealing at 100 through 600 F, and embrittlement increased after annealing at 900 and 1000 F. Duplicate results after annealing at 800 F did not agree.

The second group of tests described in Table 8 were run to determine the effect of annealing time on the reduction of embrittlement at 100 F. In this test group even the untreated samples were ductile. It was obvious, therefore, that some source of error was entering into the test. The most logical cause of trouble was believed to be sample heating during testing in air to a point above the maximum temperature of embrittlement such that embrittlement would be reduced or eliminated. To check this, two additional untreated samples were tested in air, while a third sample was tested in a water bath. One of the air-tested samples was ductile, and one was brittle. Since the sample tested in a water bath was quite brittle, the origin of difficulty seemed definitely to be sample heating.

The annealing treatments examined in Test Group 2 were re-examined in Test Group 4. Water baths were used for heating at controlled test temperatures of 60 and 85 F. No beneficial effects of pretreatment were apparent at either temperature.

Because of the consistency of the effect observed in Test Group 1, it would be tentatively concluded that pretreatments do have a slight beneficial effect. The data from Test Group 4, however, indicate that the effect is not of great significance, and is probably operative only in cases, in which the alloy is tested at a condition quite close to the transition from

TABLE 8. EFFECT OF PRETREATMENT ON THE SUSCEPTIBILITY TO LOW-STRAIN-RATE EMBRITTLEMENT

Annealing Treatment		Hydrogen	Test Conditions		Ultimate Tensile	Reduction in
Temperature, F	Time, days	Content, ppm	Temp, F	Testing Rate, inch/minute	Strength, psi	Area, %
			Test Group 1			
None	None	375	75	0.025	149,000	19
None	None	375	75	0.025	148,000	19
100	7	375	75	0.025	149,000	43
100	7	375	75	0.025	149,500	44
150	7	375	75	0.025	149,000	38
150	7	375	75	0.025	149,000	36
200	7	375	75	0.025	148,000	30
200	7	375	75	0.025	146,000	48
300	7	375	75	0.025	149,000	38
300	7	375	75	0.025	148,000	37
600	2	375	75	0.025	149,800	43
600	2	375	75	0.025	150,000	31
800	1	375	75	0.025	148,000	42
800	1	375	75	0.025	149,000	17
900	1	375	75	0.025	146,500	19
900	1	375	75	0.025	147,000	15
1000	1	375	75	0.025	145,000	11
1000	1	375	75	0.025	149,000	14
			Test Group 2			
None	None	375	75	0.025	149,500	33
None	None	375	75	0.025	149,000	47
100	1/3	375	75	0.025	150,000	46
100	1/3	375	75	0.025	148,000	30
100	1	375	75	0.025	148,000	44
100	1	375	75	0.025	150,000	30
100	2	375	75	0.025	149,000	47
100	2	375	75	0.025	147,000	45
100	7	375	75	0.025	148,000	52
100	7	375	75	0.025	150,000	22
			Test Group 3			
None	None	400	75 (in air)	0.025	147,000	48
None	None	400	75 (in air)	0.025	145,000	12
None	None	400	75 (bath)	0.025	146,500	14
			Test Group 4			
None	None	400	60 (bath)	0.025	146,300	11
100	1/3	400	60 (bath)	0.025	145,500	13

TABLE 8. (Continued)

Annealing Treatment		Hydrogen	Test Conditions		Ultimate Tensile	Reduction in
Temperature, F	Time, days	Content, ppm	Temp, F	Testing Rate, inch/minute	Strength, psi	Area, %
			Test Group 4 (Continued)			
100	1	400	60 (bath)	0.025	148,000	9
100	2	400	60 (bath)	0.025	148,000	11
100	7	400	60 (bath)	0.025	148,000	11
None	None	400	85 (bath)	0.025	148,000	23
100	1/3	400	85 (bath)	0.025	147,300	17
100	1	400	85 (bath)	0.025	147,000	16
100	2	400	85 (bath)	0.025	147,000	22
100	7	400	85 (bath)	0.025	146,000	18

ductile to brittle failure. Because of time limitations, further study of pretreatments could not be carried out.

Segregation of Hydrogen at the Fracture

Previous studies[2] have indicated that a large increase in beta lattice constant occurs near the fracture in hydrogen embrittled Ti-8Mn alloy. This suggested that hydrogen was concentrating in the fracture region. Several attempts to confirm the initial data have been made using Ti-2Fe-2Cr-2Mo.

Two standard 0.250-inch-diameter round tensile specimens were prepared from Ti-2Fe-2Cr-2Mo containing 375 ppm hydrogen. These samples were broken in tension and immediately examined by X-ray for lattice constant of the beta phase at the fracture. The incident beam was adjusted to strike either the center of the fracture or the fracture lip. Following the fracture examination, a section was cut from the unstrained shoulder portion of the bar for a lattice determination of material away from the fracture. Results of the X-ray examination are shown in Table 9.

TABLE 9. SUMMARY OF X-RAY TESTS TO CHECK FOR HYDROGEN SEGREGATION AT THE FRACTURE

Sample	Hydrogen Content, ppm	Tensile-Test Conditions		Reduction in Area, %	Beta Lattice Constant, angstrom units		
		Temp	Platen Speed		Shoulder	Lip of Fracture	Center of Fracture
Ti-2Fe-2Cr-2Mo	375	75 F	0.005 inch/min	21	3.226(b)	3.229(c)	
Ti-2Fe-2Cr-2Mo	375	32 F	0.005 inch/min	15	3.224(b)	3.221(c)	3.216(c)
Ti-8Mn(a)	400	75 F	0.005 inch/min	6	3.202	3.213-3.218	--

(a) Sample tested previously.[2]
(b) Probably accurate to ± 0.001 angstrom unit.
(c) Probably accurate to ± 0.005 angstrom unit.

On the basis of these data, it would appear that the original results may have been misleading. It is also possible, however, that the region of hydrogen-induced failure was missed in the present work and that the X-ray patterns were made on regions of the fracture which failed in a ductile manner after cracking had initiated from hydrogen embrittlement in another area. Also, Ti-2Fe-2Cr-2Mo may not be so suitable for such studies as Ti-8Mn because of differences in lattice distortion of the beta phase by hydrogen.

Hydride Formation in Torsion and Compression

A study was initiated at the start of the investigation to determine whether strain-induced hydride could be developed in torsion or on the compression side of bends. Hydride formed under such conditions would not lead to complete failure, and thus the relationship between crack formation and hydride location could be more accurately determined.

Bend samples were prepared from Ti-2Fe-2Cr-2Mo sheet containing 250 ppm hydrogen and stressed in an effort to produce cracking on the tension side of the bend. No cracks were developed, however, and sectioning to examine for differences in hydride precipitation of tension and compression sides of the bend was not carried out.

Torsion loading was carried out by applying a twisting moment to Ti-8Mn wire containing 600 ppm. Very fine circumferential cracks were observed on the surface after 2 or 3 days in test. When the wire was sectioned for metallographic examination, the cracks could not be located. It is possible that they closed on removal of stress. Some hydride was observed, but its random orientation suggested a thermal origin.

Further studies of hydride formation in torsion or compression loading were halted since metallographic examination of the notched stress-rupture samples being examined concurrently showed a number of excellent examples of hydride formation. Studies of the relationship between cracking and hydride formation were made conveniently on this material. The various types of strain-induced hydride observed and their relationship to cracking are described in a later section of this report.

Hydride Re-Solution During Heat Treatment

Ti-2.7Cr-1.3Fe-0.2O alloy (Ti150A) is known to develop large amounts of strain-induced and thermal hydride quite easily. It was felt that an indication of the hydrogen solubility in this alloy might be obtained by quenching the alloy from successively higher temperatures and observing any change in hydride content which might occur. A sample containing 1000 ppm was aged for 1 week at 200 F, 300 F, and 400 F. After annealing, the samples were either slow cooled or water quenched. Metallographic examination showed all samples to contain large amounts of needlelike hydride. The original structure was predominantly alpha plus martensite with very little beta, and was not visibly affected by these heat treatments. Unalloyed alpha titanium would dissolve about 400 ppm hydrogen at 400 F (see Figure 13), while dissolving only about 10 ppm at room

temperature. Thus, a large amount of hydride would be expected to dissolve during this heat treatment, assuming iron and chromium do not greatly affect hydrogen solubility in alpha because of their own low solubility in alpha.

In the absence of any visible structural change during heat treatment, it must be concluded either that hydride once formed is quite difficult to redissolve at low temperatures or that hydride is able to reprecipitate in an almost identical form, both on slow cooling and on water quenching. Samples quenched after annealing 24 hours at 800 F and 1000 F suggested that the former explanation was more probable since noticeable structural changes had occurred in hydride present in these samples. Since the present study did not appear capable of providing the desired information on low-temperature hydrogen solubility, further studies of this type were halted.

Discussion of Results

The present investigation has indicated that low-strain-rate embrittlement can be explained satisfactorily on the basis of precipitation of hydride from a supersaturated solid solution of hydrogen in titanium. Changes in the equilibrium solubility of hydrogen lead to the initial loss of ductility as temperature decreases, while a further decrease in temperature results in recovery of ductility due to decreased rate of rejection of hydride. The rate-controlling step apparently is the diffusion rate of hydrogen.

In most cases, the change in solubility of hydrogen in the beta phase is probably the principal contributor to embrittlement. However, suitably alloyed alpha titanium may also retain greater than equilibrium amounts of hydrogen at room temperature and thus serve as a source of hydrogen for embrittlement. Alpha-beta alloys appear most susceptible to embrittlement because of the ease with which hydride nucleates at the alpha-beta interface. An all-beta alloy, Ti-20Mo with 3600 ppm hydrogen, was susceptible to embrittlement, but strain-induced hydride was not observed. An all-alpha alloy, Ti-5Al, on the other hand, showed strain-induced hydride and slight embrittlement at 300 ppm hydrogen, but not at 150 ppm hydrogen. Embrittlement was more pronounced in an alpha-compound alloy, presumably due to the ability of the compound phase to nucleate hydride. The ease of precipitation of hydride from beta on an alpha substrate apparently is related to the ease with which hydride precipitates along the prism planes in alpha. It has been suggested[8] that hydride nucleates with considerable difficulty in beta titanium because of lattice mismatch. If so, the special susceptibility of alpha-beta alloys can be related to the tendency for hydride to nucleate heterogeneously along the alpha-beta interface leading ultimately to a highly localized semicontinuous hydride distribution. The tendency for alpha-beta interface precipitation of hydride and for cracking to occur along the interface in alpha-beta alloys is well known.

In the present discussion, embrittlement has been related to hydride formation. It has occasionally been suggested, particularly by those quite familiar with hydrogen embrittlement in steel, that embrittlement is due to hydrogen segregation at the alpha-beta interface or to precipitation of hydrogen gas. Although the relationship between embrittlement and hydride has not been conclusively proven, the extensive metallographic evidence showing hydride in alpha-beta interfacial areas, cracking following the hydride phase, highly localized strain-oriented hydride, etc. (see, for example, the following sections of this report), would suggest that attempts to relate embrittlement to some factor other than hydride formation are unnecessary.

The most perplexing question yet remaining unanswered regarding the mechanism of low-strain-rate hydrogen embrittlement would appear to be the effect of strain on the embrittlement reaction. It is apparent that, in the absence of strain, the embrittling reaction does not occur. That is, alloys aged for long periods at low temperature do not become brittle during the aging period. This is quite unexpected, since diffusion data indicate that the rate of hydrogen movement is relatively rapid, even at room temperature and lower. Calculations suggest that only a few seconds are needed to move appreciable amounts of hydrogen through beta regions of the size generally observed in titanium alloys. * One must assume either that hydrogen does not diffuse as rapidly as predicted, or that nucleation of hydride occurs only with difficulty.

The assumption that hydrogen does not diffuse rapidly is one factor leading to the theory in which the movement of dislocations forms an essential part of the mechanism. The second factor is that microsegregation at the interface is increased during plastic deformation. Hydrogen would have a greater rate of diffusion along dislocations, and since the dislocations are probably anchored at the alpha-beta interface in most cases, a tendency for hydrogen concentration at the interface is developed. Alternatively, it might be assumed that an atmosphere of hydrogen follows the moving dislocations during straining. Again, since the dislocation would finally be blocked by the alpha-beta interface, a tendency toward hydrogen segregation at the interface would develop. When the hydrogen concentration at the interface built up sufficiently, nucleation of hydride would occur and embrittlement would result.

A dependence of diffusion on dislocation movement is quite attractive, since embrittlement is almost always found only after plastic flow. Also,

*The diffusion data for iodide beta titanium indicate that the diffusivity at room temperature is 2×10^{-8} cm^2/sec. Using the approximate relationship that the concentration of diffusing substance is midway between its initial and final concentration when $t = x^2/D$ (where t is diffusion time, x is diffusion distance, and D is diffusivity), a time of only 4.5 seconds is required assuming x to be 3×10^{-4} cm (based on the approximate radius of beta regions in the 375 ppm Ti-2Fe-2Cr-2Mo sample). Thus, the buildup of hydrogen at the alpha-beta interface should be very rapid if a concentration gradient is developed.

it can be argued that some plastic flow occurs even during relief of residual forming stresses, leading to the type of embrittlement referred to as delayed cracking.

If diffusion of hydrogen is not assumed to be prohibitively slow in the absence of strain, a strain dependence could be developed if it is assumed that embrittlement is a deviation from the equilibrium state caused by a pile-up of hydrogen at the interface by dislocation movement. This implies that the dislocations carry along with them atmospheres of hydrogen. This nonequilibrium segregation of hydrogen, if it became sufficiently great, might precipitate as a reasonably stable hydride before back diffusion to the equilibrium state can occur. Although this theory would explain the effects observed in cyclic loading[2], in which increased life was obtained in rupture testing when samples were allowed to "rest" at zero load at various intermediate points in the test,[a] it would also predict a lack of embrittlement at very low strain rates. That is, a strain rate should be reached at which the pile-up of hydrogen at the interface is occurring at a lesser rate than its removal by thermal diffusion. No evidence for such an effect has been reported.

It is also possible to develop a theory in which the effect of strain is related to nucleation. In this approach, it is assumed that nucleation cannot occur without the aid of either plastic flow or regions of very high elastic stress in the material. Such a mechanism would suggest that nucleation would be quite oriented with respect to stress and thus highly localized. Localized hydride precipitation is often observed, as shown by the photomicrograph reproduced in Figure 17. The apparent strain-rate dependence of the embrittlement reaction would then be actually a time dependence, as described previously in the section "Critical Nucleation Stress". This theory must assume that the nucleation stress or strain becomes less as time under stress increases in order to explain delayed cracking under the action of residual stress. This is a reasonable assumption, however.

It is apparent from the foregoing discussion that the dependence of hydrogen embrittlement upon the application of plastic strain, or possibly high elastic stresses, is not yet understood. It seems likely that this dependence is due either to dislocation-directed diffusion or to stress-dependent nucleation. Possibly both factors enter into the mechanism under different conditions. Further work will be required to resolve this question.

(a) It should be noted that these effects could not be confirmed in the present investigation (see page 40).

500X N28655

FIGURE 17. LOCALIZED PRECIPITATION OF HYDRIDE IN A Ti-6Mn ALLOY CONTAINING 600 PPM HYDROGEN

THE EFFECT OF ALLOY COMPOSITION AND HEAT TREATMENT ON LOW-STRAIN-RATE EMBRITTLEMENT

In the previous investigation, reported in WADC 54-616 Part IV[2], 80 titanium-base alloys were examined in the stabilized condition to determine the effect of alloy content on hydrogen embrittlement. At the same time four titanium-base alloys in a number of different heat-treated conditions were examined to determine the effect of heat treatment and microstructure on hydrogen embrittlement. Hydrogen embrittlement was detected in the original investigation by means of impact testing, unnotched tensile testing at two test speeds, and unnotched stress-rupture testing. The hydrogen tolerances obtained in the study were rather high, in view of the amount of hydrogen observed to cause delayed cracking in the field. Therefore, the present investigation was conducted on the same material

by using notched stress-rupture tests to redetermine the hydrogen tolerance of the various alloys and conditions.

Experimental Procedure

Preparation of Material

The same alloys as previously studied were used for the present investigation. A complete discussion of alloy preparation and fabrication is given in WADC TR 54-616, Part IV[2]. Material used in this investigation was in one of three forms:

(1) Unnotched tensile specimens or impact specimens

(2) Hydrogenated 1/4-inch-diameter swaged rod

(3) Unhydrogenated 5/8-inch-diameter swaged rod.

Before testing, all hydrogenated material was given a heat treatment consisting of a portion of the final heat treatment originally given the material to eliminate any hydrogen segregation which might have arisen from room-temperature aging. Heat treatments were as follows:

Stabilized material: 1 hour at 1100 F and air cooled

Solution-heat-treated material: 1 hour at 1300 F and water quenched

Aged material: 1 hour at 900 F and air cooled.

Whenever possible, notched testing was conducted on material hydrogenated in the previous study. Where this was not possible, additional material was hydrogenated. In most cases, 1/4-inch-diameter swaged rod was hydrogenated. In some cases, machined samples were hydrogenated. In a few of the microstructural studies, hydrogenation was conducted on 5/8-inch-diameter rod as in the original program. Hydrogenation procedures are described in WADC 54-616, Part IV[2]. When additional 1/4-inch-diameter rod was needed, swaging was accomplished in the same manner as in the original investigation.

The bulk of the stress-rupture testing was conducted with the samples illustrated in Figure 18. Figure 18a illustrates the specimen prepared by machining a notch into the gage section of a tensile specimen. This specimen was designated as Specimen B. The specimen machined from previously prepared impact samples is shown in Figure 18b. The specimen was designated as Specimen A. A few samples similar to Specimen A but

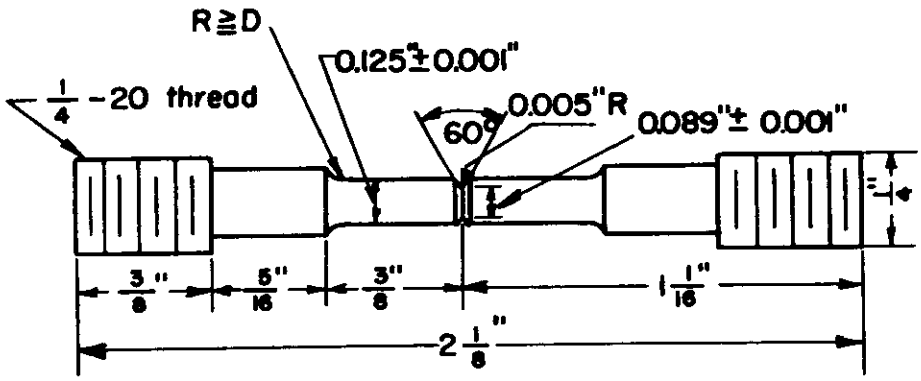

a. $2\frac{1}{8}$ - Inch Notched Test Specimen
(Specimen B)

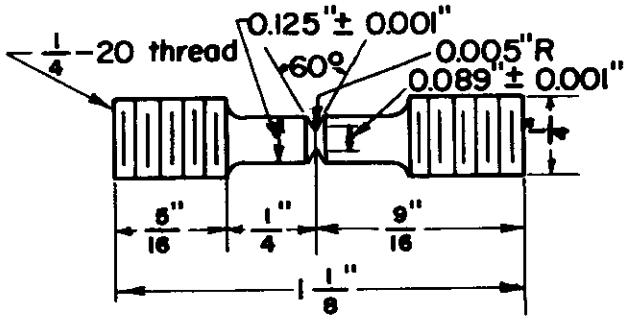

b. $1\frac{1}{8}$ - Inch Notched Test Specimen
(Specimen A)

A-23658

FIGURE 18. NOTCHED TEST SPECIMENS USED IN THIS INVESTIGATION

enlarged to 0.212-inch diameter, 0.150-inch diameter under the notch, were prepared from 1/4-inch-diameter rod, but this design, designated Specimen C, was abandoned early in the research program in favor of Specimen A. All three specimens had a stress concentration factor of 3 in tension. As shown in Table 10, the data from all three test specimens appeared to be equivalent; i.e., a consistent variation of rupture life with applied stress was observed regardless of specimen configuration.

Notched Stress-Rupture Testing

Notched stress-rupture testing was conducted at 78 F in a controlled-temperature, -humidity room. Lever-arm creep racks were used to load the specimen. Time to failure and reduction in area under the notch were determined.

Initial rupture tests were conducted over a range of stresses to determine the effect of hydrogen on the rupture behavior. Curves showing the variation in life caused by hydrogen are shown in Figures 19 through 24. Embrittlement was manifested in these alloys by a considerable loss of rupture life. The Ti-2Mn-2Cr alloy, shown in Figure 19, was not embrittled at 20 ppm, but showed appreciable reductions in life with 200, 300, and 400 ppm of hydrogen. A similar large decrease in life was apparent in Ti-4Fe, Ti-4Mo, and stabilized Ti-4Al-4Mn as shown in Figures 20, 21, and 22. Ti-20Mo and solution heat treated Ti-4Al-4Mn, on the other hand, were not susceptible to hydrogen embrittlement with 800 ppm hydrogen as shown by Figures 23 and 24.

In the previous studies with unnotched specimens, ductility (per cent reduction in area) was the primary criterion of embrittlement, while time to rupture was not greatly affected. In the present work, ductility under the notch was not used as a criterion for detecting embrittlement, since it was not as consistent an indication as time to failure. This can be illustrated quite well by the notched-tensile-test results given in Table 11 and by reference to the stress-rupture ductility data given in the Appendix. Ti-4Mo showed an indication of ductility loss at 600 ppm of hydrogen and definite embrittlement at 800 ppm of hydrogen. In rupture testing, the ductility under the notch decreased from about 20 per cent at 20 ppm to 8 per cent at 400 ppm, the hydrogen level where embrittlement was first observed. Agreement between embrittlement level as determined by rupture life and ductility was quite good in this alloy. Ti-20Mo and Ti-4Fe, on the other hand, showed no significant ductility change in the notched tensile tests, both being initially relatively brittle. Some evidence of decreased ductility was apparent in rupture testing of Ti-4Fe, but the loss in ductility – from 8.0 to 1.2 per cent – is observed only if the unembrittled samples are allowed to fail in test. This requires adjustment of the testing stress for each alloy and hydrogen content. Time to rupture showed

TABLE 10. SELECTED TEST DATA SHOWING EQUIVALENCE OF THREE NOTCHED STRESS-RUPTURE SPECIMENS

Alloy	Nominal Composition (Balance Titanium), weight per cent	Hydrogen Content, ppm	Specimen Type	Stress, % of unnotched UTS	Time to Failure, hours	Reduction in Area, %
K-1	4Mo	600	A	110	6.7	6.5
			A	95	4.0	5.2
			A	80	39.6	2.4
			B	75	16.3	4.0
K-1	4Mn	800	A	110	2.3	4.5
			A	95	8.0	3.9
			A	80	18.0	1.5
			B	70	19.0	0.5
K-25	2Mn-2Cr	30	C	110	11.7	4.6
			B	110	13.0	5.7
			C	95	31.0	3.6
			B	80	95.1	3.1
K-25	2Mn-2Cr	400	C	110	8.8	2.6
			B	110	5.8	3.7
			C	95	18.2	0.6
			B	80	90.3	1.1

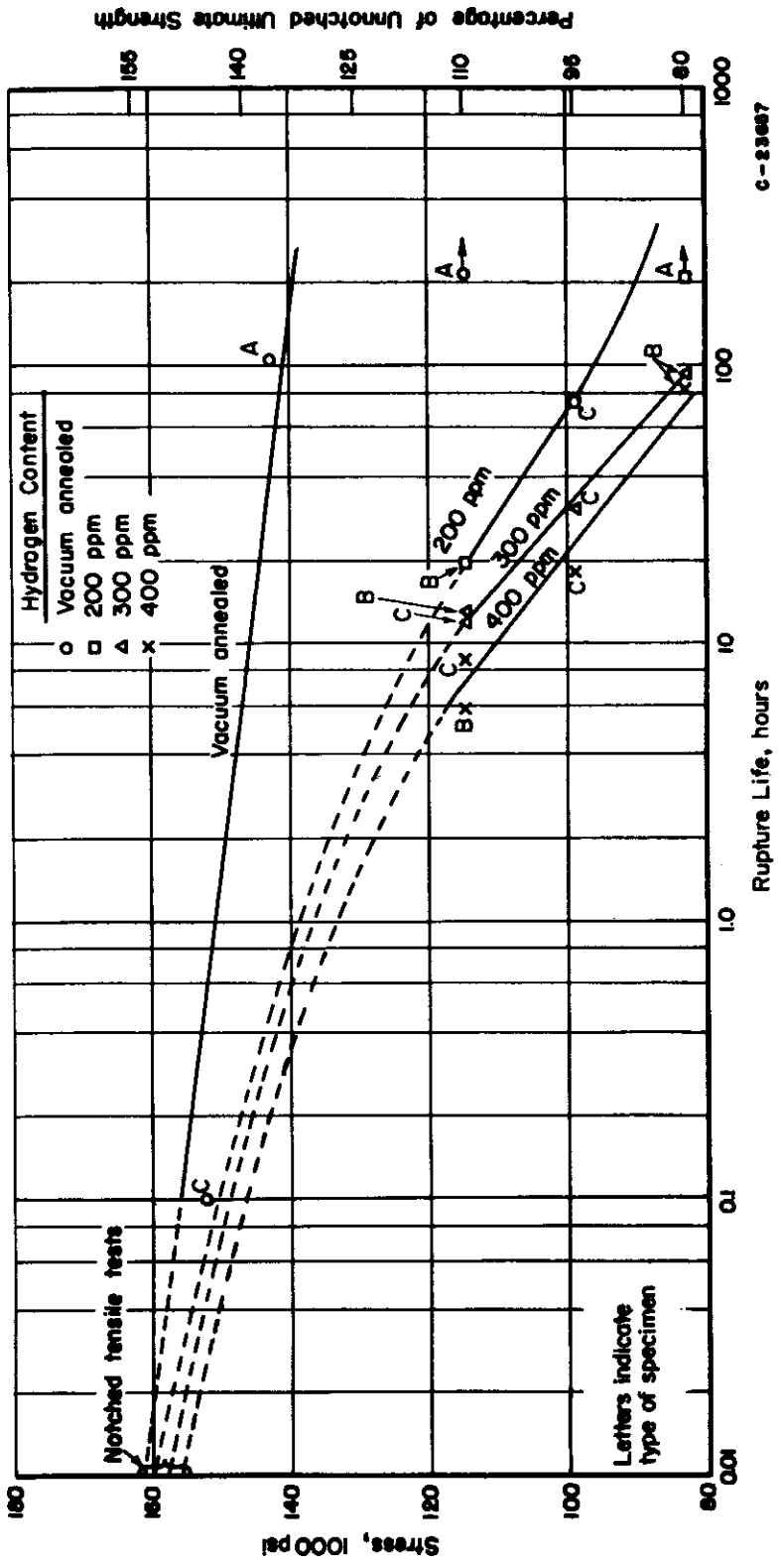

FIGURE 19. THE EFFECT OF HYDROGEN ON THE NOTCHED STRESS-RUPTURE PROPERTIES OF Ti-2Mn-2Cr

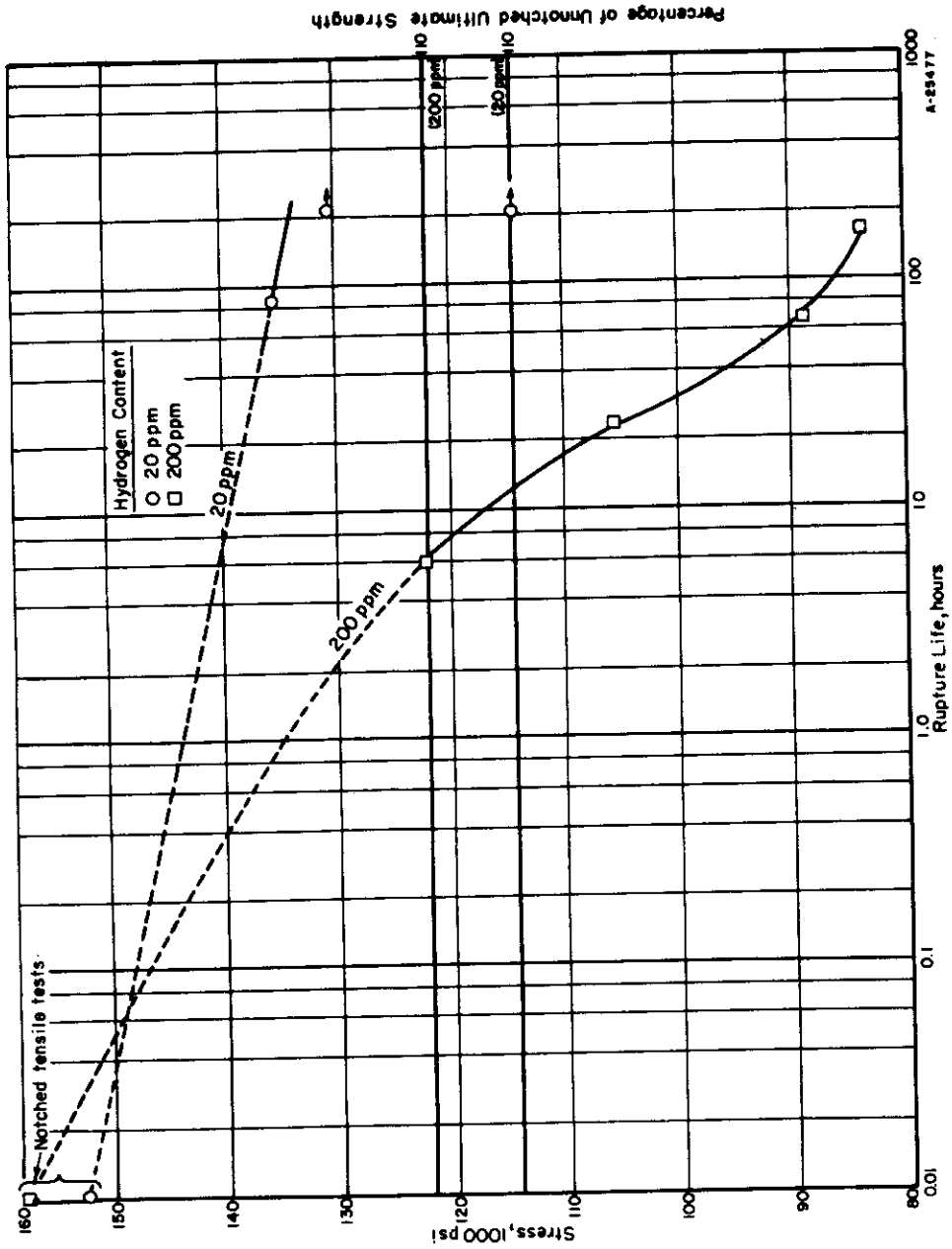

FIGURE 20. THE EFFECT OF HYDROGEN ON THE NOTCHED STRESS-RUPTURE PROPERTIES OF Ti-4Fe (F-15)

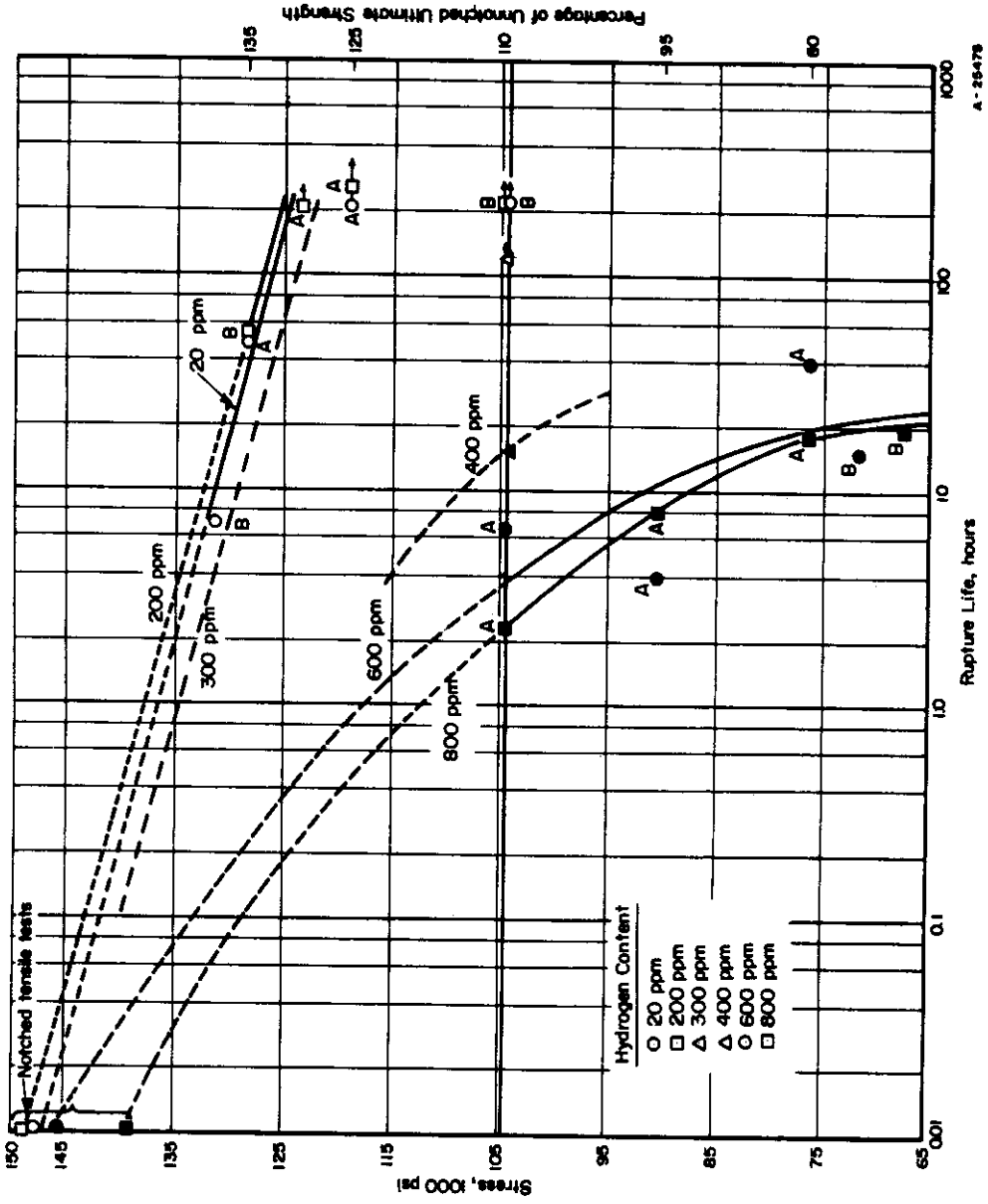

FIGURE 21. THE EFFECT OF HYDROGEN ON THE NOTCHED STRESS-RUPTURE PROPERTIES OF Ti-4Mo (K-1)

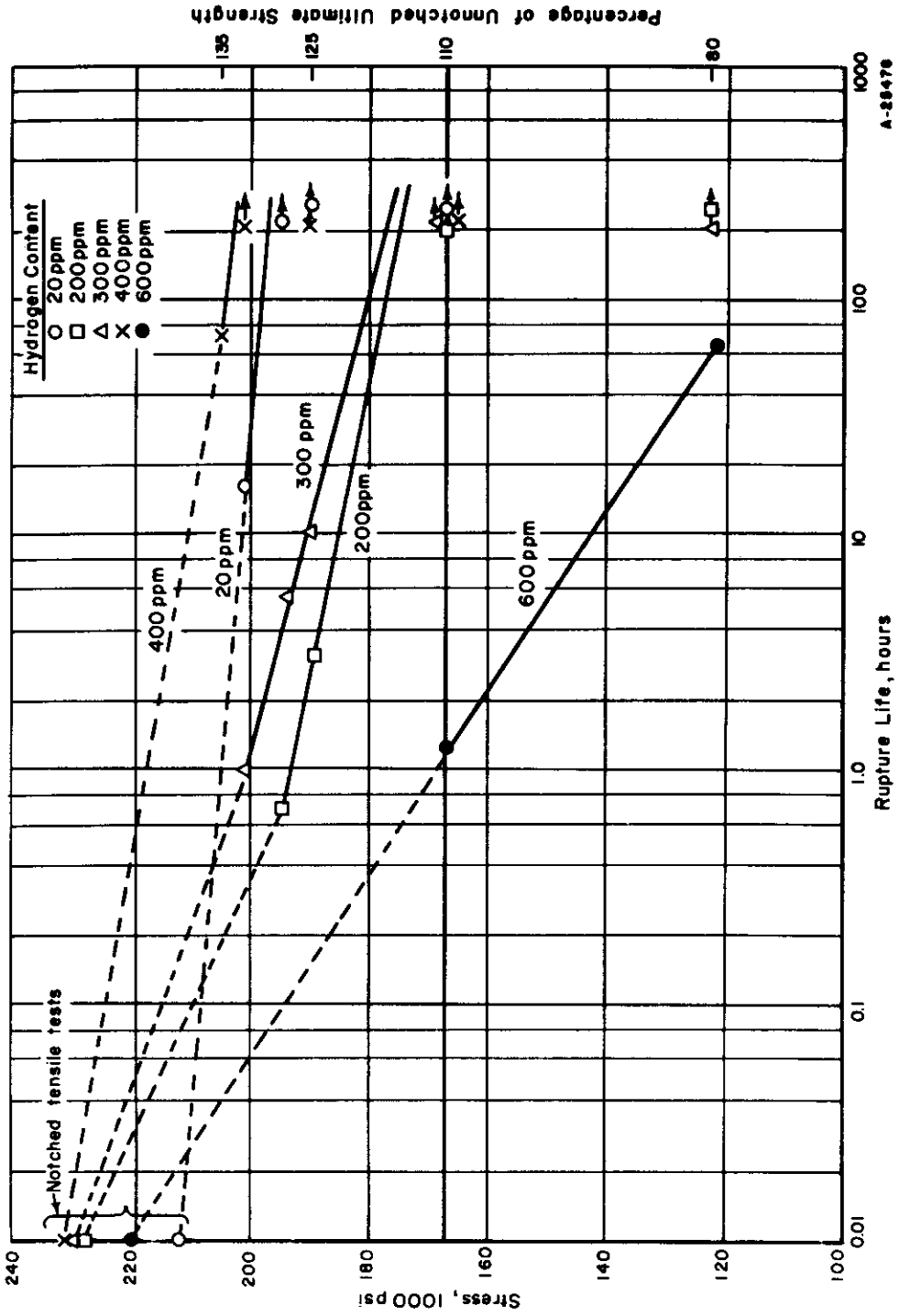

FIGURE 22. THE EFFECT OF HYDROGEN ON THE NOTCHED STRESS-RUPTURE PROPERTIES OF Ti-4Al-4Mn IN THE AS-STABILIZED, FINE EQUIAXED ALPHA CONDITION (K-38-1)

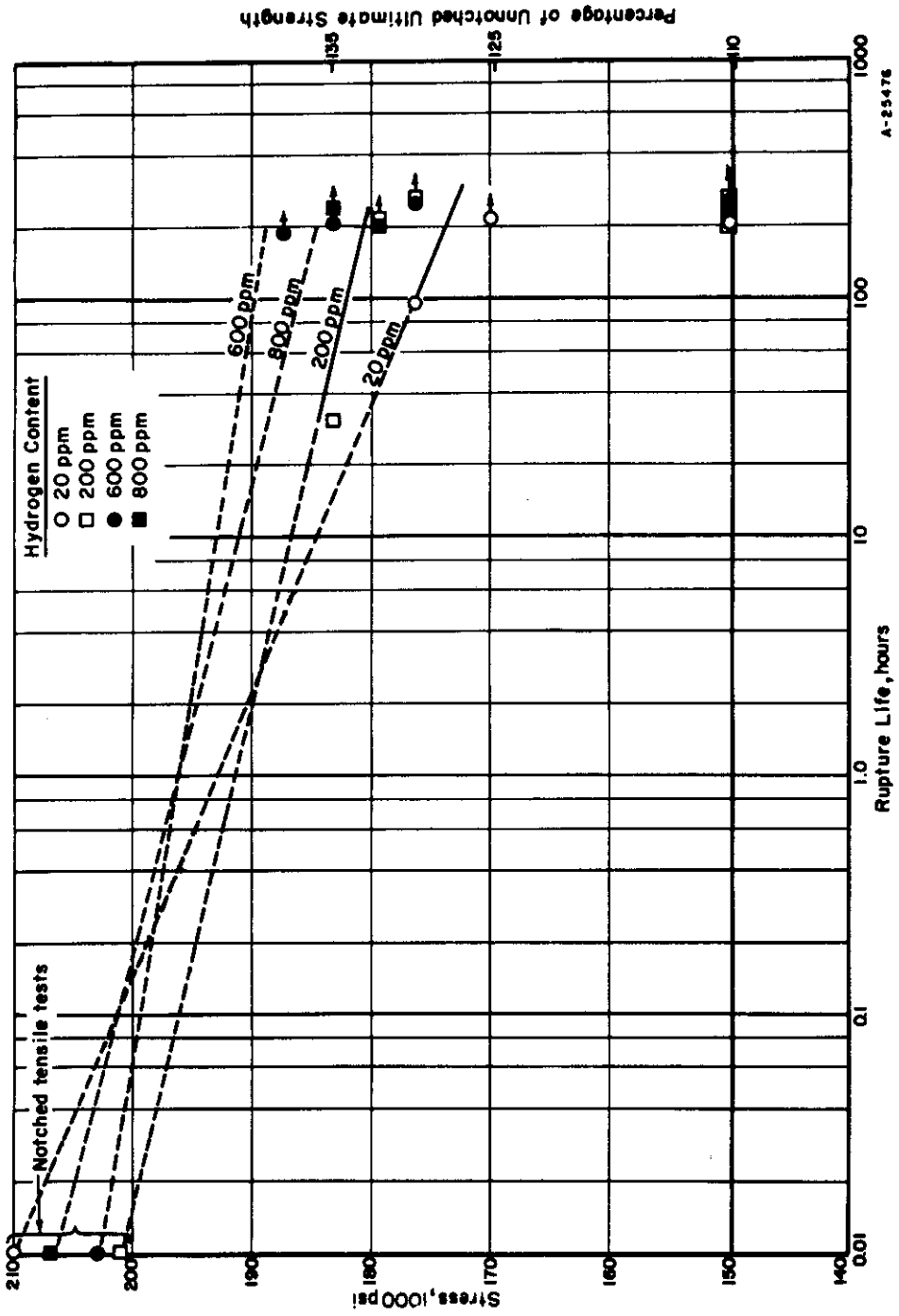

FIGURE 23. THE EFFECT OF HYDROGEN ON THE NOTCHED STRESS-RUPTURE PROPERTIES OF Ti-20Mo (K-3)

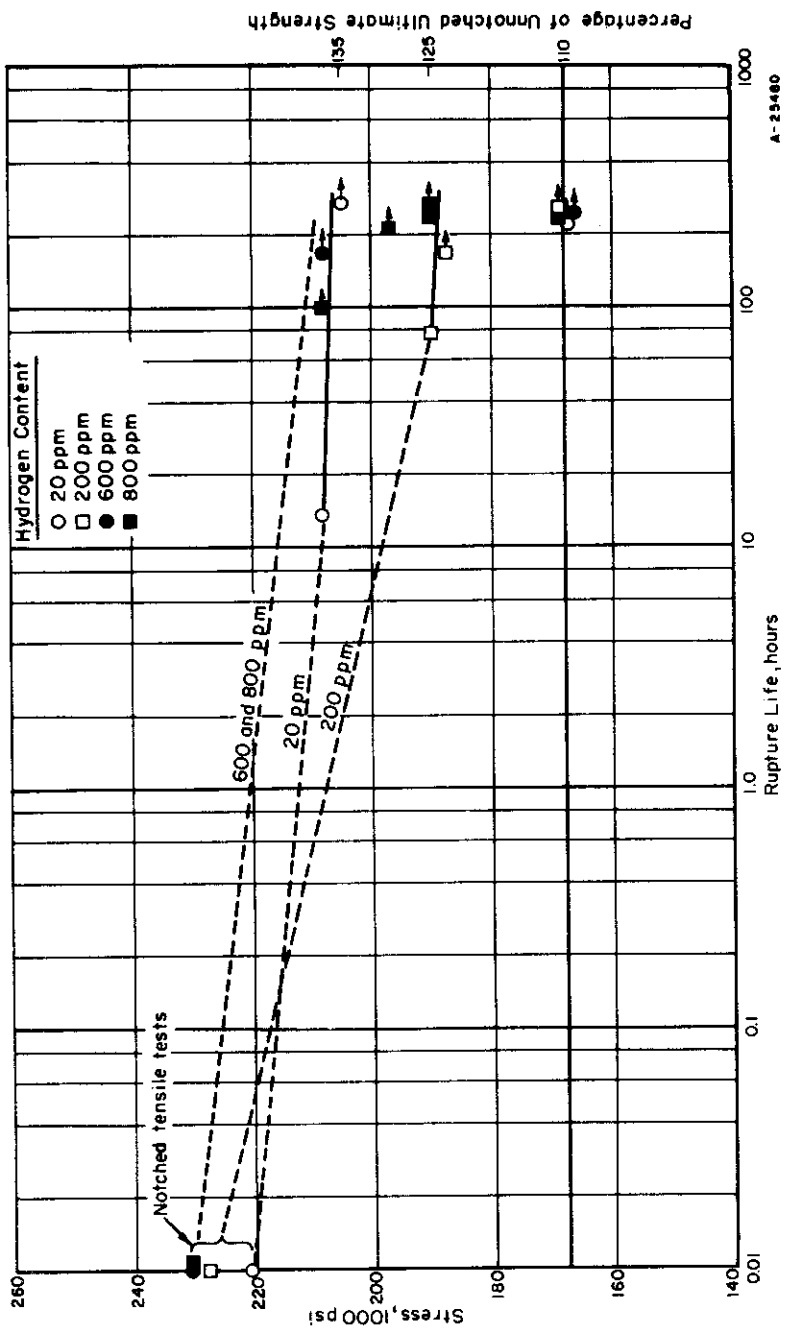

FIGURE 24. THE EFFECT OF HYDROGEN ON THE NOTCHED STRESS-RUPTURE PROPERTIES OF Ti-4Al-4Mn IN THE AS-SOLUTION HEAT-TREATED, FINE EQUIAXED ALPHA CONDITION (K-38-2)

TABLE 11. NOTCHED TENSILE PROPERTIES OF ALLOYS TESTED AT 0.005 INCH/MINUTE PLATEN SPEED

Alloy	Nominal Composition (Balance Titanium), weight per cent	Hydrogen Content, ppm	Notched Tensile Properties, $K_t = 3$	
			Ultimate Strength, psi	Reduction in Area, %
K-1	4Mo	20	148,000	21.2
		200	148,600	25.0
		600	146,000	17.3
		800	138,800	8.1
K-20	20Mo	20	209,600	6.0
		200	200,900	2.7
		600	203,400	4.6
		800	206,900	4.3
K-15	4Fe	20	153,000	6.9
		200	157,500	5.1
K-25	2Mn-2Cr	20	162,100	22.4
		300	157,500	17.1
		400	156,000	13.4
K-38-1	4Al-4Mn (Stabilized, fine equiaxed)	20	212,300	8.5
		200	227,800	11.1
		300	228,800	10.7
		400	231,000	10.8
		600	220,200	7.4
K-38-2	4Al-4Mn (Solution heat treated, fine equiaxed)	20	221,200	9.8
		200	227,700	12.0
		600	230,900	12.2
		800	230,800	10.9
K-38-4	4Al-4Mn (Stabilized, coarse acicular)	20	204,800	11.3
		100	210,200	7.2
		200	219,900	9.3

embrittlement quite clearly, however, as shown by comparing Figure 20 with Figure 23. Ti-2Mn-2Cr, which was embrittled at 200 ppm of hydrogen, showed progressive loss in ductility under the notch in tensile testing, but was still reasonably ductile at 400 ppm of hydrogen. An abrupt loss in ductility was observed at 200 ppm of hydrogen in rupture testing, showing that loss in ductility was a useful criterion for embrittlement in this alloy. The stabilized Ti-4Al-4Mn sample (K-38-1) reacted differently. In this alloy the following behavior was observed.

Embrittlement based on time to failure	400 to 600 ppm
Ductility loss in notched stress-rupture testing	Progressive from 20 ppm
Ductility loss in notched tensile testing	None

Selection of the embrittlement level in this alloy on the basis of notched ductility was impossible. However, the drop in rupture life was quite definite. Although ductility is apparently lost in notched stress-rupture testing when embrittlement occurs, the variations in notched ductility inherent in the alloys seem to overshadow the ductility loss due to embrittlement. Therefore, rupture life was used as the only criterion for embrittlement in this investigation.

The notched tensile data given in Table 11 also illustrate a second effect of hydrogen. Hydrogen in solution can have a significant strengthening effect. Increased strength was most often noticed in aluminum-containing alloys and is apparently due to the increased solubility of hydrogen in alpha titanium alloyed with aluminum.

On the basis of the above program, it was apparent that embrittlement could be detected by loading notched samples to a stress equal to about 110 per cent of the unnotched ultimate tensile strength. Embrittled alloys in this test would fail in a short time, generally 10 hours or less, while alloys free from embrittlement would withstand loading for 100 hours or more without failure. The following test procedure was therefore selected for evaluating the alloy and compositional variations being examined:

(1) For each alloy, the hydrogen level just below the unnotched embrittlement level found previously[2] was tested at a stress level of 110 per cent of the unnotched tensile strength. This hydrogen level was chosen because preliminary testing indicated embrittlement in the notched test would be at or below the unnotched-embrittlement level.

(2) If embrittlement was indicated at this level (as shown by short-time failure), the next lower hydrogen level was tested under the same stress conditions. Failure in less than 50 hours was assumed to indicate embrittlement.

(3) If no brittleness was indicated in the first sample (as evidenced by a 100-hour runout), the next higher hydrogen level was tested.

(4) Depending on the results obtained above, additional tests were run to bracket the hydrogen embrittlement level. The embrittlement level was considered bracketed when a runout was obtained at a particular hydrogen level and the next higher level produced a short-time failure. Where an alloy containing 800 ppm of hydrogen ran out, however, the tolerance level was taken as being greater than 800 ppm.

(5) The alloys were examined at hydrogen levels of 20, 200, 300, 400, 600, and 800 ppm. Studies on the effect of heat treatment included the 100-ppm hydrogen level in addition to those already mentioned.

The notched rupture-stress level was generally based upon an average tensile strength of the alloy taken, without regard to hydrogen content, from the unnotched tensile strengths obtained previously. In most cases the average unnotched tensile strength taken from tests at several different hydrogen levels did not deviate significantly from the individual strength values. If consistent strength changes were observed to occur as hydrogen content was varied, the notch testing stress was based on the tensile strength of the hydrogen level being tested.

Metallographic and Hardness Examination

Following rupture testing, the notched specimens were sectioned longitudinally to examine the region of flow or fracture for the presence of hydride. If hydride was present at the notch, but not in unstrained portions of the specimen, it was assumed to have been precipitated under strain. Hardness readings were taken on an unstrained portion of the metallographic specimen. These data, in conjunction with metallographic examination of the structure, were used primarily to insure that sample mixups did not occur during processing of the large number of alloys examined.

Results

A complete tabulation of the results of notch stress-rupture testing, hardness testing, and metallographic examination is given in the Appendix. The results of these studies are summarized and compared with data reported in WADC TR 54-616, Part IV[2] in Tables 12 through 17. Embrittlement is reported by giving both the highest hydrogen content showing ductile behavior and the lowest hydrogen content resulting in embrittlement. The hydrogen tolerance of the alloys to low-strain-rate embrittlement is assumed to lie between these values.

Effect of Alloy Content

The hydrogen tolerance of binary titanium-base alloys is given in Table 12. In general, notched stress-rupture testing resulted in the observation of embrittlement at lower hydrogen contents than unnotched stress-rupture testing. Some of the alloys appeared to be notch sensitive, so that notched stress-rupture testing was especially severe. The chromium-containing alloys had to be tested at 102 rather than 110 per cent of the unnotched tensile strength, for example, to observe ductile behavior at 20 ppm. The Ti-7Ni alloy was also generally brittle in notch testing. As in previous work, the binary Ti-Ta, Ti-Cu, and Ti-Ni alloys showed no low strain-rate embrittlement tendencies. Molybdenum-containing alloys were significantly more tolerant of hydrogen than the other alloys tested. The superiority of Ti-Cr or Ti-Cb alloys to Ti-Mn, Ti-Fe, or Ti-V alloys previously noted in unnotched examination was lost in notched stress-rupture testing. This is probably a result of differences in the basic notch sensitivity of the various alloys.

Increased hydrogen tolerance with increased amounts of beta was apparent in Ti-Mo, Ti-V, and Ti-Mn alloys. Ti-Cr alloys became more susceptible to embrittlement as the beta content increased, while Ti-Fe and Ti-Cb alloys showed the abrupt decrease in tolerance with increased beta content indicative of a shift from an alpha matrix to a semicontinuous beta matrix.

Strain-induced hydride was observed in Ti-Cb, Ti-Mn, Ti-Cr, and Ti-Fe alloys. Thermally precipitated hydride was seen in Ti-Ta, Ti-Cb, and Ti-Fe alloys but not, contrary to expectations, in Ti-Cu or Ti-Ni alloys. Strain-induced hydride was not identified definitely in Ti-V and Ti-Mo alloys. The Ti-V samples were inadvertently mounted in bakelite, and the moderately high temperatures occurring during the mounting process may have caused re-solution of any hydride present. Usually, specimens were mounted in a room-temperature-setting resin.

TABLE 12. LOW-STRAIN-RATE EMBRITTLEMENT IN BINARY TITANIUM-BASE ALLOYS

Composition, weight per cent	Alloy	Volume Per Cent Beta	Metallographic Evidence of Strain-Induced Hydride, ppm	Results of Unnotched Tests		Results of Notched Tests	
				Ductile, ppm hydrogen	Brittle, ppm hydrogen	Ductile, ppm hydrogen	Brittle, ppm hydrogen
Ti-4Mo	K1	20	>800	600	800	300	400
Ti-8Mo	K2	35	>800	800	--	800	--
Ti-20Mo	K3	80	>800	800	--	800	--
Ti-4V	K4	20	>200	20	200	20	200
Ti-8V	K5	35	>200	20	200	20	200
Ti-20V	K6	70	>800	800	--	800	--
Ti-4Ta	K7	10	<400(a)	400	--	800	--
Ti-8Ta	K8	15	None	800	--	800	--
Ti-4Cb	K9	20	<600(a)	800	--	600	800
Ti-8Cb	K10	35	200	400	600	20	200
Ti-4Mn	K11	30	200	20	200	20	200
Ti-6Mn	K12	40	400(?)	400	600	20	200
Ti-8Mn	K13-1	50	400	200	300	300	400
Ti-4Cr	K16	25	200	20	200	20	200
Ti-6Cr	K17	30	200	200	300	20	200
Ti-8Cr	K18	40	200	400	600	--	20
Ti-2Fe	K14	30	200	600	--	600	800
Ti-4Fe	K15	40	200	20	200	20	200
Ti-4Cu	K19	0	>800	200	--	800	--
Ti-7Cu	K20	0	>800	20	--	800	--
Ti-4Ni	K68	0	>800	800	--	800	--
Ti-7Ni	K69	0	>800	400	--	--	20

(a) Probably thermally precipitated hydride.

TABLE 13. LOW-STRAIN-RATE EMBRITTLEMENT IN TITANIUM-BASE ALLOYS CONTAINING MULTIPLE BETA STABILIZERS

Composition, weight per cent	Alloy	Metallographic Evidence of Strain-Induced Hydride, ppm	Results of Unnotched Tests		Results of Notched Tests	
			Ductile, ppm hydrogen	Brittle, ppm hydrogen	Ductile, ppm hydrogen	Brittle, ppm hydrogen
			Beta-Isomorphous : Beta-Isomorphous			
Ti-20Mo	K3	>800	800	--	800	--
Ti-8Mo-8V	K23	None	800	--	800	--
Ti-20V	K6	>800	800	--	800	--
Ti-8Mo	K2	>800	800	--	800	--
Ti-4Mo-4V	K22	>600	200	800	400	600
Ti-8V	K5	>200	20	200	20	200
Ti-4Mo	K1	>800	600	800	300	400
Ti-2Mo-2V	K21	200	400	--	20	200
Ti-4V	K4	>200	20	200	20	200
			Beta-Isomorphous : Sluggish-Eutectoid			
Ti-4Mo	K1	>800	600	800	300	400
Ti-2Mo-2Mn	K29	>200	200	300	20	200
Ti-4Mn	K11	200	20	200	20	200
Ti-4Mo	K1	>800	600	800	300	400
Ti-2Mo-2Cr	K32	>300	200	300	20	200
Ti-4Cr	K16	200	20	200	20	200
Ti-4Mo	K1	>800	600	800	300	400
Ti-2Mo-2Fe	K30	>200	200	300	20	200
Ti-4Fe	K15	200	20	200	20	200
Ti-4V	K4	>200	20	200	20	200
Ti-2V-2Fe	K31	200	20	200	20	200
Ti-4Fe	K15	200	20	200	20	200

TABLE 13. (Continued)

Composition, weight per cent	Alloy	Metallographic Evidence of Strain-Induced Hydride, ppm	Results of Unnotched Tests		Results of Notched Tests	
			Ductile, ppm hydrogen	Brittle, ppm hydrogen	Ductile, ppm hydrogen	Brittle, ppm hydrogen
Beta-Isomorphous : Sluggish-Eutectoid (Continued)						
Ti-4Mo	K1	>800	600	800	300	400
Ti-4Fe	K15	200	20	200	20	200
Ti-6Cr	K17	200	200	300	20	200
Ti-2Mo-2Fe-2Cr	K33-1	>300	300	--	100	200
Sluggish-Eutectoid : Sluggish-Eutectoid						
Ti-4Mn	K11	200	20	200	20	200
Ti-2Mn-2Cr	K25	300	300	400	20	200
Ti-4Cr	K16	200	20	200	20	200
Ti-4Mn	K11	200	20	200	20	200
Ti-2Mn-2Fe	K24	200	20	200	20	200
Ti-4Fe	K15	200	20	200	20	200
Ti-4Cr	K16	200	20	200	20	200
Ti-2Cr-2Fe	K26	>200	20	200	20	200
Ti-4Fe	K15	200	20	200	20	200
Ti-6Cr	K17	200	200	300	20	200
Ti-3Cr-3Fe	K27	>200	20	200	20	200
Ti-4Fe	K15	200	20	200	20	200
Ti-4Fe	K15	200	20	200	20	200
Ti-6Mn	K12	400(?)	400	600	20	200
Ti-6Cr	K17	200	200	300	20	200
Ti-2Fe-2Mn-2Cr	K28	>200	20	200	20	200
Beta-Isomorphous : Active-Eutectoid						
Ti-4Mo	K1	>800	600	800	300	400
Ti-2Mo-2Cu	K71	--	200	--	--	200
Ti-4Cu	K19	>800	200	--	800	--

TABLE 13. (Continued)

Composition weight per cent	Alloy	Metallographic Evidence of Strain-Induced Hydride, ppm	Results of Unnotched Tests		Results of Notched Tests	
			Ductile, ppm hydrogen	Brittle, ppm hydrogen	Ductile, ppm hydrogen	Brittle, ppm hydrogen
		Sluggish Eutectoid : Active-Eutectoid				
Ti-4Mn	K11	200	20	200	20	200
Ti-2Mn-2Cu	K70	200	200	800	20	200
Ti-4Cu	K19	>800	200	--	800	--

TABLE 14. LOW-STRAIN-RATE EMBRITTLEMENT IN ALUMINUM- AND TIN-CONTAINING TITANIUM-BASE ALLOYS

Composition, weight per cent	Alloy	Metallographic Evidence of Strain-Induced Hydride, ppm	Results of Unnotched Tests		Results of Notched Tests	
			Ductile, ppm hydrogen	Brittle, ppm hydrogen	Ductile, ppm hydrogen	Brittle, ppm hydrogen
Ti-4Mo	K1	>800	600	800	300	400
Ti-4Al-4Mo	K34	>800	800	--	800	--
Ti-6Al-4Mo	K35	>800	800	--	800	--
Ti-12Sn-4Mo	K73	>800	800	--	800	--
Ti-4V	K4	>200	20	200	20	200
Ti-4Al-4V	K36	800	600	--	300	400
Ti-6Al-4V	K37-1	>800	800	--	800	--
Ti-12Sn-4V	K74	>400	300	--	300	400
Ti-4Mn	K11	200	20	200	20	200
Ti-4Al-4Mn	K38-1	>600	300	400	400	600
Ti-6Al-4Mn	K39	>800	800	--	800	--
Ti-12Sn-4Mn	K75	>300	200	300	20	200
Ti-4Cr	K16	200	20	200	20	200
Ti-4Al-4Cr	K42	>400	400	600	20	200
Ti-6Al-4Cr	K43	--	--	20	--	--
Ti-12Sn-4Cr	K77	>400	200	--	300	400
Ti-2Fe	K14	200	600	--	800	800
Ti-4Al-2Fe	K40	200[a]	20	200	20	200
Ti-6Al-2Fe	K41	600[a]	400	600	400	600
Ti-12Sn-2Fe	K76	200	20	200	20	200
Ti-2Cr-2Fe	K26	>200	20	200	20	200
Ti-4Al-2Cr-2Fe	K44	>400	400	600	300	400
Ti-2Mo-2Fe-2Cr	K33-1	>300	300	--	100	200
Ti-4Al-1.3Mo-1.3Fe 1.3Cr	K45	>600	300	600	300	400
Ti-7Cu	K69	>800	800	--	800	--
Ti-4Al-7Cu	K72	>800	200	800	600	800
Ti-12Sn-7Cu	K78	>800	200	--	600	800

TABLE 15. LOW-STRAIN-RATE EMBRITTLEMENT IN TITANIUM-BASE ALLOYS FOR VARYING INTERSTITIAL CONTENT

Composition, weight per cent	Alloy	Metallographic Evidence of Strain-Induced Hydride, ppm	Results of Unnotched Tests		Results of Notched Tests	
			Ductile, ppm hydrogen	Brittle, ppm hydrogen	Ductile, ppm hydrogen	Brittle, ppm hydrogen
Ti-4Mo						
Iodide	K46	>800	800	--	--	800
Sponge	K1	>800	600	800	300	400
O_2 added	K48	>300	200	400	200	300
Ti-20Mo						
Iodide	K47	>800	800	--	800	--
Sponge	K3	>800	800	--	800	--
O_2 added	K49	600	400	600	400	600
Ti-4V						
Iodide	K50	--	400	--	200	--
Sponge	K4	>200	20	200	20	200
O_2 added	K52	100	20	100	20	100
Ti-20V						
Iodide	K51	>800	800	--	800	--
Sponge	K6	>800	800	--	800	--
O_2 added	K53	>800	800	--	800	--
Ti-8Mn						
Iodide	K54	--	300	400	--	400
Sponge	K13-1	400	200	300	300	400
O_2 added	K55	>300	200	300	200	300
Ti-6Cr						
Iodide	K56	--	400	--	--	400
Sponge	K17	200	200	300	20	200
O_2 added	K57	>200	200	300	20	200

TABLE 15. (Continued)

Composition, weight per cent	Alloy	Metallographic Evidence of Strain-Induced Hydride, ppm	Results of Unnotched Tests		Results of Notched Tests	
			Ductile, ppm hydrogen	Brittle, ppm hydrogen	Ductile, ppm hydrogen	Brittle, ppm hydrogen
Ti-7Cu						
Iodide	K80	800[a]	800	--	800	--
Sponge	K20	>800	20	--	800	--
O_2 added	K79	>800	800	--	800	--
Ti-6Al-4Mo						
Iodide	K58	>800	800	--	800	--
Sponge	K35	>800	800	--	800	--
O_2 added	K59	>800	800	--	800	--
Ti-6Al-4V						
Iodide	K60	--	600	--	600	--
Sponge	K37-1	>800	800	--	800	--
O_2 added	K61	>800	400	600	800	--
Ti-4Al-4Mn						
Iodide	K62	--	400	--	400	--
Sponge	K38-1	>600	300	400	400	600
O_2 added	K63	>600	200	300	300	400
Ti-4Al-4Fe						
Iodide	K64	--	200	400	--	400
O_2 added	K65	>300	200	300	200	300
Ti-4Al-4Cr						
Iodide	K66	--	400	--	--	--
Sponge	K42	>400	400	600	20	200
O_2 added	K67	--	--	20	--	--

(a) Acicular hydride in alpha.

TABLE 16. EFFECT OF HEAT TREATMENT ON THE HYDROGEN TOLERANCE OF FIVE TITANIUM-BASE ALLOYS

Heat Treatment and Type of Alpha	Alloy	Metallographic Evidence of Strain-Induced Hydride, ppm	Results of Unnotched Tests		Results of Notched Tests	
			Ductile, ppm hydrogen	Brittle, ppm hydrogen	Ductile, ppm hydrogen	Brittle, ppm hydrogen
		Ti-8Mn				
Solution heat treated, equiaxed	K13-2	>800	300	600	600	800
Stabilized, equiaxed	K13-1	400	200	300	300	400
Solution heat treated and aged, equiaxed	K13-3	200	100	200	100	200
Solution heat treated, acicular	K13-5	>800	400	--	600	800
Stabilized, acicular	K13-4	>300	200	300	200	300
Solution heat treated and aged, acicular	K13-6	200	20	100	20	100
		Ti-2Mo-2Fe-2Cr				
Solution heat treated, equiaxed	K33-2	400	200	600	300	400
Stabilized, equiaxed	K33-1	>300	300	--	100	200
Solution heat treated and aged, equiaxed	K33-3	200	200	300	20	100
Solution heat treated, acicular	K33-5	>300	300	400	200	300
Stabilized, acicular	K33-4	300	200	300	100	200
Solution heat treated and aged, acicular	K33-6	100	100	200	20	100
		Ti-6Al-4V				
Solution heat treated, equiaxed	K37-2	>800	600	800	800	--
Stabilized, equiaxed	K37-1	>800	800	--	800	--
Solution heat treated and aged, equiaxed	K37-3	>600	400	--	400	600
Solution heat treated, acicular	K37-5	>800	600	800	800	--
Stabilized, acicular	K37-4	>800	200	600	800	--
Solution heat treated and aged, acicular	K37-6	>300	200	400	200	300
		Ti-4Al-4Mn				
Solution heat treated, equiaxed	K38-2	>800	800	--	800	--
Stabilized, equiaxed	K38-1	>600	300	400	400	600
Solution heat treated and aged, equiaxed	K38-3	>300	100	200	200	300
Solution heat treated, acicular	K38-5	>800	800	--	800	--
Stabilized, acicular	K38-4	>600	100	200	400	600
Solution heat treated and aged, acicular	K38-6	100	100	200	20	100

TABLE 17. THE EFFECT OF GRAIN SIZE ON THE HYDROGEN TOLERANCE OF FOUR TITANIUM ALLOYS

Alpha Grain Size and Type	Alloy	Results of Unnotched Tests		Results of Notched Tests	
		Ductile, ppm hydrogen	Brittle, ppm hydrogen	Ductile, ppm hydrogen	Brittle, ppm hydrogen
		Ti-8Mn			
Fine (4 μ) equiaxed	K13-7	200	--	--	--
Medium (6 μ) equiaxed	K13-1	200	300	300	400
Coarse (8 μ) equiaxed	K13-8	200	300	--	--
Medium acicular	K13-9	200	300	200	--
Coarse acicular	K13-4	200	300	200	300
		Ti-6Al-4V			
Fine (6 μ) equiaxed	K37-1	800	--	800	--
Medium (12 μ) equiaxed	K37-7	400	--	--	--
Coarse (24 μ) equiaxed	K37-8	20	200	--	--
Medium acicular	K37-9	400	--	400	--
Coarse acicular	K37-4	200	600	800	--
		Ti-4Al-4Mn			
Fine (4 μ) equiaxed	K38-1	300	400	400	600
Medium (16 μ) equiaxed	K38-7	300	--	800	--
Coarse (24 μ) equiaxed	K38-8	20	200	600	800
Fine acicular	K38-9	300	--	400	600
Coarse acicular	K38-4	100	200	400	600

The effect on hydrogen tolerance of multiple beta-stabilizing additions is shown in Table 13. Notched stress-rupture testing confirmed the previous conclusion[2] that the susceptibility of complex alloys to low-strain-rate embrittlement is intermediate between those of the equivalent binary alloys. In most instances, notch testing indicated the hydrogen tolerance to be 100 ppm or more lower than that indicated by unnotched testing.

The effects of aluminum and tin on low-strain-rate embrittlement are summarized in Table 14. Hydrogen tolerance was greatly improved by aluminum and somewhat improved by tin in most cases. However, as previously noted, both aluminum and tin resulted in the beta-free Ti-4Al-7Cu and Ti-12Sn-7Cu alloys showing low-strain-rate embrittlement. Strain-induced hydride was observed in the alpha phase in two of the titanium-aluminum alloys, but very rarely in the alpha-beta interface, even in cases where pronounced embrittlement was indicated (see, for example, Ti-4Al-1.3Mo-1.3Fe-1.3Cr). Aluminum, and possibly tin also, appear to retard hydride formation. Thus Ti-4Al-4V showed embrittlement at 400 ppm, but visible hydride was not seen until 800 ppm hydrogen was present.

Increasing interstitial content resulted in decreasing hydrogen tolerance, as shown in Table 15. The results presented in this table also show the trend for the hydrogen tolerance to be lower in notched than in unnotched rupture testing. It is of interest that hydride was observed in the high interstitial Ti-Mo and Ti-V alloys and in an iodide Ti-Cu alloy. Hydride was not observed in low-interstitial samples of these alloys.

Effect of Heat Treatment

A complete description of the properties of the alloys heat treated to various strengths for this program is given in WADC 54-616, Part IV[2]. In general, tolerance was observed to vary with final heat treatment temperature (1300 F for solution heat treated, 1100 F for stabilized, and 900 F for aged material) instead of strength. The hydrogen tolerances as determined by notched testing are summarized in Table 16. As in unnotched testing, a direct correlation with final heat treatment temperature and embrittlement in notched rupture testing was observed. The aluminum-free alloys tended to show a reduction in hydrogen tolerance of 100 to 200 ppm in notched testing, and hydride was often observed. The aluminum-containing alloys, on the other hand, showed hydride in only one sample, and the hydrogen tolerance was higher in notched than in unnotched testing in several cases. This may be a reflection of the strengthening effect of hydrogen in these alloys demonstrated by the notched tensile testing summarized in Table 11. If strengthening occurs, the alloy may show increasing resistance to flow as hydrogen is increased, and thus tend to be less

sensitive to embrittlement when testing is conducted at a constant stress based on the average unnotched tensile strength. Strengthening was not nearly as pronounced in unnotched as in notched tensile tests. The low reduction in area observed in samples which did not fail, supports this conjecture.

Testing in all microstructural conditions was conducted on only one of the four alloy series designed to demonstrate the effects of grain size on hydrogen tolerance. Ti-4Al-4Mn was selected for this examination. The results of notched and unnotched stress-rupture tests are summarized in Table 17. Notch testing was conducted on freshly heat-treated material. To avoid difficulties previously encourtered with patches of acicular structure, the coarse equiaxed grain sizes were produced by slightly different heat treatments. The new heat treatments were as follows:

K-38-7: 6 hours at 1550 F, furnace cool to 1100 F, hold 1 hour, air cool (in argon)

K-38-8: 48 hours at 1550 F, furnace cool to 1100 F, hold 1 hour, air cool (in argon)

Hydrogen tolerance as indicated by notched stress-rupture testing did not agree well with those indicated by unnotched testing. Again, the origin of this difference may have been strengthening of the alloy by hydrogen in solution.

Strain-Induced Hydride

Three separate types of structures tentatively identified[a] as strain-induced hydride were observed in these alloys: grain boundary, massive, and acicular. The appearance of grain-boundary hydride is shown in Figure 25. This type of hydride was most commonly observed in alloys containing large amounts of beta phase and hydrogen contents at or slightly in excess of the hydrogen tolerance to low-strain-rate embrittlement. Massive hydride is illustrated in Figure 26. This type of hydride was most common in alloys containing semicontinuous patches of beta in an alpha matrix. The hydride had apparently completely replaced beta in certain regions. The third type of strain-induced hydride, acicular hydride, was seen in only a few aluminum-containing alloys. It is shown in Figure 27. Acicular hydride differed from the other two types in that it was normally found only in the alpha phase.

(a) The identification of this phase as hydride is based upon its correlation with hydrogen content. No X-ray or analytical determinations have been made.

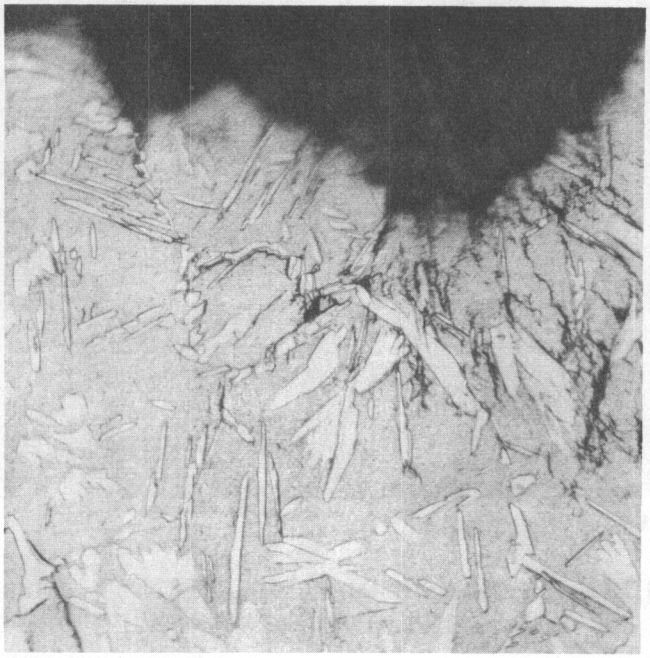

500X N45183

FIGURE 25. GRAIN BOUNDARY HYDRIDE IN Ti-8Mn (K-13-6) CONTAINING 200 PPM HYDROGEN

Much of the strain-induced hydride observed was secondary in origin, apparently precipitating along regions of high residual stress remaining after fracture rather than during the original stress-rupture test. Hydride precipitation of this type, accompanied by cracking perpendicular to the fracture surface, is illustrated in Figure 28.

In some series of samples, grain-boundary hydride was replaced by massive hydride as the hydride content increased. This suggests that massive hydride may form by the further growth of hydride initially formed in the alpha-beta interface until the beta phase is completely consumed.

Discussion of Results

The notched stress-rupture examination has resulted in a confirmation of most of the conclusions regarding the effects of alloying and heat treatment on hydrogen tolerance of titanium alloys resulting from the

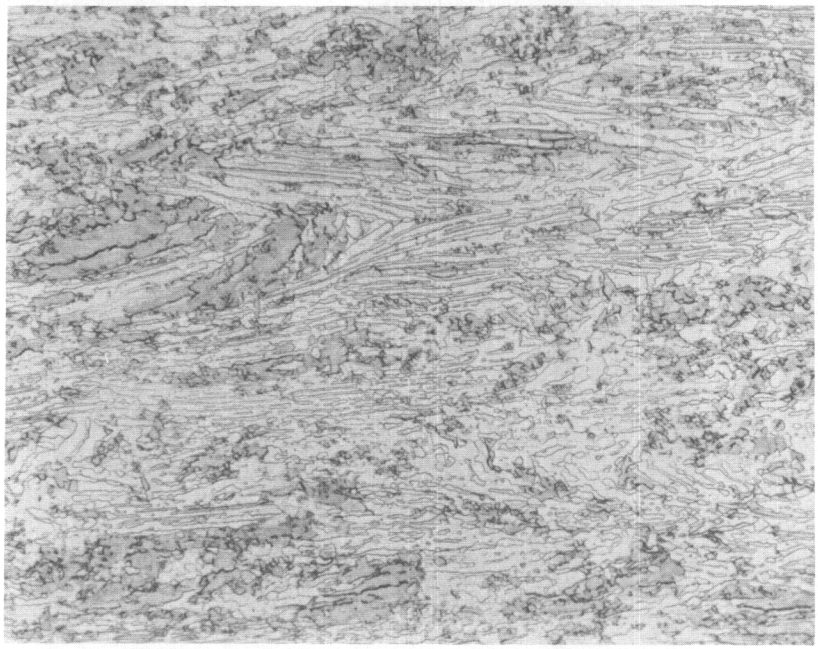

500X N44812

FIGURE 26. MASSIVE HYDRIDE IN Ti-2Mn-2Fe (K-24) CONTAINING 200 PPM HYDROGEN

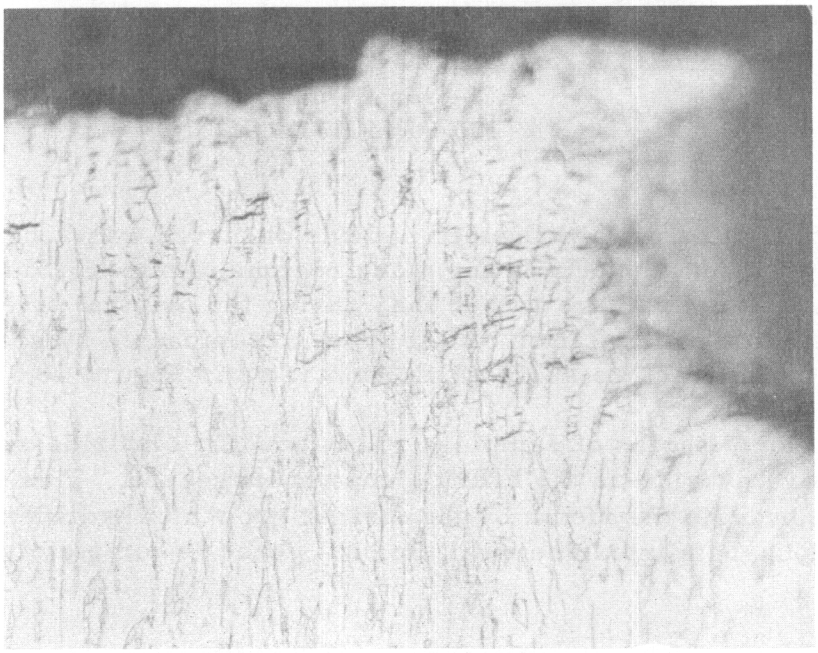

500X N44811

FIGURE 27. ACICULAR HYDRIDE IN THE ALPHA PHASE IN Ti-6Al-2Fe (K-41) CONTAINING 600 PPM HYDROGEN

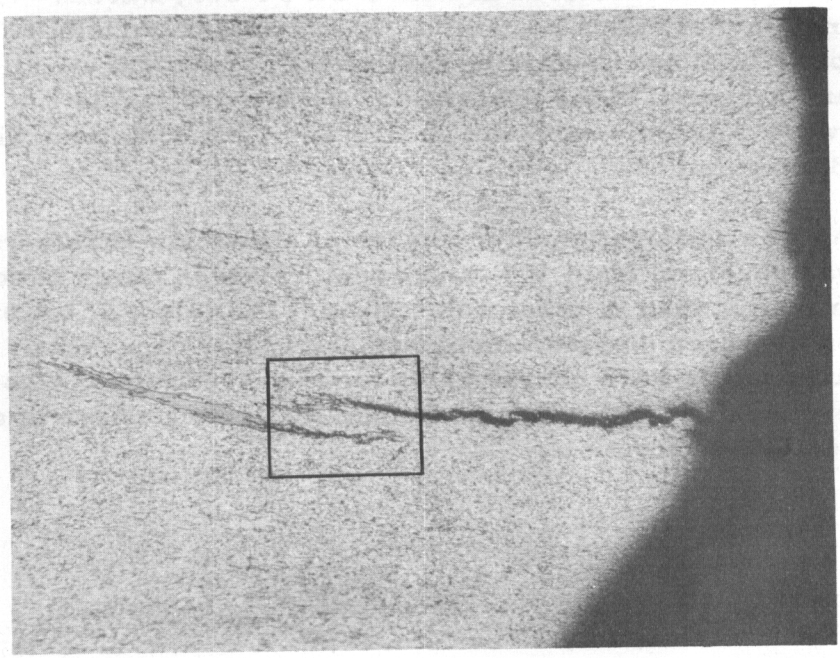

75X (a) N45177

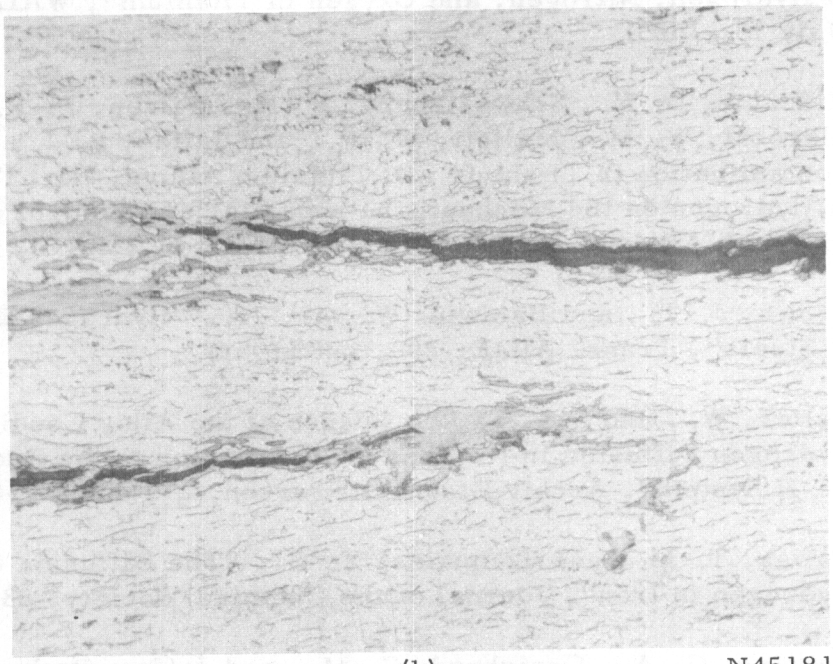

500X (b) N45181

FIGURE 28. SECONDARY STRAIN-INDUCED HYDRIDE IN A FRACTURED NOTCHED-STRESS-RUPTURE SAMPLE OF Ti-4V-0.95O_2 ALLOY (K-52) CONTAINING 100 PPM HYDROGEN

The lower photomicrograph is an enlargement of the region outlined in the upper.

original research described in WADC TR 54-616, Part IV(2). The principal difference is that alloys containing chromium and columbium lost their superiority to alloys containing manganese, iron, and vanadium in ability to withstand hydrogen in the presence of a notch. Titanium-molybdenum alloys were markedly superior to all other beta-containing binary alloys in notched examination.

As was anticipated, in a number of alloys low-strain-rate embrittlement was observed from 100 to 200 ppm hydrogen lower in notched stress-rupture testing than in unnotched testing. The effect of the presence of a notch on hydrogen embrittlement was quite alloy dependent. Chromium-containing alloys were considerably more susceptible to embrittlement in the presence of a notch while aluminum-containing alloys in some cases appeared less susceptible.

REFERENCES

(1) Wasilewski, R. J., and Kehl, G. L., "Summary Report on Diffusion of Hydrogen, Nitrogen, and Oxygen in Titanium", WAL 401/149-11A (July 13, 1953).

(2) Williams, D. N., Schwartzberg, F. R., Wilson, P. R., Albrecht, W. M., Mallett, M. W., and Jaffee, R. I., "Hydrogen Contamination in Titanium and Titanium Alloys, Part IV: The Effect of Hydrogen on the Mechanical Properties and Control of Hydrogen in Titanium Alloys", WADC TR 54-616, Part IV (March, 1957).

(3) Brown, J. T., and Baldwin, W. M., Jr., "Hydrogen Embrittlement of Steels", Trans. AIME, 200, 298 (1954).

(4) Geller, W., and Sun, T., "Influence of the Alloy Condition on the Hydrogen Diffusion in Iron and a Contribution to the Knowledge of the Fe-H System", Archiv Eisenhuttenwesen, 21, 423 (1950).

(5) Stross, T. M., and Tompkins, F. C., "The Diffusion Coefficient of Hydrogen in Iron", Journal of the Chemical Society, 230 (1956).

(6) Lenning, G. A., Craighead, C. M., and Jaffee, R. I., "Constitution and Mechanical Properties of Titanium-Hydrogen Alloys", Trans. AIME, 200, 367 (1954).

(7) Köster, W., Bangert, L., and Evers, M., "Damping Behavior of Hydrogen-Loaded Titanium", Z. Metall., 47, 564 (1956).

(8) McQuillan, A. D., "Hydrogen in Titanium and Its Alloys", NYU Titanium Course, Lecture No. 11 (September 12, 1956).

(9) **DOUGLASS, R. W., HOLDEN, F. C., OGDEN, H. R., and JAFFEE, R. I., "An Investigation of the Effects of Impurities and Metallurgical Variables On The Notch Sensitivity of Titanium Alloys", WADC TR 58-438, February 1958.**

(10) Lenning, G. A., Craighead, C. M., and Jaffee, R. I., "The Effect on Hydrogen on the Mechanical Properties of Titanium and Titanium Alloys", Summary Report to Watertown Arsenal, Contract No. DA-33-019-ORD-938 (July 31, 1954).

APPENDIX A

TABULATED TEST RESULTS

TABLE A-1. COMPLETE RESULTS OF THE ROOM-TEMPERATURE NOTCHED STRESS-RUPTURE TEST PROGRAM

Alloy	Composition (Balance Titanium), weight per cent	Specimen	Specimen Type	Hydrogen Content, ppm	Hardness (10-Kg Load), VHN	Applied Stress		Time to Failure, hr(a)	Reduction in Area, per cent(a)	General Microstructural Characteristics	Visible Hydride at Notch
						PSI	Per Cent of Unnotched UTS				
K-1	4Mo	04N	B	20	–	131,500	138	7.0	18.2	–	–
		03N	A	20	–	128,600	135	48.9	23.0	–	–
		02N	A	20	–	119,000	125	(212.8)	(3.3)	–	–
		01N	B	20	228	104,800	110	(215.7)	(1.1)	Alpha matrix	None
		24N	B	200	–	128,600	138	54.1	23.2	–	–
		22N	A	200	–	123,800	130	(209.9)	(5.3)	–	–
		23N	A	200	–	119,000	125	(256.6)	(6.7)	–	–
		21N	B	200	236	104,800	110	(215.3)	(2.5)	Alpha matrix	None
		31N	A	300	236	104,800	110	(117.0)	(2.0)	Ditto	None
		41N	A	400	238	104,800	110	17.5	8.0	"	Fine massive type(?)
		61N	A	600	230	104,800	110	6.7	6.5	"	None(?)
		62N	A	600	–	90,500	95	4.0	5.2	–	–
		63N	A	600	–	76,400	80	39.6	2.4	–	–
		64N	B	600	–	71,500	75	16.3	4.0	–	–
		81N	A	800	228	104,800	110	2.3	4.5	Alpha matrix	None(?)
		82N	A	800	–	90,500	95	8.0	3.9	–	–
		84N	A	800	–	76,400	80	18.0	1.5	–	–
		83N	B	800	–	66,700	70	19.0	0.5	–	–
K-2	8Mo	81N	A	800	266	120,700	110	(114.4)	(0.0)	About 25% equiaxed alpha; beta stained	None
K-3	20Mo	02N	B	20	–	176,500	130	97.0	4.6	–	–
		03N	A	20	–	169,800	125	(214.6)	(1.1)	–	–
		01N	B	20	289	149,400	110	(206.9)	(0.9)	Stringers of alpha particles in beta	None
		23N	A	200	–	183,200	135	30.7	3.7	–	–
		24N	B	200	–	179,200	132	(215.5)	(2.3)	–	–
		22N	A	200	–	176,500	130	(261.8)	(1.8)	–	–
		61N	A	200	297	149,400	110	(206.9)	(0.3)	Fewer alpha particles than 01N	None
		64N	A	600	–	187,400	138	(193.7)	(2.6)	–	–
		63N	A	600	–	183,200	135	(209.5)	(3.7)	–	–
		62N	A	600	–	176,500	130	(261.8)	(2.1)	–	–
		61N	B	600	289	149,400	110	(256.5)	(0.2)	Fewer alpha particles than 21N	None
		83N	A	800	–	183,200	135	(239.2)	(3.3)	–	–
		82N	A	800	–	179,200	132	(209.6)	(2.2)	–	–
		84N	A	800	–	176,500	120	199.9	6.6	–	–
		81N	B	800	297	149,400	110	(215.7)	(1.5)	Fewer alpha particles than 61N	None

TABLE A-1. COMPLETE RESULTS OF THE ROOM-TEMPERATURE NOTCHED STRESS-RUPTURE TEST PROGRAM (Continued)

Alloy	Composition (Balance Titanium), weight per cent	Specimen	Specimen Type	Hydrogen Content, ppm	Hardness (10-Kg Load), VHN	Applied Stress, PSI	Applied Stress, Per Cent of Unnotched UTS	Time to Failure, hr (a)	Reduction in Area, per cent (a)	General Microstructural Characteristics	Visible Hydride at Notch
K-4	4V	01N	B	20	254	114,800	110	(137.6)	(3.4)	Stringered beta in alpha matrix	None (Bakelite mount)
		21N	B	200	254	114,800	110	4.6	4.2	Ditto	Ditto
		22N	B	200	–	99,200	95	12.6	1.8	–	–
K-5	8V	01N	B	20	272	125,400	110	(137.7)	(1.2)	Alpha stringered in beta matrix	None (Bakelite mount)
		21N	A	200	270	128,800	110	6.3	7.0	Ditto	Ditto
		22N	A	200	–	111,200	95	105.8	4.9	–	–
K-6	20V	81N	A	800	264	136,200	110	(167.8)	(2.9)	Fine alpha particles in beta matrix	None (Bakelite mount)
K-7	4Ta	41N	B	400	224	97,300	110	(168.5)	(3.9)	Fine-grained alpha	Acicular type
		81N	A	800	240	97,300	110	(114.7)	(0.8)	Ditto	Course acicular type
K-8	8Ta	82N	B	800	230	108,600	110	(119.5)	(4.2)	Single-phase alpha (?)	None
K-9	4Cb	61N	B	600	210	96,800	110	113.8	5.2	–	Massive type
		81N	A	800	–	96,900	110	32.0	6.4	–	–
		82N	B	800	215	96,900	110	21.8	1.8	–	Massive and acicular types
K-10	8Cb	01N	A	20	230	101,300	110	(101.1)	1.7	Alpha matrix, wrought structure	None
		21N	A	200	228	101,300	110	9.5	4.0	Ditto	Heavy grain-boundary type
		42N	B	400	228	101,300	110	6.5	0.2	"	Ditto
K-11	4Mn	01N	A	20	254	120,800	110	(100.1)	(1.0)	Stringered beta in alpha matrix	None
		22N	A	200	243	120,800	110	6.2	6.1	Ditto	Heavy grain-boundary type
		31N	A	300	262	120,800	110	10.5	4.3	"	Ditto
		42N	B	400	253	120,800	110	3.5	2.6	"	"
K-12	6Mn	01N	A	20	270	132,500	110	(115.2)	(0.6)	Matrix appeared to be alpha	None
		21N	A	200	274	132,500	110	26.4	3.9	Ditto	None
		42N	B	400	272	132,500	110	0.9	1.2	"	Small amount of grain-boundary type (?)
K-13	8Mn	Data given following Alloy K-80									
K-14	2Fe	21N	A	200	207	94,500	110	132.3	5.0	Small amount of beta in fine-grained alpha matrix	Grain-boundary type
		61N	B	600	218	94,500	110	65.6	3.0	Ditto	Large amount of grain-boundary type
		81N	A	800	228	94,500	110	38.0	4.0	Inclusion in fracture region	Ditto
K-15	4Fe	04N	A	20	–	137,700	132	49.3	7.9	–	–
		03N	A	20	–	135,500	130	86.7	8.0	–	–
		02N	A	20	–	130,400	125	(214.3)	(2.6)	–	–

TABLE A-1. COMPLETE RESULTS OF THE ROOM-TEMPERATURE NOTCHED STRESS-RUPTURE TEST PROGRAM (Continued)

Alloy	Composition (Balance Titanium), weight per cent	Specimen	Specimen Type	Hydrogen Content, ppm	Hardness (10-Kg Load), VHN	Applied Stress PSI	Applied Stress Per Cent of Unnotched UTS	Time to Failure, hr(a)	Reduction in Area, per cent(a)	General Microstructural Characteristics	Visible Hydride at Notch
K-15	4Fe	01N	A	20	253	114,700	110	(207.4)	(0.6)	Small amount of stringered beta in alpha	None (?)
		21N	A	200	253	122,200	110	6.0	3.3	–	Extensive massive type
		22N	A	200	–	105,500	95	23.7	0.8	–	–
		23N	A	200	–	88,900	80	67.3	3.6	–	–
		24N	A	200	–	83,400	75	166.7	0.3	–	–
K-16	4Cr	01N	A	20	260	120,700	110	(162.4)	(1.7)	Stringered beta in alpha matrix	None
		22N	A	200	256	120,700	110	28.3	0.5	Ditto	Course grain-boundary type
K-17	6Cr	01N	B	20	–	135,000	110	(137.4)	(0.7)	Alpha matrix	None
		2NN	B	200	–	135,000	110	3.3	1.6	–	Grain-boundary type
K-18	8Cr	01N	B	20	283	130,600	110	7.9	1.8	Wrought structure, beta matrix	None
		02N	A	20	270	121,000	102	(165.8)	(3.0)	Ditto	None
		21N	A	200	287	130,600	110	2.8	1.3	"	Some grain-boundary type
		22N	A	200	281	121,000	102	5.2	0.6	"	Some grain-boundary type (?)
		41N	B	400	281	130,600	110	0.5	2.1	"	None (?)
		42N	A	400	287	121,000	102	2.6	0.5	"	Some grain-boundary type (?)
		61N	A	600	283	121,000	102	18.4	1.6	"	Grain-boundary hydride
K-19	4Cu	22N	B	20	213	95,900	110	(99.4)	(2.1)	Alpha plus compound	None
		61N	A	600	235	95,900	110	(100.6)	(1.2)	Ditto	None (?)
		81N	A	800	227	95,900	110	(139.0)	(1.3)	Alpha plus compound (compound more defined)	None (?)
K-20	7Cu	41N	B	400	238	112,700	110	(99.3)	(4.1)	Alpha plus uniform compound dispersion	None (?)
		81N	A	800	245	112,700	110	(114.3)	(0.9)	Ditto	None (?)
K-21	2Mo-2V	01N	B	20	228	105,000	110	(100.0)	(1.6)	Fine beta stringers in alpha matrix	None
		21N	B	200	227	105,000	110	19.9	5.3	Ditto	Massive type
		41N	A	400	230	105,000	110	8.6	1.3	"	Large amount of massive type
		61N	A	600	228	105,000	110	6.3	1.9	Hydride present in unstrained areas	Ditto
K-22	4Mo-4V	21N	A	200	262	122,500	110	(114.5)	(0.0)	Very fine structure, stringered alpha in beta matrix	None
		41N	A	400	259	122,500	110	(100.9)	(1.2)	–	None
		61N	B	600	263	122,500	110	1.0	7.6	More beta than in 21N or 41N	None
K-23	8Mo-8V	81N	A	800	297	145,500	110	(118.9)	(0.0)	Alpha stringers in beta	None
K-24	2Mn-2Fe	01N	A	20	240	114,600	110	(143.0)	(1.6)	Stringered beta in alpha matrix	None
		21N	A	200	254	114,600	110	10.6	2.0	Ditto	Massive type

TABLE A-1. COMPLETE RESULTS OF THE ROOM-TEMPERATURE NOTCHED STRESS-RUPTURE TEST PROGRAM (Continued)

Alloy	Composition (Balance Titanium), weight per cent	Specimen	Specimen Type	Hydrogen Content, ppm	Hardness (10-Kg Load), VHN	Applied Stress		Time to Failure, hr[a]	Reduction in Area, per cent[a]	General Microstructural Characteristics	Visible Hydride at Notch
						PSI	Per Cent of Unnotched UTS				
K-25	2Mn-2Cr	02N	C	20	–	152,500	146	0.1	20.0	–	–
		01NX	A	20	–	143,000	137	103.6	19.3	–	–
		01N	A	20	249	114,700	110	(205.6)	(2.3)	Wrought structure, alpha matrix	None
		23N	B	200	256	114,700	110	19.6	6.4	Extensive staining	None
		22N	C	200	–	99,100	95	72.6	3.3	–	–
		21N	A	200	–	83,400	80	(205.6)	(0.5)	–	–
		33N	C	300	251	114,700	110	11.7	4.6	–	Some grain-boundary type
		34N	B	300	–	114,700	110	13.0	5.7	–	–
		32N	C	300	–	99,100	95	31.0	3.6	–	–
		35N	B	300	–	83,400	80	95.1	3.1	–	–
		43N	C	400	256	114,700	110	8.8	2.6	Hydride seems to completely fill beta areas, grain-boundary type approaching massive type	Large amount of grain-boundary type
		44N	B	400	–	114,700	110	5.8	3.7	–	–
		42N	C	400	–	99,100	95	18.2	0.6	–	–
		45N	B	400	–	83,400	80	90.3	1.1	–	–
K-26	2Cr-2Fe	01N	B	20	233	114,200	110	(151.9)	(1.8)	Wrought structure, beta matrix (?)	None
		21N	B	200	245	114,200	110	9.7	3.5	–	None
K-27	3Cr-3Fe	01N	B	20	261	133,200	110	(116.7)	(0.7)	Wrought structure	None
		21N	B	200	261	133,200	110	2.9	3.2	Beta-phase stained	None
K-28	2Mn-2Cr-2Fe	01N	B	20	281	131,400	110	(112.9)	(0.7)	Beta matrix, grain-boundary alpha, alpha particles in beta	None
		21N	A	200	283	138,000	110	4.0	3.4	–	None (Bakelite mount)
		22N	A	200	–	119,200	95	19.7	2.7	–	–
K-29	2Mo-2Mn	01N	B	20	262	116,600	110	(144.3)	(0.6)	Wrought structure, alpha matrix	None
		21N	A	200	253	116,600	110	22.3	5.2	–	None (Bakelite mount)
		22N	B	200	–	100,800	95	64.4	3.1	–	–
K-30	2Mo-2Fe	01N	B	20	276	128,200	110	(117.0)	(2.5)	Beta in alpha matrix	None
		21N	A	200	281	128,200	110	6.0	3.5	–	None (?)
		22N	B	200	–	110,800	95	6.7	1.1	–	–
K-31	2V-2Fe	01N	B	20	238	113,600	110	(143.0)	(2.5)	Alpha matrix, some fine precipitate	None
		21N	B	200	240	113,600	110	18.5	2.7	–	Massive type
K-32	2Mo-2Cr	01N	B	20	251	121,000	110	(143.1)	(2.3)	Acicular alpha in beta matrix	None
		21N	B	200	253	121,000	110	37.7	5.8	–	None
		31N	A	300	258	121,000	110	13.4	6.0	–	None (?)

TABLE A-1. COMPLETE RESULTS OF THE ROOM-TEMPERATURE NOTCHED STRESS-RUPTURE TEST PROGRAM (Continued)

Alloy	Composition (Balance Titanium), weight per cent	Specimen	Specimen Type	Hydrogen Content, ppm	Hardness (10-Kg Load), VHN	Applied Stress PSI	Applied Stress Per Cent of Unnotched UTS	Time to Failure, hr[a]	Reduction in Area, per cent[a]	General Microstructural Characteristics	Visible Hydride at Notch
K-33	2Mo-2Cr-2Fe	Data given following Alloy K-80									
K-34	4Al-4Mo	81N	B	800	342	157,500	110	(141.2)	(1.0))	Stringers of beta in an alpha matrix	None
K-35	6Al-4Mo	81N	B	800	383	190,800	110	(137.3)	(0.5)	Stringers of beta in an alpha matrix	None
K-36	4Al-4V	01N	B	20	319	152,000	110	(100.0)	(0.3)	Fine uniformly distributed beta in alpha matrix	None
		21N	A	200	319	152,000	110	(164.1)	(1.4)	–	None
		31N	A	300	330	152,000	110	78.3	5.0	–	None
		41N	B	400	317	152,000	110	22.2	4.8	–	None
		61N	B	600	317	152,000	110	24.3	3.5	–	None
		81N	A	800	314	152,000	110	12.4	3.0	–	Massive type
K-37	6Al-4V	Data given following Alloy K-80									
K-38	4Al-4Mn	Data given following Alloy K-80									
K-39	6Al-4Mn	81N	B	800	405	205,000	110	(141.5)	(0.3)	Stringers of alpha in beta	None
K-40	4Al-2Fe	01N	B	20	304	150,800	110	(162.5)	(1.1)	Wrought structure, alpha matrix	None
		21N	A	200	325	150,800	110	45.3	1.0	–	Acicular type in alpha
K-41	6Al-2Fe	41N	A	400	397	191,500	110	(141.1)	(0.0)	Stringered beta in an alpha matrix	None
		61N	B	800	383	199,200	110	5.0	1.9	–	Acicular type in alpha (?)
K-42	4Al-4Cr	01N	A	20	348	158,000	110	(115.4)	(0.8)	Wrought structure; beta appears to contain a precipitate: alpha matrix	None
		21N	A	200	339	158,000	110	1.7	2.0	–	None (?)
		41N	A	400	336	158,000	110	40.9	0.8	–	None (?)
K-43	6Al-4Cr	No notch tests were completed									
K-44	4Al-2Cr-2Fe	21N	B	200	376	180,100	110	(162.2)	(1.1)	Equiaxed alpha with uniformly distributed beta	None
		31N	A	300	390	180,100	110	(112.7)	(0.5)	–	None
		41N	A	400	383	180,100	110	13.1	3.1	–	None
K-45	4Al-1.3Cr-1.3Mo-1.3Fe	31N	B	300	327	189,400	110	(143.2)	(1.3)	Fine-grained, uniform alpha plus beta	None
		41N	B	400	390	189,400	110	25.0	2.8	–	None
		61N	A	600	387	189,400	110	9.3	0.2	–	None
K-46	4Mo (I)	81N	B	800	–	87,200	110	24.9	2.4	–	–

TABLE A-1. COMPLETE RESULTS OF THE ROOM-TEMPERATURE NOTCHED STRESS-RUPTURE TEST PROGRAM (Continued)

Alloy	Composition (Balance Titanium), weight per cent	Specimen	Specimen Type	Hydrogen Content, ppm	Hardness (10-Kg Load), VHN	Applied Stress PSI	Applied Stress Per Cent of Unnotched UTS	Time to Failure, hr [a]	Reduction in Area, per cent [a]	General Microstructural Characteristics	Visible Hydride at Notch
K-47	20Mo (I)	81N	B	800	240	118,500	110	(118.7)	(1.2)	Fine equiaxed beta, small amount of alpha	None
K-48	4Mo (O)	21N	B	200	302	132,300	110	(121.1)	(2.0)	Very fine spheroidal beta in alpha matrix	None
		31N	A	300	299	132,300	110	9.2	4.0	–	None
K-49	20Mo (O)	41N	A	400	297	158,800	110	(143.1)	(0.5)	Beta with small amount of alpha in grain boundaries	None
		61N	A	600	–	158,800	110	0.9	6.0	–	
		62N	A	600	294	158,800	110	0.8	8.5	–	Massive type (?)
K-50	4V (I)	21N	B	200	–	87,000	110	(118.8)	(4.2)	–	–
K-51	20V (I)	81N	B	800	236	109,100	110	(118.6)	(0.5)	Fine equiaxed beta	None
K-52	4V (O)	01N	B	20	270	124,200	110	(161.9)	(1.3)	Beta in an alpha matrix	None
		11N	B	100	270	124,200	110	12.7	2.6	–	Massive type
K-53	20V (O)	81N	B	800	249	118,100	110	(120.6)	(0.0)	Small amount of alpha precipitate in beta matrix	None
K-54	8Mn (I)	41N	B	400	–	132,800	110	0.4	2.8	–	–
K-55	8Mn (O)	21N	B	200	357	168,900	110	(114.9)	(0.0)	Equiaxed alpha in beta matrix	None
		31N	B	300	357	168,900	110	1.1	–	–	None
		32N	A	300	360	168,900	110	2.7	1.6	–	None
K-56	6Cr (I)	41N	B	400	–	108,700	110	2.7	1.1	–	–
K-57	6Cr (O)	01N	A	20	327	151,600	110	120.8	2.2	Alpha stringers in a beta matrix	None
		21N	B	200	327	151,600	110	20.4	4.4	This sample showed a fine precipitate near the fracture	None (Bakelite mount)
K-58	6Al-4Mn (I)	81N	B	800	342	164,500	110	(102.6)	(5.6)	Stringers of beta in an alpha matrix	None
K-59	6Al-4Mo (O)	81N	B	800	373	193,000	110	(101.0)	(2.2)	Stringers of beta in an alpha matrix	None
K-60	6Al-4V (I)	61N	A	600	–	162,800	110	(118.1)	(0.2)	–	–
K-61	6Al-4V (O)	61N	B	600	409	202,000	110	(100.7)	(1.5)	Small amount of beta in alpha matrix	None
		81N	A	800	401	202,000	110	(163.6)	(2.0)	–	None
K-62	4Al-4Mn (I)	41N	B	400	–	158,700	110	(114.3)	(0.0)	–	–

TABLE A-1. COMPLETE RESULTS OF THE ROOM-TEMPERATURE NOTCHED STRESS-RUPTURE TEST PROGRAM (Continued)

Alloy	Composition (Balance Titanium), weight per cent	Specimen	Specimen Type	Hydrogen Content, ppm	Hardness (10-Kg Load), VHN	Applied Stress PSI	Applied Stress Per Cent of Unnotched UTS	Time to Failure, hr[a]	Reduction in Area, per cent[a]	General Microstructural Characteristics	Visible Hydride at Notch
K-63	4Al-4Mn (O)	21N	B	200	213	190,500	110	(119.4)	(4.2)	Stringered beta in an alpha matrix	None
		31N	B	300	216	190,500	110	(163.4)	(0.3)	–	None
		41N	A	400	217	190,500	110	28.4	2.0	–	None
		61N	A	600	214	190,500	110	1.6	1.1	–	None
K-64	4Al-4Fe (I)	41N	B	400	–	161,700	110	4.9	0.5	–	–
K-65	4Al-4Fe (O)	21N	A	200	–	191,800	110	65.8	2.1	–	–
		22N	A	200	397	191,800	110	(126.0)	(0.0)	Alpha in a beta matrix	None
		31N	B	300	401	191,800	110	0.8	3.1	–	None (?)
K-66	4Al-4Cr (I)	No notch tests were completed									
K-67	4Al-4Cr (O)	No notch tests were completed									
K-68	4Ni	81N	A	800	201	83,200	110	(165.5)	(1.0)	Acicular alpha plus compound	None (Bakelite mount)
K-69	7Ni	01N	B	20	251	113,300	110	0.4	4.0	Large compound particles in alpha	None
		02N	B	20	249	100,000	102	23.8	1.6	–	None
		41N	B	400	254	113,300	110	11.9	1.8	–	None
		81N	A	800	–	113,300	110	6.3 3	–	–	–
		82N	A	800	254	100,000	102	20.1	0.9	Cracks or grain-boundary hydride	None (?)
K-70	2Mn-2Cu	01N	B	20	232	107,100	110	(113.6)	(1.3)	Alpha plus coarse compound(?); perhaps as much as 10 per cent beta	None
		02N	B	20	221	99,300	102	(162.6)	(2.0)	–	None
		21N	A	200	224	107,100	110	15.0	5.2	–	Grain-boundary type
		21NX	A	200	221	99,300	102	33.7	5.0	–	Massive type
		81N	A	800	233	99,300	102	14.5	1.1	–	Ditto
K-71	2Mo-2Cu	21N	B	200	–	108,000	110	33.9	4.5	–	–
K-72	4Al-7Cu	21N	B	200	339	161,500	110	(142.8)	(0.0)	Acicular alpha plus compound	None
		61N	A	600	–	167,200	110	50.8-60.1	1.8	–	–
		62N	A	600	348	167,200	110	49.9	1.2	–	None
		82N	A	800	350	168,500	110	26.3	0.9	Compound finer when 200 ppm hydrogen added	None
		81N	A	800	336	167,200	–	49.9	1.2	–	None
K-73	12Sn-4Mo	21N	B	200	327	153,800	110	(164.0)	(0.2)	Fine-grained alpha containing stringers of beta	None
		81N	A	800	302	153,800	110	(137.8)	(0.6)	–	None

TABLE A-1. COMPLETE RESULTS OF THE ROOM-TEMPERATURE NOTCHED STRESS-RUPTURE TEST PROGRAM (Continued)

Alloy	Composition (Balance Titanium), weight per cent	Specimen	Specimen Type	Hydrogen Content, ppm	Hardness (10-Kg Load), VHN	Applied Stress		Time to Failure, hr[a]	Reduction in Area, per cent[a]	General Microstructural Characteristics	Visible Hydride at Notch
						PSI	Per Cent of Unnotched UTS				
K-74	12Sn-4V	31N	B	300	330	167,000	110	(100.1)	(0.2)	Fine equiaxed alpha in beta matrix	None
		41N	A	400	333	167,000	110	4.4	7.0	–	None
K-75	12Sn-4Mn	01N	B	20	330	164,900	110	(138.2)	(1.6)	Equiaxed alpha in beta matrix	None
		21N	B	200	333	164,900	110	49.1	4.4	–	None
		31N	A	300	336	164,900	110	11.7	4.6	–	None
K-76	12Sn-2Fe	01N	B	20	325	159,500	110	(162.7)	(0.5)	Stringered beta in alpha matrix	None
		22N	A	200	330	159,500	110	2.7	1.5	–	Massive type
K-77	12Sn-4Cr	21N	B	200	339	163,500	110	(100.2)	(0.0)	Grain-boundary alpha in prior beta grain boundaries; fine, uniform alpha particles in beta matrix	None
		31N	A	300	336	163,500	110	(161.6)	(0.0)	–	None
		41N	A	400	342	163,500	110	4.9	3.0	–	None
K-78	12Sn-7Cu	21N	B	200	229	162,100	110	(100.3)	(0.0)	Alpha plus mixed-size compound	None
		41N	A	600	234	162,100	110	(100.1)	(0.5)	–	None
		81N	A	800	241	162,100	110	19.4	1.3	–	None (?)
K-79	7Cu (O)	81N	B	800	281	123,100	110	(100.7)	(1.4)	Alpha plus fine compound	None
K-80	7Cu (I)	81N	B	800	188	85,100	110	(165.0)	(0.5)	Alpha plus coarse compound	Acicular type in alpha

TABLE A-1. COMPLETE RESULTS OF THE ROOM-TEMPERATURE NOTCHED STRESS-RUPTURE TEST PROGRAM (Continued)

Alloy	Composition (Balance Titanium), weight per cent	Heat Treatment(b)	Specimen	Specimen Type	Hydrogen Content, ppm	Hardness (10-Kg Load), VHN	Applied Stress PSI	Applied Stress Per Cent of Unnotched UTS	Time to Failure, hr(a)	Reduction in Area, per cent(a)	General Microstructural Characteristics	Visible Hydride at Notch
K-13-1	8Mn	S – Eq.	2-11N	B	200	299	140,000	110	(235.2)	(0.3)	–	None
			3-11N	A	300	299	140,000	110	(165.9)	(1.2)	–	None
			4-11N	A	400	309	140,000	110	5.1	2.0	–	Some grain-boundary type
K-13-2	8Mn	SHT – Eq.	3-21N	A	300	351	168,000	110	(145.0)	(1.4)	–	None
			6-21N	A	600	357	168,000	110	107.2	2.2	–	None
			8-21N	A	800	348	168,000	110	38.1	2.2	–	None
K-13-3	8Mn	SHT + A – Eq.	0-31N	B	20	357	174,000	110	(210.0)	(1.0)	–	–
			1-32N	A	100	351	174,000	110	59.7	3.9	Hydride or cracking at fracture	None (?)
			2-31N	A	200	383	174,000	110	0.5	2.0	–	Grain-boundary hydride
K-13-4	8Mn	S – Ac.	2-41N	B	200	279	134,000	110	(215.7)	(1.9)	–	None
			3-41N	A	300	285	134,000	110	3.3	5.2	–	None
K-13-5	8Mn	SHT – Ac.	2-51N	A	200	339	167,500	110	(214.9)	(0.7)	–	None
			4-51N	A	400	336	167,500	110	(137.7)	(0.2)	–	None
			6-51N	A	600	342	167,500	110	(139.3)	(1.0)	Alpha stained	None
			8-51N	A	800	345	167,500	110	1.2	2.2	Alpha stained, heavy at fracture	None
K-13-6	8Mn	SHT + A – Ac.	0-61N	B	20	322	166,400	110	(163.0)	(0.3)	–	None
			1-62N	B	100	336	166,400	110	0.4	2.8	Some cracking along alpha-beta interface near fracture	None
			1-63N	B	100	–	143,600	95	0.6	0.3	–	–
			2-61N	B	200	351	166,400	110	0.2	1.6	–	Grain-boundary hydride
			2-62N	A	200	–	143,600	95	0.1	3.2	–	–
K-13-7	8Mn	S – F. – Eq.	No notch tests were completed									
K-13-8	8Mn	S – C. – Eq.	No notch tests were completed									
K-13-9	8Mn	S – M – Ac.	2-91N	B	200	–	135,100	110	(162.2)	(1.0)	–	–
K-33-1	2Mo-2Fe-2Cr	S – Eq.	1-11N	A	100	253	123,500	110	(117.1)	(0.8)	–	None
			2-11N	B	200	256	123,500	110	38.3	2.0	–	None (?)
			3-11N	A	300	253	123,500	110	8.2	5.2	–	None
			3-21N	B	300	–	106,600	95	51.8	2.0	–	–
K-33-2	2Mo-2Fe-2Cr	SHT – Eq.	2-21N	B	200	287	169,400	110	(239.3)	(3.4)	–	None
			3-21N	A	300	289	169,400	110	(113.7)	(2.3)	–	None
			4-21N	A	400	309	169,400	110	16.2	6.3	–	Grain-boundary type

TABLE A-1. COMPLETE RESULTS OF THE ROOM-TEMPERATURE NOTCHED STRESS-RUPTURE TEST PROGRAM (Continued)

Alloy	Composition (Balance Titanium), weight per cent	Heat Treatment[b]	Specimen	Specimen Type	Hydrogen Content, ppm	Hardness (10-Kg Load), VHN	Applied Stress PSI	Applied Stress Per Cent of Unnotched UTS	Time to Failure, hr[a]	Reduction in Area, per cent[a]	General Microstructural Characteristics	Visible Hydride at Notch
K-33-3	2Mo-2Fe-2Cr	SHT + A – Eq.	0-31N	B	20	299	133,800	110	(101.1)	(0.4)	–	None
			1-31N	A	100	262	133,800	110	45.0	1.3	–	None (?)
			2-31N	B	200	304	133,800	110	17.9	3.4	–	Grain-boundary type
			2-32N	A	200	–	115,500	95	(216.3)	(0.0)	–	–
K-33-4	2Mo-2Fe-2Cr	S – Ac.	1-41N	A	100	240	120,000	110	(120.3)	(1.5)	–	None
			2-41N	B	200	242	120,000	110	6.4	6.0	–	None
			3-41N	B	300	242	120,000	110	2.1	6.1	–	Grain-boundary type
			3-42N	A	300	–	103,600	95	3.8	4.8	–	–
K-33-5	2Mo-2Fe-2Cr	SHT – Ac.	2-51N	B	200	272	142,900	110	(135.8)	(1.6)	–	None
			3-51N	B	300	281	142,900	110	7.9	6.4	–	None (?)
			3-52N	B	300	–	123,400	95	16.8	4.4	–	–
K-33-6	2Mo-2Fe-2Cr	SHT + A – Ac.	0-61N	B	20	289	148,700	110	(118.9)	(1.1)	–	None
			1-61NX	A	100	276	148,700	110	0.6	4.6	Hydride visible some distance from fracture	Grain-boundary type
K-37-1	6Al-4V	S – Eq.	8-11N	B	800	336	165,200	110	(239.3)	(0.5)	–	None
K-37-2	6Al-4V	SHT – Eq.	6-21N	B	600	317	161,500	110	(238.4)	(0.8)	–	None
			8-21N	A	800	348	161,500	110	(163.9)	(0.8)	–	None
K-37-3	6Al-4V	SHT + A – Eq.	2-31N	B	200	354	172,100	110	(208.3)	(0.3)	–	None
			3-31N	A	300	363	172,100	110	(161.7)	(0.0)	–	None
			4-31N	B	400	354	172,100	110	85.9	5.1	–	None
			6-31N	A	600	354	172,100	110	30.9	4.0	–	None
K-37-4	6Al-4V	S – Ac.	2-41N	A	200	287	160,500	110	(207.0)	(0.7)	–	None
			6-41N	B	600	285	160,500	110	(114.0)	(0.7)	–	None
			8-41N	B	800	272	160,500	110	(137.9)	(0.7)	–	None
K-37-5	6Al-4V	SHT – Ac.	6-51N	B	600	283	153,300	110	(214.7)	(1.7)	Twinning visible around notch	None
			8-51N	A	800	287	153,300	110	(112.1)	(0.0)	–	None
K-37-6	6Al-4V	SHT + A – Ac.	1-61NX	A	100	339	156,700	110	(120.3)	(0.0)	–	None
			2-61NX	A	200	312	156,700	110	(163.5)	(0.8)	–	None
			3-61N	A	300	314	156,700	110	20.5	2.1	–	None
K-37-7	6Al-4V	S – M.– Eq.	No notch tests were completed									
K-37-8	6Al-4V	S – C.–Eq.	No notch tests were completed									

TABLE A-1. COMPLETE RESULTS OF THE ROOM-TEMPERATURE NOTCHED STRESS-RUPTURE TEST PROGRAM (Continued)

Alloy	Composition (Balance Titanium), weight per cent	Heat Treatment[b]	Specimen	Specimen Type	Hydrogen Content, ppm	Hardness (10-Kg Load), VHN	Applied Stress PSI	Applied Stress Per Cent of Unnotched UTS	Time to Failure, hr[a]	Reduction in Area, per cent[a]	General Microstructural Characteristics	Visible Hydride at Notch
K-37-9	6Al-4V	S – M – Ac.	4-91N	A	400	–	155,000	110	(160.1)	(0.0)	–	–
K-38-1	4Al-4Mn	S – Eq.	0-14N	A	20	–	201,000	132	16.3	11.6	Alloy segregation evident in some samples of the 4Al-4Mn alloy	–
			0-15N	A	20	–	195,000	128	(208.5)	(3.7)	–	–
			0-12N	B	20	–	190,200	125	(255.4)	(1.7)	–	–
			0-11N	B	20	333	167,500	110	(250.0)	(1.2)	–	None
			2-14N	A	200	–	201,000	132	0.0	7.7	–	–
			2-15N	A	200	–	195,000	128	0.7	11.1	–	–
			2-16N	A	200	–	190,200	125	3.1	5.8	–	–
			2-11N	A	200	351	167,500	110	(205.6)	(0.9)	–	None
			2-12N	B	200	–	121,800	80	(235.8)	(0.0)	–	–
			3-14N	A	300	–	201,000	132	1.0	9.6	–	–
			3-15N	A	300	–	195,000	128	5.6	3.6	–	–
			3-16N	A	300	–	190,200	125	10.5	4.2	–	–
			3-11N	A	300	360	167,500	110	(202.1)	(0.9)	–	None
			3-12N	B	300	–	121,800	80	(203.4)	(0.2)	–	–
			4-15N	A	400	–	205,300	135	71.3	8.6	–	–
			4-14N	A	400	–	201,000	132	(205.8)	(1.9)	–	–
			4-12N	A	400	–	190,200	125	(212.1)	(3.1)	–	–
			4-11N	A	400	330	167,500	110	(204.1)	(0.5)	–	None
			6-11N	B	600	345	167,500	110	1.3	5.1	–	None
			6-12N	B	600	–	121,800	80	67.9	3.2	–	–
K-38-2	4Al-4Mn	SHT – Eq.	0-23N	A	20	–	208,200	137	13.5	11.9	–	–
			0-22N	A	20	–	205,300	135	(264.4)	(5.3)	–	–
			0-24N	A	20	–	187,500	123	(214.4)	(1.4)	–	–
			0-21N	A	20	342	167,300	110	(210.6)	(1.1)	–	None
			2-22N	A	200	–	190,000	125	78.6	11.4	–	–
			2-24N	A	200	–	187,500	123	(165.5)	(1.1)	–	–
			2-23N	A	200	–	182,500	120	(214.9)	(1.0)	–	–
			2-21N	A	200	354	167,300	110	(257.7)	(0.8)	–	None
			6-24N	A	600	–	208,200	137	(165.7)	(4.5)	–	–
			6-23N	A	600	–	197,700	130	(210.2)	(2.9)	–	–
			6-22N	B	600	–	190,000	125	(262.3)	(2.5)	–	–
			6-21N	A	600	342	167,300	110	(239.4)	(0.0)	–	None
			8-24N	A	800	–	208,200	137	(100.0)	(3.1)	–	–
			8-23N	A	800	–	197,700	130	(210.1)	(1.8)	–	–
			8-22N	A	800	–	190,000	125	(239.2)	(2.1)	–	–
			8-21N	A	800	345	167,300	110	(235.8)	(0.0)	–	None

TABLE A-1. COMPLETE RESULTS OF THE ROOM-TEMPERATURE NOTCHED STRESS-RUPTURE TEST PROGRAM (Continued)

Alloy	Composition (Balance Titanium), weight per cent	Heat Treatment(b)	Specimen	Specimen Type	Hydrogen Content, ppm	Hardness (10-Kg Load), VHN	Applied Stress, PSI	Applied Stress, Per Cent of Unnotched UTS	Time to Failure, hr(a)	Reduction in Area, per cent(a)	General Microstructural Characteristics	Visible Hydride at Notch
K-38-3	4Al-4Mn	SHT + A – Eq.	1-31N	B	100	360	178,900	110	(214.0)	(0.7)	–	None
			2-31NX	A	200	333	178,900	110	(115.3)	(0.0)	Hydride in segregated area	None
			3-31N	A	300	370	178,900	110	12.4	6.4	–	None
K-38-4	4Al-4Mn	S – Ac.	0-42N	A	20	–	179,200	125	1.9	7.7	–	–
			0-43N	A	20	–	172,200	120	12.1	8.0	–	–
			0-44N	A	20	–	167,900	117	(193.5)	(1.8)	–	–
			0-41N	A	20	299	157,900	110	(215.5)	(0.8)	Some alloy segregation	None
			1-44N	A	100	–	186,500	130	(239.6)	(5.1)	–	–
			1-42N	A	100	–	179,200	125	(260.9)	(1.8)	–	–
			1-41N	A	100	317	157,900	110	(210.5)	(1.1)	–	None
			2-42N	A	200	–	179,200	125	7.0	7.1	–	–
			2-44N	A	200	–	172,200	120	(239.5)	(0.6)	–	–
			2-41N	A	200	306	157,900	110	(239.5)	(0.6)	Alpha stained on etching	None
			3-41N	A	300	325	157,900	110	(115.0)	(0.0)	–	None
			4-41N	A	400	325	157,900	110	(117.4)	(0.2)	–	None
			6-41N	B	600	345	157,900	110	31.3	4.0	Several alloy segregations	None
K-38-5	4Al-4Mn	SHT – Ac.	8-51N	A	800	327	162,800	110	(239.2)	(0.2)	–	None
K-38-6	4Al-4Mn	SHT + A – Ac.	0-61N	B	20	348	179,400	110	(162.9)	(0.6)	–	None
			1-61NX	A	100	360	179,400	110	0.3	3.2	–	Grain-boundary type
			2-61N	B	200	339	179,400	110	1.7	1.3	–	Grain-boundary type
K-38-7	4Al-4Mn	S – M.– Eq.	2-71N	B	200	333	149,900	110	(167.5)	(1.1)	–	None
			3-71N	A	300	336	149,900	110	(140.7)	(0.6)	–	None
			4-71N	A	400	336	149,900	110	(163.4)	(0.3)	–	None
			6-71N	B	600	342	149,900	110	63.2	2.0	–	None
			8-71N	A	800	339	149,900	110	(115.5)	(0.8)	–	None
K-38-8	4Al-4Mn	S – C.– Eq.	0-81N	B	20	319	146,100	110	(114.1)	(0.9)	Very coarse equiaxed structure	None
			2-81N	A	200	319	146,100	110	(115.5)	(0.3)	–	None
			3-81N	A	300	348	146,100	110	(120.4)	(0.0)	Hydride in segregated area	None
			4-81N	A	400	339	146,100	110	(119.3)	(0.2)	–	None
			6-81N	A	600	339	146,100	110	(161.4)	(0.3)	–	None
			8-81N	A	800	342	146,100	110	16.3	3.0	May be a small amount of grain-boundary hydride at fracture	None(?)
			8-82N	A	800	–	151,800	110	12.2	2.2	–	–
K-38-9	4Al-4Mn	S – F.– Ac.	3-91N	B	300	325	167,800	110	(165.6)	(0.3)	–	None
			4-91N	A	400	325	167,800	110	(121.1)	(0.0)	–	None
			6-91NX	A	600	345	167,800	110	8.6	5.0	Severe alloy segregation	None

(a) Values in parenthesis from samples removed from test before rupture.
(b) S = stabilized, SHT = solution heat treated, A = aged, Ac. = acicular, Eq. = equiaxed, F = fine grain size, C = coarse grain size, M = medium grain size.